

COMPUTATIONAL DEVELOPMENTS FOR *AB INITIO* MANY-BODY THEORY

By

Justin Gage Lietz

A DISSERTATION

Submitted to
Michigan State University
in partial fulfillment of the requirements
for the degree of

Physics - Doctor of Philosophy
Computational Math, Science and Engineering - Dual Major

2019

ABSTRACT

COMPUTATIONAL DEVELOPMENTS FOR *AB INITIO* MANY-BODY THEORY

By

Justin Gage Lietz

Quantum many-body physics is the body of knowledge which studies systems of many interacting particles and the mathematical framework for calculating properties of these systems. Methods in many-body physics which use a first principles approach to solving the many-body Schrödinger equation are referred to as *ab initio* methods, and provide approximate solutions which are systematically improvable. Coupled cluster theory is an *ab initio* quantum many-body method which has been shown to provide accurate calculations of ground state energies for a wide range of systems in quantum chemistry and nuclear physics. Calculations of physical properties using *ab initio* many-body methods can be computationally expensive, requiring the development of efficient data structures, algorithms and techniques in high-performance computing to achieve numerical accuracy.

Many physical systems of interest are difficult or impossible to measure experimentally, and so are reliant on predictive and accurate calculations from many-body theory. Neutron stars in particular are difficult to collect observational data for, but simulations of infinite nuclear matter can provide key insights to the internal structure of these astronomical objects. The main focus of this thesis is the development of a large and versatile coupled cluster program which implements a sparse tensor storage scheme and efficient tensor contraction algorithms. A distributed memory data structure for these large, sparse tensors is used so that the code can run in a high-performance computing setting, and can thus handle the computational challenges of infinite nuclear matter calculations using large basis sets. By

validating these data structures and algorithms in the context of coupled cluster theory and infinite nuclear matter, they can be applied to a wide range of many-body methods and physical systems.

Dedicated to my loving parents.

ACKNOWLEDGMENTS

This dissertation is the culmination of six years of graduate school, all of which has been under the guidance of my PhD advisor, Morten Hjorth-Jensen. I am incredibly lucky to have been on this journey with Morten, as he is not only an excellent teacher, scientist, and mentor, but he is also a wonderful person who is overflowing with kindness. It is hard to imagine what this dissertation would look like if I had never met Morten, as his influence is in every one of its pages. My thoughts surrounding physics, research, and philosophy have been profoundly shaped by Morten and that extends much beyond just this work. Thank you so much Morten, while this dissertation marks the end of my time as your student, I know it also marks the beginning of a lifelong friendship.

Next, I would like to thank Scott Bogner and Heiko Hergert who also have had a huge impact on this dissertation by creating an intellectually stimulating and friendly environment for the nuclear many-body group. It has been a pleasure to share this journey with you and with the other grad students in the group: Sam Novario, Nathan Parzuchowski, Titus Morris and Fei Yuan. The times I got to travel to summer schools with all of you and explore new cities are some of my favorite memories of grad school.

Outside of those who directly contributed to this dissertation, I also want to thank those who have made a positive impact on my life while I was working on it. First I want to thank my girlfriend, Rachel, for all of your love and support. You helped make my time in grad school the best years of my life, and I can't wait for our next adventure together. I am also grateful for the time shared with my other grad student friends, and in particular the great times I got to spend with Dennis, Terri, Michael, and Brent in the last few months. It was tough to push through at the end of grad school, but getting to spend time with you all

helped immensely.

Next I would like to thank my brother, Jordan who has been my friend and role model for my entire life and continues to be to this day, and my sister-in-law Sarah who can bring a smile to anyone in my family. You guys are the best, and I can't wait for many more visits to see you, Annabelle, and Ollie. Lastly, and certainly most importantly, I have to give thanks to my parents, Kim and Steve, to whom this dissertation is dedicated to. They have provided unconditional love and selfless support so that I could pursue what I love doing, and I am incredibly grateful for everything they have done for me.

Thank you so much mom and dad.

TABLE OF CONTENTS

LIST OF TABLES	ix
LIST OF FIGURES	x
KEY TO ABBREVIATIONS	xiii
Chapter 1 Introduction	1
1.1 Nuclear Theory as a Window into the the Stars	1
1.2 <i>Ab initio</i> methods in Nuclear Theory	3
1.3 Quantum Many-Body Methods	4
1.4 Infinite Matter Calculations	5
1.5 Computational Challenges	6
1.6 Thesis Overview	8
Chapter 2 Quantum Many-Body Physics	9
2.1 Bra-ket Notation	11
2.2 Many-fermion wave functions and spaces	14
2.3 Occupation Number Representation	21
2.4 Creation and annihilation operators	23
2.5 Number Operator	26
2.6 Anti-commutation relations	28
2.7 Operators in Second Quantized Form	29
2.8 Wick's Theorem	33
2.9 Generalized Wick's Theorem	38
2.10 Slater-Condon Rules	38
2.11 The Fermi Vacuum	44
2.12 Configuration Interaction	50
2.13 Hartree-Fock Theory	53
2.14 Many-Body Perturbation Theory	58
2.15 In-Medium Similarity Renormalization Group	65
2.16 The Magnus Formulation of IM-SRG	72
Chapter 3 Physical Systems	84
3.1 Pairing Model	85
3.2 Single-Particle Basis for Infinite Fermionic Matter	89
3.3 Two-Nucleon Interaction	93
3.4 Homogeneous Electron Gas	97
Chapter 4 Coupled Cluster	99
4.1 Prologue to Coupled Cluster	99

4.2	Coupled Cluster Theory	103
4.3	Coupled Cluster Diagrams	106
4.4	Diagrammatic Derivation of the Coupled Cluster Equations	117
4.5	Computational Scaling of Coupled Cluster Theory	127
Chapter 5	Computational Methodology	132
5.1	Code Validation	132
5.1.1	Pairing Model	133
5.1.2	Infinite Neutron Matter	135
5.2	Taming the Two-Body Basis	136
5.3	Performance Testing Matrix-Matrix Multiplication	141
5.4	Tensor Contractions as Matrix Multiplication	145
5.5	Parallel Computing	151
5.6	Distributed Memory Parallelization	156
5.7	Final Parallel Algorithm	158
Chapter 6	Results	163
6.1	Neutron Matter	164
6.2	Homogeneous Electron Gas	171
6.3	Computational Results	174
Chapter 7	Conclusions and Perspectives	184
BIBLIOGRAPHY	187

LIST OF TABLES

Table 2.1:	Single-Particle Index Conventions	45
Table 3.1:	Single-particle states and their quantum numbers and their energies from Eq. (3.3). The degeneracy for every quantum number p is equal to two due to the two possible spin values.	86
Table 3.2:	Total number of particle filling $N_{\uparrow\downarrow}$ for various $n_x^2 + n_y^2 + n_z^2$ values for one spin-1/2 fermion species. Borrowing from nuclear shell-model terminology, filled shells correspond to all single-particle states for one $n_x^2 + n_y^2 + n_z^2$ value being occupied. For matter with both protons and neutrons, the filling degree increased with a factor of 2.	92
Table 3.3:	Parameters used to define the Minnesota interaction model [53]. . .	97
Table 4.1:	Sign table for the four terms of eq. (4.37).	115
Table 5.1:	Coupled cluster and MBPT2 results for the simple pairing model with eight single-particle levels and four spin-1/2 fermions for different values of the interaction strength g	134
Table 5.2:	CCD and MBPT2 results for infinite neutron matter with $N = 66$ neutrons and a maximum number of single-particle states constrained by $N_{max} = 36$ (36 plane wave energy shells).	136
Table 5.3:	All possible particle-hole sectors are listed in the left column. In the right column are 6 particle hole sectors which contain all of the information of the whole matrix, plus how the other 10 can be equivalently expressed.	138
Table 5.4:	A straight forward scheme to organize the two-body basis in columns.	139

LIST OF FIGURES

Figure 2.1:	SRG with direct integration and with the Magnus expansion.	81
Figure 2.2:	Magnus SRG with the exact unitary transformation and with a BCH expansion truncated after a fixed number of terms	82
Figure 2.3:	Magnus SRG with the exact unitary transformation and with a BCH expansion truncated after a fixed tolerance is met	83
Figure 3.1:	Correlation energy for the pairing model with exact diagonalization, MBPT2 and perturbation theory to third order MBPT3 for a range of interaction values. A canonical Hartree-Fock basis has been employed in all MBPT calculations.	88
Figure 5.1:	Correlation energy for the pairing model with exact diagonalization, CCD and perturbation theory to third (MBPT3) and fourth order (MBPT4) for a range of interaction values.	135
Figure 5.2:	The pp-pp sector of a two-body interaction matrix for a simple neutron matter system with 40 single-particle states above the Fermi level.	140
Figure 5.3:	Implementation of the same mathematics can have very different run times.	144
Figure 5.4:	MBPT2 contribution to the correlation for pure neutron matter with $N = 14$ neutrons and periodic boundary conditions. Up to approximately 1600 single-particle states have been included in the sums over intermediate states in Eqs. (5.7) and (5.8)	148
Figure 5.5:	A cartoon of how the interaction matrix might be split into work loads for different threads of execution for the naive storage and the block storage schemes.	155
Figure 5.6:	Performance of MBPT2 calculations with increasing number of MPI ranks. The speed of the calculation is measured in s^{-1} , the black data are the inverse time required to finish the calculation on the fastest rank, and the red data are the speeds of the slowest rank. . .	157

Figure 5.7:	The blocks are distributed to the ranks to try and keep the number of non-zero matrix elements equal among ranks. The histogram shows that the time it takes to load these blocks is dominated by an enormous amount of small blocks, which is ideal for load balancing.	159
Figure 5.8:	The t -amplitudes are permuted as needed for the tensor contractions which are not aligned as a matrix-matrix product. In the histogram, the larger blocks have begun to take more of the total time relative to the previous step.	160
Figure 5.9:	The largest tensor contractions are now performed, which are already aligned as matrix-matrix products. The $\mathcal{O}(N^3)$ scaling of the matrix-matrix product causes the larger matrices to contribute significantly to the total processing time in this step.	161
Figure 5.10:	The t -amplitudes are summed together and the correlation energy is calculated. If the energy has not converged to the set tolerance, another iteration of the CC equations are performed, using these new t -amplitudes in step 2.	161
Figure 6.1:	Two different energy per particle plots at low densities of neutron matter with the Minnesota potential [53] computed in the CCD approximation with 54 neutrons and an $N_{\max} = 100$ truncation (100 plane-wave energy shells), corresponding to 10754 single particle states.	165
Figure 6.2:	Energy per particle of pure neutron matter computed in the CCD approximation with the Minnesota interaction model [53].	166
Figure 6.3:	The relative error shows how much the CCD correlation energy is changing between subsequent calculations at different model spaces sizes ranging from $N_{\max} = 10$ to 70 for neutron matter with the Minnesota potential at density 0.2 fm^{-3}	167
Figure 6.4:	Finite-size effects in different energies of pure neutron matter computed with the Minnesota interaction model [53] as a function of the number of particles for both periodic boundary conditions (PBC) and twist-averaged boundary conditions (TABC5).	169
Figure 6.5:	Energy per particle for pure neutron matter with the Minnesota potential [53]. Here the calculations have been performed with IM-SRG(2), CCD, CIMC [77], and the ADC(3) Self-Consistent Green's Function scheme [77].	170
Figure 6.6:	The CCD energy per particle for the homogeneous electron gas for a range of Wigner-Seitz Radii with $A = 14$ electrons	172

Figure 6.7:	Contributions to the energy from purely CCD many-body correlations.	173
Figure 6.8:	Fractional contribution to the energy from the Hartree-Fock reference state.	173
Figure 6.9:	The relative error shows how much the CCD correlation energy is changing between model spaces sizes ranging from $N_{\max} = 10$ to 60 for the electron gas at $r_s = 0.5$	174
Figure 6.10:	The relative error shows how much the CCD correlation energy is changing between model spaces sizes ranging from $N_{\max} = 10$ to 60 for the electron gas at $r_s = 0.1$	175
Figure 6.11:	The relative error of the CCD correlation energy is changing between model spaces sizes ranging from $N_{\max} = 100$ to 200 for the neutron matter with the Minnesota potential at $A = 54$ and $\rho = 0.08$	176
Figure 6.12:	The time required for the large basis set Minnesota potential calculations.	177
Figure 6.13:	Strong scaling of distributed memory code, dark green line shows ideal case.	178
Figure 6.14:	Weak scaling of distributed memory code, the dark green line shows the ideal case.	180
Figure 6.15:	Number of tensor elements required for the 3-body force in the infinite matter basis with and without block-diagonal compression.	181
Figure 6.16:	Size of tensor in gigabytes required for the 3-body force in the infinite matter basis with and without block-diagonal compression.	182
Figure 6.17:	On node timing tests for the tensor contraction of three-body force diagrams.	183

KEY TO ABBREVIATIONS

- NSCL - National Superconducting Cyclotron Laboratory (East Lansing MI, USA)
- CC - Coupled Cluster
- CC(S)(D)(T) - Coupled Cluster with (Singles)(Doubles)(Triples)
- IM-SRG - In-Medium Similarity Renormalization Group
- EoS - Equation of State
- d.o.f. - Degree of Freedom
- QCD - Quantum Chromodynamics
- LQCD - Lattice QCD
- GPU - Graphics Processing Unit
- χ -EFT - Chiral Effective Field Theory
- FCI - Full Configuration Interaction
- CISD - Configuration Interaction Singles and Doubles
- CIMC - Configuration Interaction Monte Carlo
- MBPT - Many-Body Perturbation Theory
- BCH - Baker - Campbell - Hausdorff
- HEG - Homogeneous Electron Gas
- BLAS - Basic Linear Algebra Subroutines
- cuBLAS - CUDA BLAS
- OMP - Open Multi-Processing
- MPI - Message Passing Interface
- ADC - Algebraic Diagrammatic Construction

Chapter 1

Introduction

1.1 Nuclear Theory as a Window into the the Stars

Stars are objects of extreme forces. Spheres of crushing gravitational forces being held up by the violent nuclear reactions at their core. Until they aren't. Eventually the nuclear fuel at the core of every star depletes, giving way to gravitational contraction, and in some cases cataclysmic collapse. Many bright burning stars will collapse onto their own cores, creating one of the brightest events in the galaxy, a supernova. The extreme explosions of some dying stars blast off a significant fraction of their total material, and leave behind a spent core. If the resulting core is large enough, the gravitational compression will crush the remaining matter to extreme densities. In the cases that are not quite large enough for a black hole to form, a neutron star remains at the center of a once bright burning star. Neutron stars get their name because the extreme densities caused by the gravitational collapse have pushed beyond the limits of electron degeneracy, collapsing the bulk of protons and electrons into neutrons. In a region around 1-3 solar masses, the resulting neutron degeneracy pressure together with the very close range nuclear force are enough to push back against further gravitational collapse, forming an incredible astronomical object that is composed of a very unique state of matter. Neutron stars tend to be around one solar mass, but are only about 10km in size, as the entire macroscopic object is around nuclear density. After this bright supernova, the resulting neutron star core is left cold and dim. This makes direct observation

of these fascinating objects very difficult, and can only rarely be done. In the case of pulsars, direct electromagnetic radiation can be detected, however it is only from a directed beam out of the magnetic axis of the star. Otherwise, indirect measurements of nearby stars must be done. Looking for the gravitational footprint on the orbits of stars, such as a bright star in a binary system with a neutron star can determine with some accuracy the mass of the binary neutron star partner. A direct astronomical measurement of the neutron star radius might not be possible, as they are just too dim and too far away. Since telescopes are largely unable to see neutron stars, it is up to theoretical physics to help paint a picture of these extreme objects.

To figure out how neutron stars respond to gravitational compression, and how they eventually equilibrate to some radius, the equation of state (EoS) of the neutron star must be known. Currently, there are many proposed equations of state [1, 2], which lead to a large spread of possible radii given a particular observed mass. This is due to the difficult nature of calculating the nuclear EoS, which in principle requires knowing the exact composition of a neutron star, and calculating the energetic state of this quantum system. A large part of a neutron star is thought to be pure neutron matter, although some amount of proton and lepton matter is likely present in a state of β -stable matter. Some theories posit that the extreme densities towards the core of the neutron star could cause the formation of hyperons in the nuclear matter, or that the matter could be pushed into a state of pure quarks [1]. Regardless of the composition, the resulting calculation is a difficult problem of quantum many-body physics. A comprehensive treatment of this problem would involve calculating the strong interactions of an absurd number of particles, and many attempts have been made using a slew of different approximations. Regardless of the exact framework, it seems that theoretical nuclear physics, the study of some of the smallest particles, could be our best

tool to determine properties of these massive celestial bodies.

1.2 *Ab initio* methods in Nuclear Theory

Nuclear theory as a field is currently in an exciting period of growth due to theoretical and computational developments in *ab initio* methods over the last two decades. *Ab initio*, latin for “from the beginning”, is a phrase used to describe work done from first principles, which for nuclear theory means starting from the building blocks of the atomic nucleus: protons and neutrons. While nucleons are composite particles made up of quarks and gluons, they are well bound (on the order of GeV) compared to the interactions between them (MeV) so they function well as the basic degrees of freedom (d.o.f). The “hard core” nature of the nucleon-nucleon force has made the *ab initio* approach to calculating nuclear properties intractable in the past, as this leads to the coupling of high and low momentum modes, creating difficulties in calculating all but the smallest nuclei. Many strategies have been used to evade this problem, perhaps most notable are the phenomenological models used to great effect with shell model (SM) calculations. By developing nuclear interactions using nuclear data input near regions of interest, high accuracy calculations of properties of nuclei have been made [3]. In this approach however, many nucleonic d.o.f.’s are “frozen out”, meaning that they are ignored and some contact with the underlying physics is lost. Another approach has been the development of similarity renormalization group (SRG) methods, which have lead to the proper decoupling of these high and low momentum modes, leading to softer interactions that are able to converge much faster, and make many more calculations possible [4, 5]. Potentials generated from chiral effective field theory (χ -EFT) [6, 7], which connect the nuclear force to the underlying symmetries of the QCD langrangian, can now be softened with SRG [4, 5]

leading to a class of potentials that have connections to the underlying physics, and are tractable for calculations of nuclei. This progress has allowed properties of medium mass nuclei to be calculated with links to fundamental forces at modest computational cost. This has opened a whole new way of studying nuclei, as now methods that keep track of all of the nucleonic d.o.f.'s can be used in realistic calculations.

1.3 Quantum Many-Body Methods

There are many ways of taking on realistic calculations of nuclear properties, and at the core of many approaches is the non-relativistic many-body Schrödinger equation. Low energy nuclear physicists can get away without using relativistic quantum mechanics because the typical binding energies of nuclei is in the range of 1 MeV to 10 MeV per nucleon, while each nucleon itself is bound together at around 1 GeV. Even with this non-relativistic approximation, the task of calculating any many-body problem is daunting. The second approximation that must be done is to pick a finite basis to perform the calculation in. These basis sets are in principle infinite, but we must have a finite system for our finite computers. Within this framework, the task of a complete energy spectrum calculation of N particles in a basis with M single-particle states, would require diagonalizing an $\binom{M}{N}$ by $\binom{M}{N}$ sized matrix where $\binom{M}{N} = \frac{M!}{N!(M-N)!}$ is a factorially growing number. This means that for all but small systems in small basis sets, this factorial growth will quickly grow beyond current computational power. Full configuration interaction (FCI) is a method which uses a minimal number of approximations, and computes a nearly exact energy of the system, but at a massive computational cost [8, 9, 10, 11]. This unfavorable scaling has led to the development of an entire industry of approximations to solving the full many-body problem.

Each method approaches the many-body problem in its own way, with its own series of advantages and disadvantages. In particular, coupled cluster theory [12, 13, 14, 15, 16] has been in use in many-body theory since the 60's, starting with the work of Coester [17, 18] and Kummel [19], and saw enormous success in quantum chemistry, and more recently nuclear theory as well [20, 21]. Coupled cluster theory is centered around a way to organize the many-body basis by grouping states in excitation “clusters” that lead to very favorable truncations of less important terms. Truncations are almost always needed in practical calculations, but by restoring the truncations term by term we can systematically improve the solution and eventually restore the exact FCI answer. With this improved many-body basis truncation, coupled cluster theory has a favorable polynomial scaling, and sacrifices only a small amount of accuracy. In quantum chemistry, CC theory has been used to calculate molecular properties to chemical accuracy at a fraction of the computational cost of a total FCI calculation. In nuclear physics, coupled cluster's many-body truncation errors are typically minimal when compared to errors in the approximation of the nuclear forces. With this success, CC has shown to be one of the premier *ab initio* many-body methods in nuclear physics.

1.4 Infinite Matter Calculations

This thesis focuses on *ab initio* many-body calculations relevant for neutron stars. The ultimate goal is to learn more about neutron stars while still maintaining a link to the underlying theory of the strong force, quantum chromodynamics, while at the same time studying the tools and approximations needed to make this possible. Simulating an entire star at the quantum level is an impossible task. However, by studying a small periodic chunk

of neutron star matter, we can extract properties like the equation of state while maintaining these important links[1].

This idea of studying a periodic box of quantum matter is not a new idea, and the so called “infinite matter” problem is an often revisited system for many-body theorists [22]. By simulating a finite number of particles in a periodic box, an approximation to an infinite space filled with these particles can be made. Infinite matter is studied in quantum chemistry [23] to simulate electrons moving in a neverending lattice of atoms, and in nuclear physics it can be studied as a large block of neutron star matter [2].

Many-body physicists in general study the infinite matter problem as a sandbox to examine their theoretical machinery. The periodic box in which infinite matter is frequently studied leads to a natural choice of basis, that of plane waves. The flat periodic boundaries that are chosen lead to a quantization of momentum modes, which give a basis of fixed momenta waves moving through the box. Despite being a theoretically convenient basis, the plane waves can be computationally challenging, as realistic simulations of neutron matter can need hundreds of particles and thousands of basis states to converge to a point that resembles a true infinite slab of matter.

1.5 Computational Challenges

Despite the polynomial scaling, *ab initio* methods like coupled cluster theory can begin to struggle with the computational load that thousands of basis states require. It is here that a deep inspection of the many-body tools in use must be done. Approximations in coupled cluster theory organize the many-body basis in terms that (typically) decrease in importance for higher excitation levels. For infinite matter calculations, the first non-zero

terms are that of doubles excitations, that is, exciting pairs of particles together, in what is called coupled cluster doubles (CCD). Even in this restrictive approximation, storage of the two-body interaction matrix scales as M^4 , where the number of single-particle basis states M can quickly grow to 10^3 , leading to matrix sizes of 10^{12} elements, which is already too large for modern computers to deal with. While these matrices are very large, by exploiting the sparsity of this many-body basis, these matrices can be tamed to sizes that can run on a single large computer, or a small cluster. However, studies of modern nuclear potentials have shown that three-body forces are necessary for accurate calculations, leading to a three-body interaction matrix that scales as M^6 . Furthermore, CCD alone is often too restrictive of an approximation, and either partial or full inclusion of triples excitations (CCDT) is necessary for modern state-of-the-art calculations of infinite nuclear matter. These complications mean that tools from high-performance computing are necessary to meet the precision and accuracy demands of *ab initio* many-body theory. First, to even store the three-body interaction matrix which can quickly grow to hundreds of terabytes (TB) in size, distributed memory algorithms must be used. Only by distributing these large interaction matrices across a computational cluster can the calculation even be started. Next, the floating point operations (FLOPs) required by a CCDT calculation with three-body forces will scale as M^9 , meaning that massively parallel algorithms are needed to get these calculations finished in a reasonable amount of time. This massively parallel paradigm of supercomputing usually means writing custom code for the architecture of the computer that will be used, and in the case of the current largest computers, this means leveraging the enormous power of graphics processing units (GPUs) to get the job done. Along with a growing demand for computational power is a growing problem with reproducible science and portable codes. To maximize the scientific effort of computational physicists, research that is maintainable, extensible and reproducible

needs code that is well tested, well documented, well designed and version controlled.

1.6 Thesis Overview

This thesis will review the basics of quantum mechanics and many-body theory as it pertains to coupled cluster calculations in Chapter 2 to establish the language and notation needed for the subsequent chapters. To establish the context of the field, we will go through the relevant theory derivations, and Chapter 3 will describe the quantum systems which will be tackled with these methods. A focus will be on coupled cluster theory, and Chapter 4 will show how to derive CC theory using the development of diagrammatic techniques. Once this foundation is laid, we dive into the main object of this thesis: a large and versatile computer program which can calculate properties of a variety of quantum systems using a variety of many-body methods. In Chapter 5 we describe the distributed memory data structures and algorithms that implement these many-body methods efficiently in a high performance computing setting. Lastly, the numerical results and performance testing of the program for infinite matter calculations are discussed in Chapter 6.

Chapter 2

Quantum Many-Body Physics

This work will focus on *ab initio* calculations of many interacting particles where *ab initio*, meaning “from the beginning”, refers to the fact that we want these calculations to be as fundamental as possible. By starting from the basic building blocks, we can make accurate predictions of properties over a wide range of systems. Choosing these degrees of freedom is a game of compromise. Degrees of freedom that are too “macroscopic” will have limited applicability, but degrees of freedom that are too “microscopic” yield a wide range of applicability, but coupling the very small scales up to the large scales of the system size can become computationally impossible. The target systems of nuclear physics frequently land in a regime where using the constituent protons and neutrons as the degrees of freedom can be too microscopic, as calculating properties of nuclei rapidly grows too complex. Historically, phenomenological models, like the shell model, have had success by generating effective interactions for a few valence nucleons on top of an inert closed shell core. Accurate properties can be computed relatively quickly by “freezing out” the nucleon degrees of freedom in the closed shell. However, the shell model interactions rely on known experimental data in the region of interest to fit the matrix elements, and so any given shell model interaction can only function well in this limited space. Extrapolating into regions where there is little experimental data is very challenging, as the interaction was only tuned to the region of interest.

In the other extreme, the nucleons that make up nuclei are themselves composite particles

of quarks and gluons. So a truly fundamental calculation would build up the properties with all quark and gluon degrees of freedom active. Such calculations are done in the field of lattice quantum chromodynamics (LQCD) [24, 25], but due to the extreme microscopic nature of these degrees of freedom they quickly become overwhelmingly difficult, leaving only the smallest nuclear systems accessible this way .

This work operates in between these regimes, where the quarks and gluons are frozen out, but all of the protons and neutrons remain active in the calculation. As a trade off, the interactions between nucleons are generated from chiral effective field theory (χ -EFT) [6, 7], which bring the symmetries from the fundamental QCD Lagrangian. While these calculations are expensive, truncations are made to the possible configurations of nucleons to make them feasible, and techniques in high performance computing allow relatively large systems to be calculated. In principle, interactions fit once to few nucleon data have much larger ranges of applicability, and would accurately compute properties from small to medium mass nuclei to infinite nuclear matter. In reality, the current state of the art predictive models need additional data like the binding energy and radii of small to medium mass nuclei [26, 27]. In this sense, the philosophy of *ab initio* quantum many-body physics is to keep all nucleons active, and while truncations are made, there is a systematically improvable scheme for both the interaction and the many-body correlations. To provide the foundation to make these statements concrete, this chapter will briefly walk through single-particle quantum mechanics and then survey a few quantum many-body techniques.

2.1 Bra-ket Notation

A concise formalism for describing quantum states is bra-ket notation, also called Dirac notation. In bra-ket notation, a quantum state is represented as an abstract **ket**, $|\psi\rangle$. This notation distinguishes itself from wave mechanics where the state is written explicitly as $\psi(x)$, a function of \mathbf{R} space, or matrix mechanics where the state is expanded in some orthonormal basis, and referenced as a set of basis components (c_0, c_1, \dots) . The abstract nature of the ket allows for a formalism where derivations and manipulations can be done in an *invariant* way, and a choice of coordinates or a basis can be chosen at any point where it is convenient.

There are many texts covering the formalism of bra-ket notation, so we'll just look at a few interesting pieces to have footing for later discussions. In bra-ket formalism, the quantum state $|\psi\rangle \in \mathcal{H}$ is an element of state space, which is a abstract complex Hilbert space that is infinite dimensional and separable (i.e. can have a countable orthonormal basis).

One property of Hilbert spaces that is central to quantum mechanics is that they are closed under linear combinations. As a consequence, superpositions of states are themselves states in the space

$$|\psi\rangle = c_1 |\psi_1\rangle + c_2 |\psi_2\rangle. \quad (2.1)$$

Additionally, Hilbert spaces come with an inner product $\text{IP} : (\mathcal{H}, \mathcal{H}) \rightarrow \mathbb{C}$ which can be written many different ways. However the last notation written below using the angled brackets is where bra-ket notation gets its name

$$\text{IP}(|\phi\rangle, |\psi\rangle) = \langle |\phi\rangle, |\psi\rangle \rangle \equiv \langle \phi | \psi \rangle = \langle \psi | \phi \rangle^*. \quad (2.2)$$

This leads to the definition of the bra state $\langle\phi|$. For any state $|\phi\rangle \in \mathcal{H}$, we can associate a linear functional $\langle\phi| \equiv f_{|\phi\rangle} : \mathcal{H} \rightarrow \mathbb{C}$, where for $|\psi\rangle \in \mathcal{H}$

$$f_{|\phi\rangle}(|\psi\rangle) = \langle\phi|(|\psi\rangle) = \text{IP}(|\phi\rangle, |\psi\rangle) = \langle\phi|\psi\rangle. \quad (2.3)$$

Only the bra-ket notation of the inner product will be used from now on, the function argument style was just to draw attention to the fact that these bras are linear maps from the Hilbert space to the complex numbers. The Hermitian conjugate (conjugate transpose) is used to go from a ket state to the corresponding bra state,

$$|\psi\rangle^\dagger = \langle\psi| \quad \langle\psi|^\dagger = |\psi\rangle. \quad (2.4)$$

A distinct advantage to this notation is now the projection operator P_ψ onto the state $|\psi\rangle$ is compactly written as

$$P_\psi = |\psi\rangle \langle\psi|. \quad (2.5)$$

A set of ket vectors is considered an orthonormal basis $\{|\psi_i\rangle \equiv |i\rangle\}_{i \in \mathbb{N}}$ if they satisfy the orthonormality relation

$$\langle i|j\rangle = \delta_{ij}, \forall i, j \in \mathbb{N}, \quad (2.6)$$

and the completeness relation

$$\sum_{i \in \mathbb{N}} |i\rangle \langle i| = \mathbb{1}_{\mathcal{H}}. \quad (2.7)$$

From here, we can represent the quantum state in any basis of our choosing, by applying

the completeness relation (2.7) above on any ket $|\psi\rangle$

$$|\psi\rangle = \sum_{i=0}^{\infty} |i\rangle \langle i|\psi\rangle. \quad (2.8)$$

Next, we introduce linear operators on \mathcal{H} . An operator A maps a ket $|\psi\rangle$ into a new ket $A|\psi\rangle = |A\psi\rangle \in \mathcal{H}$ and $\langle\psi|A = \langle A^\dagger\psi|$, where A^\dagger is the adjoint of A . The adjoint is defined by the operation of the operator under the inner product

$$\text{IP}(|\phi\rangle, A|\psi\rangle) = \text{IP}(A^\dagger|\phi\rangle, |\psi\rangle). \quad (2.9)$$

In bra-ket notation notice that $\langle\phi|\psi\rangle = \langle\psi|\phi\rangle^*$, so if $|\psi\rangle$ is acted on by A then projected onto $\langle\phi|$ we get

$$\langle\phi|(A|\psi\rangle) = \langle\phi|A\psi\rangle = \langle A^\dagger\psi|\phi\rangle^*, \quad (2.10)$$

which defines the bra-ket notation of the adjoint. There are some technicalities regarding the domain of A in contrast to the domain of A^\dagger which can in general cause problems, which are detailed in[28]. If this is not a concern, as is the case in all calculations in this work, then bra-ket notation actually provides an equivalent interpretation that the operator A acts on the bra state, which is then projected onto by the ket state. In the case of self-adjoint operators where $A = A^\dagger$, there are no worries even in bra-ket notation since

$$\langle\phi|A\psi\rangle = \langle A\phi|\psi\rangle = \langle\phi|A|\psi\rangle. \quad (2.11)$$

Self-adjoint operators are of particular interest, since they correspond to physical observables to ground the theory in reality.

Since this is a work in computational physics, everything must be truncated to fit the calculations on a computer. In this case, one must select a representation for the calculation to be carried out in, and then the basis is truncated

$$|\psi\rangle = \sum_{i=0}^{\infty} \langle i|\psi\rangle |i\rangle \approx \sum_{i=0}^N \langle i|\psi\rangle |i\rangle. \quad (2.12)$$

The accuracy of this approximation will be discussed in later chapters. The quantum state is fully encoded in N coefficients of orthonormal basis states and operators are fully described by their matrix elements $\langle i|A|j\rangle$. In this regime, observables are represented by Hermitian matrices where, $\langle i|A|j\rangle = \langle j|A|i\rangle^*$, which have real eigenvalues.

Let us now consider a Hamiltonian as an operator on a Hilbert space in the following way: The eigenkets of \hat{H} , denoted $|i\rangle$, provide an orthonormal basis for the Hilbert space. The spectrum of allowed energy levels of the system is given by the set of eigenvalues, denoted $\{\varepsilon_i\}$, solving the equation:

$$\hat{H} |i\rangle = \varepsilon_i |i\rangle. \quad (2.13)$$

Since \hat{H} is a Hermitian operator, the energy is always a real number.

2.2 Many-fermion wave functions and spaces

To calculate energies of quantum many-body systems, we must find the eigenkets of the many-body Hamiltonian

$$\hat{H} |\Psi_\mu\rangle = E_\mu |\Psi_\mu\rangle, \quad \hat{H} = \hat{Z} + \hat{V} + \dots \quad (2.14)$$

where \hat{Z}, \hat{V} are the one-body and two-body pieces of the Hamiltonian, and in general these terms go up to A -body interactions for a system of A particles. The many-body state is an element of the A -body Hilbert space

$$|\Psi\rangle \in \mathcal{H}_A. \quad (2.15)$$

To express the many-body state in terms of single-particle quantum mechanics, let's first try the A -body Hilbert space as the tensor product of A single-particle Hilbert spaces

$$\mathcal{H}_A = \underbrace{\mathcal{H} \otimes \mathcal{H} \otimes \cdots \otimes \mathcal{H}}_A, \quad (2.16)$$

where there i th single particle state is $|\psi_i\rangle \in \mathcal{H}$. This accurately represents a many-body state where none of the particles are interacting with each other

$$|\Psi\rangle = |\psi_{p_1} \psi_{p_2} \cdots \psi_{p_A}\rangle \stackrel{\text{def}}{=} |\psi_{p_1}\rangle \otimes |\psi_{p_2}\rangle \otimes \cdots \otimes |\psi_{p_A}\rangle, \quad (2.17)$$

where the positions of the kets matters, as $|\psi_a\rangle |\psi_b\rangle$ means that particle 1 is in state $|\psi_a\rangle$ and particle 2 is in state $|\psi_b\rangle$, and is in general different from $|\psi_b\rangle |\psi_a\rangle$. The many-body state written as a many-body wavefunction:

$$\langle x_1, x_2, \dots, x_A | \Psi \rangle = \Psi(x_1, x_2, \dots, x_A) = \langle x_1, x_2, \dots, x_A | \psi_{p_1} \psi_{p_2} \cdots \psi_{p_A} \rangle \quad (2.18)$$

$$= \psi_{p_1}(x_1) \psi_{p_2}(x_2) \cdots \psi_{p_A}(x_A), \quad (2.19)$$

where x_1, x_2, \dots, x_A represent the coordinates of the degrees of freedom (like position and spin for example) of each particle. These are called “product states” as the wave functions

simply multiply together, and they form a complete A -body basis

$$\Psi(x_1, \dots, x_A) = \sum_{p_1, \dots, p_A} d_{p_1 \dots p_A} \psi_{p_1}(x_1) \dots \psi_{p_A}(x_A), \quad (2.20)$$

$$d_{p_1 \dots p_A} = \langle \psi_{p_1} \dots \psi_{p_A} | \Psi \rangle, \quad (2.21)$$

where $d_{p_1 \dots p_A}$ defines the overlap between the states. In the case of identical particles, interchanging any two particles in a state should leave any observable unchanged. The particle permutation operator P_{ij} takes two particles, i in state $|\psi_a\rangle$ and j in state $|\psi_b\rangle$ and swaps them so that they occupy each other's state. Two states are physically equivalent if they only differ by a complex phase, so

$$P_{12} |\psi_a\rangle |\psi_b\rangle = \pm |\psi_b\rangle |\psi_a\rangle, \quad (2.22)$$

gives two classes of indential particles. Particles that are symmetric under particle interchange are called bosons, and particles that are antisymmetric under particle interchange are called fermions. We will primarily be working with systems of fermions, so we introduce the antisymmetrization operator because the product wave functions do not guarantee antisymmetry

$$\hat{\mathcal{A}} = \frac{1}{A!} \sum_{\hat{Q} \in S_A} (-1)^{R_{\hat{Q}}} \hat{Q}, \quad (2.23)$$

where A is the number of particles, S_A is the symmetric group, and Q is a permutation operator in the symmetric group, with $(-1)^R$ the associated phase of the permutation. This will be talked about further, but for each pair of particles that are interchanged, a minus

sign is incurred. So if there are an even number of swaps, the sign is $+$, and if there are an odd number of swaps, the sign is $-$. The antisymmetrizer is hermitian

$$\hat{\mathcal{A}}^\dagger = \hat{\mathcal{A}}, \quad (2.24)$$

and idempotent

$$\hat{\mathcal{A}}^2 = \hat{\mathcal{A}}. \quad (2.25)$$

The antisymmetrizer projects any many-body wave function into an antisymmetric subspace. A fermionic state is already antisymmetric, so the antisymmetrizer will act as the identity operator when acting on a fermion wave function

$$|\Psi\rangle_{\text{fermionic}} = \hat{\mathcal{A}} |\Psi\rangle_{\text{fermionic}}. \quad (2.26)$$

We can write our many-fermion ket state as the antisymmetric projection of the product ket state space

$$|\Psi\rangle_{\text{fermionic}} \equiv |\Psi\rangle = \sum_{p_1, \dots, p_A} d_{p_1 \dots p_A} \hat{\mathcal{A}} |\psi_{p_1} \dots \psi_{p_A}\rangle. \quad (2.27)$$

Multiplying and dividing by $\sqrt{A!}$, we can rewrite this expression as

$$|\Psi\rangle = \sum_{p_1, \dots, p_A} \frac{1}{\sqrt{A!}} d_{p_1 \dots p_A} \sqrt{A!} \hat{\mathcal{A}} |\psi_{p_1} \dots \psi_{p_A}\rangle, \quad (2.28)$$

and we will define

$$D_{p_1 \dots p_A} \equiv \frac{1}{\sqrt{A!}} d_{p_1 \dots p_A}, \quad (2.29)$$

and

$$|\Phi_{p_1 \dots p_A}\rangle \equiv \sqrt{A!} \hat{\mathcal{A}} |\psi_{p_1} \dots \psi_{p_A}\rangle. \quad (2.30)$$

These many-body kets are explicitly antisymmetric, and they will form the basis for our many-fermion basis.

If this expression is reorganized slightly, one can see that it can be written as the determinant of a matrix, where the all of the permutations of different particles in different single-particle states are the matrix entries, that is

$$|\Phi_{p_1 \dots p_A}\rangle \rightarrow \frac{1}{\sqrt{A!}} \begin{vmatrix} \psi_{p_1}(x_1) & \dots & \psi_{p_1}(x_A) \\ \vdots & \ddots & \vdots \\ \psi_{p_A}(x_1) & \dots & \psi_{p_A}(x_A) \end{vmatrix}. \quad (2.31)$$

Since the determinant of a matrix is unchanged up to a sign under row/column permutation, this representation encodes the fermionic nature of the many-body state. This is a Slater determinant [29], and they form a complete, orthogonal and antisymmetric many-body basis to work with. For a simple example, we can look at the two-fermion case. We will try to reserve capital phi (Φ) as a variable representing a Slater determinant throughout this text

$$\Phi_{p_1 p_2}(x_1, x_2) = \frac{1}{\sqrt{2}} \begin{vmatrix} \psi_{p_1}(x_1) & \psi_{p_1}(x_2) \\ \psi_{p_2}(x_1) & \psi_{p_2}(x_2) \end{vmatrix} \quad (2.32)$$

$$= \frac{1}{\sqrt{2}} \left(\psi_{p_1}(x_1) \psi_{p_2}(x_2) - \psi_{p_1}(x_2) \psi_{p_2}(x_1) \right). \quad (2.33)$$

We see that both the antisymmetry and the Pauli exclusion principle are baked into these

Slater determinants

$$|\Phi_{p_1 p_2 \dots p_A}\rangle = -|\Phi_{p_2 p_1 \dots p_A}\rangle, \quad (2.34)$$

and if $p_1 = p_2$ the Slater determinant is zero. So again, any fermionic wave function can be expanded in this Slater determinant basis

$$|\Psi\rangle = \sum_{p_1 \dots p_A} D_{p_1 \dots p_A} |\Phi_{p_1 \dots p_A}\rangle. \quad (2.35)$$

Looking at the coefficients we see that

$$d_{p_1 \dots p_A} = \langle \psi_{p_1} \dots \psi_{p_A} | \overbrace{|\Psi\rangle}^{\text{antisymmetric}} \rangle = \langle \psi_{p_1} \dots \psi_{p_A} | \overbrace{\hat{\mathcal{A}}|\Psi\rangle}^{\text{Hermitian}} \rangle \quad (2.36)$$

$$= \langle \hat{\mathcal{A}}(\psi_{p_1} \dots \psi_{p_A}) | \Psi \rangle = \frac{1}{\sqrt{A!}} \langle \Phi_{p_1 \dots p_A} | \Psi \rangle. \quad (2.37)$$

Thus a sign change in Φ will imply the same change in D . Also, since the Slater determinant is zero if any two particles occupy the same state

$$|\Psi\rangle = \sum_{p_1 \neq p_2 \neq \dots \neq p_A} D_{p_1 \dots p_A} |\Phi_{p_1 \dots p_A}\rangle = A! \sum_{p_1 < p_2 < \dots < p_A} D_{p_1 \dots p_A} |\Phi_{p_1 \dots p_A}\rangle, \quad (2.38)$$

where the last expression accounts for the permutation of ordered states. If we define $c_{p_1 \dots p_A} = A! D_{p_1 \dots p_A}$, then our many-fermionic state can be written as

$$|\Psi\rangle = \sum_{p_1 < \dots < p_A} c_{p_1 \dots p_A} |\Phi_{p_1 \dots p_A}\rangle. \quad (2.39)$$

To keep track,

$$c_{p_1 \dots p_A} = A! \frac{1}{\sqrt{A!}} d_{p_1 \dots p_A} = \sqrt{A!} d_{p_1 \dots p_A} = \langle \Phi_{p_1 \dots p_A} | \Psi \rangle. \quad (2.40)$$

In conclusion, any quantum state of A fermions can be written as a linear combination of Slater determinants of single particle states. Let's now prove that the Slater determinant basis is orthonormal. Given an orthonormal single particle basis, let $p_1 < \dots < p_A$ and $q_1 < \dots < q_A$

$$\begin{aligned} \langle \Phi_{p_1 \dots p_A} | \Phi_{q_1 \dots q_A} \rangle &= \sqrt{A!} \sqrt{A!} \langle \hat{\mathcal{A}}(\psi_{p_1} \dots \psi_{p_A}) | \hat{\mathcal{A}}(\psi_{q_1} \dots \psi_{q_A}) \rangle \\ &= A! \langle \psi_{p_1} \dots \psi_{p_A} | \hat{\mathcal{A}}^2(\psi_{q_1} \dots \psi_{q_A}) \rangle \\ &= A! \langle \psi_{p_1} \dots \psi_{p_A} | \hat{\mathcal{A}}(\psi_{q_1} \dots \psi_{q_A}) \rangle \end{aligned} \quad (2.41)$$

$$= \frac{A!}{A!} \sum_{\hat{Q} \in \mathcal{S}_A} (-)^Q \int \psi_{p_1}^*(x_1) \dots \psi_{p_A}^*(x_A) \psi_{q_{Q_1}}(x_1) \dots \psi_{q_{Q_A}}(x_A) dx_1 \dots dx_A,$$

which if any of the q 's are different from the p 's, then the integral is zero. Assume $p_1 = q_1 \dots p_A = q_A$,

$$\langle \Phi_{p_1 \dots p_A} | \Phi_{p_1 \dots p_A} \rangle = \sum_{\hat{Q} \in \mathcal{S}_A} (-)^Q \int \psi_{p_1}^*(x_1) \dots \psi_{p_A}^*(x_A) \psi_{p_{Q_1}}(x_1) \dots \psi_{p_{Q_A}}(x_A) dx_1 \dots dx_A. \quad (2.42)$$

But since our single-particle basis is orthonormal:

$$\int \psi_{p_i}^*(x) \psi_{p_j}(x) dx = \delta_{ij}, \quad (2.43)$$

any of the permutations will make the integral equal to zero. Only the trivial permutation

of $Q = \mathbb{1}$ is nonzero, and in that case

$$\langle \Phi_{p_1 \dots p_A} | \Phi_{p_1 \dots p_A} \rangle = \int \psi_{p_1}^*(x_1) \dots \psi_{p_A}^*(x_A) \psi_{p_1}(x_1) \dots \psi_{p_A}(x_A) dx_1 \dots dx_A = 1. \quad (2.44)$$

Thus the Slater determinants are orthonormal. To recap, if we are given a complete, orthonormal single-particle space

$$\mathcal{H} = \text{Span} \{ \psi_p(x), p = 1, 2, \dots \}, \quad (2.45)$$

we can create a complete A -fermion Hilbert space

$$\mathcal{H}_A^{\text{fermion}} = \hat{\mathcal{A}}[\overbrace{\mathcal{H} \otimes \dots \otimes \mathcal{H}}^A]. \quad (2.46)$$

where the antisymmetrizer must be used to project onto the antisymmetric subspace of the full A -particle Hilbert space.

2.3 Occupation Number Representation

We are now in the proper position to begin talking about second quantization [16, 30] and occupation number representation. Given a set of ordered single particle states $1, 2, \dots, p, \dots$ we can write our Slater determinant in a slightly different way

$$|\{p_1, \dots, p_A\}\rangle \equiv |\Phi_{p_1, \dots, p_A}\rangle \xleftrightarrow{\text{isomorphic}} |0 \dots 0 \overbrace{1}^{p_1} 0 \dots 0 \overbrace{1}^{p_A} 0 \dots 0\rangle. \quad (2.47)$$

Or more compactly

$$|n_1 n_2 \dots n_p \dots\rangle, \quad n_p = 0, 1, \quad (2.48)$$

where each of the n_p terms corresponds to a one or zero from Eqn. (2.47). This now allows us to work in the Fock space [31], where the particle number is not fixed. The Fock space is the space spanned by all of such kets. In this text, we do most of our calculations with a fixed particle number, but the ability to represent a two-particle two-hole excitation as annihilating to particles below the Fermi surface and creating two particles above the Fermi surface proves to be very convenient. To ensure that the particle number is fixed, we write our A-fermion Hilbert space as

$$\mathcal{H}_A^{\text{fermion}} = \text{Span} \left\{ |n_1 \dots n_p\rangle, \quad \sum_p n_p = A \right\}, \quad (2.49)$$

while the full Fock space is the direct sum of all of such Hilbert spaces from $A = 0, 1, 2, \dots$

$$\mathcal{F}^{\text{fermion}} = \bigoplus_{A=0}^{\infty} \mathcal{H}_A^{\text{fermion}}. \quad (2.50)$$

A four particle example of such a state $|\{p_1, \dots, p_A\}\rangle$ with $p_1 = 0, p_2 = 1, p_3 = 6, p_4 = 9$, is in this representation given by

$$|\{0 \ 1 \ 6 \ 9\}\rangle = |\{\psi_0 \psi_1 \psi_6 \psi_9\}\rangle = |\Phi_{0 \ 1 \ 6 \ 9}\rangle = |110000100100\dots\rangle, \quad (2.51)$$

where here the trailing zeros can either be finite or infinite depending on how many states are in the single-particle basis.

2.4 Creation and annihilation operators

To define the annihilation operator, here is an example of what it does to a ket state,

$$\hat{X}_p |n_1 \dots n_p \dots\rangle = (-1)^{\sum_{k=1}^{p-1} n_k} n_p | \dots (1 - n_p) \dots \rangle. \quad (2.52)$$

We want to annihilate a particle in a particular state while keeping the proper phases from fermion statistics. So the $(1 - n_p)$ term is going to change a 1 to a 0 at spot p if there is a particle occupying that state. If there was not a particle occupying that state, then the n_p coefficient in front of the ket will be 0. If we multiply a ket by zero, we take this to mean that the state cannot exist, and we discard it. This is different from a ket where all of the n_p 's are zero, as that is a valid physical state, with zero particles. The sum in the expression keeps track of the phase by determining how many particles occupy lower lying states than the state we are trying to annihilate a particle from. To understand what this means more concretely, let's introduce some new notation of identifying if a single particle state is occupied or not in a ket. If a particle is in a state labeled p , with m states occupied before it, we will write

$$|\dots p \dots\rangle = \underbrace{|\dots}_{m} \overbrace{1}^p \dots\rangle, \quad n_p = 1, \quad (2.53)$$

where

$$m = \sum_{k=1}^{p-1} n_k, \quad (2.54)$$

and if a particle is not in state p with m states occupied before it, we will write it as

$$|\dots \cancel{p} \dots\rangle = \underbrace{|\dots}_{m} \overbrace{0}^p \dots\rangle, \quad n_p = 0. \quad (2.55)$$

The annihilation operator acting on these kets yields

$$\hat{X}_p |\dots p \dots\rangle = (-1)^m 1 |\dots \cancel{p} \dots\rangle, \quad (2.56)$$

$$\hat{X}_p |\dots \cancel{p} \dots\rangle = (-1)^m 0 = 0, \quad (2.57)$$

which matches with the intuition that was described above. The annihilation operator got rid of the particle occupying state p if there was a particle there, and set the whole state to 0 otherwise. Now before the creation operator is introduced, we first need to introduce the true vacuum state.

$$|0000\dots 0\dots\rangle = |0\rangle. \quad (2.58)$$

A single particle state can be written in second quantized form as

$$\psi_p = |p\rangle = |00\dots 0 \underbrace{p}_{n_p=1} 0\dots\rangle, \quad (2.59)$$

so that annihilating that single particle returns us to the true vacuum

$$\hat{X}_p |p\rangle = |00\dots 0\dots\rangle = |0\rangle. \quad (2.60)$$

We then define the creation operator as the Hermitian adjoint of the annihilation operator

$$\hat{X}_p |p\rangle = |0\rangle \rightarrow \langle p| \hat{X}_p^\dagger = \langle 0|. \quad (2.61)$$

It then follows that

$$\langle p | \hat{X}_p^\dagger | 0 \rangle = \langle 0 | 0 \rangle = 1 \implies \hat{X}_p^\dagger | 0 \rangle = | p \rangle. \quad (2.62)$$

When the creation operator acts on a state that is not the true vacuum

$$\hat{X}_p^\dagger | \{p_1 \dots p_A\} \rangle = | \{p \ p_1 \dots p_A\} \rangle, \quad (2.63)$$

$$\hat{X}_p^\dagger | \{p \ p_1 \dots p_A\} \rangle = | \{p \ p \ p_1 \dots p_A\} \rangle = 0, \quad (2.64)$$

where Eqn. (2.64) is zero since the determinant of a matrix with a repeated row is 0. This is the manifestation of the Pauli exclusion principle in the second quantization formalism, since you cannot have two fermions occupying the same state

$$\begin{aligned} & \hat{X}_p^\dagger | \{p_1 p_2 \dots p_A\} \rangle, \quad p_1 < p < p_2 \\ & = | \{p \ p_1 p_2 \dots p_A\} \rangle = - | \{p_1 \ p \ p_2 \dots p_A\} \rangle, \end{aligned} \quad (2.65)$$

or the same statement in the more compact notation

$$\hat{X}_p^\dagger | \overbrace{\dots}^m p \dots \rangle = (-1)^m | \dots p \dots \rangle, \quad (2.66)$$

and

$$\hat{X}_p^\dagger | \dots p \dots \rangle = 0. \quad (2.67)$$

Using these pieces together, we can encode these properties of the creation operator into the following definition

$$\hat{X}_p^\dagger |\dots n_p \dots\rangle \equiv (-1)^{\sum_{k=1}^{p-1} n_k} (1 - n_p) |\dots (1 - n_p) \dots\rangle. \quad (2.68)$$

2.5 Number Operator

The number operator is defined as

$$\hat{N}_p \equiv \hat{X}_p^\dagger \hat{X}_p. \quad (2.69)$$

This operator conserves particle number (it has the same number of creation and annihilation operators) and is Hermitian

$$\hat{N}_p^\dagger = (\hat{X}_p^\dagger \hat{X}_p)^\dagger = \hat{X}_p \hat{X}_p^\dagger = \hat{N}_p. \quad (2.70)$$

When \hat{N}_p acts on a ket where p is occupied, we obtain

$$\hat{N}_p |\dots p \dots\rangle = \hat{X}_p^\dagger \hat{X}_p \underbrace{|\dots p \dots\rangle}_m \quad (2.71)$$

$$= (-1)^m \hat{X}_p^\dagger |\dots \cancel{p} \dots\rangle = (-1)^m (-1)^m |\dots p \dots\rangle \quad (2.72)$$

$$= (-1)^{2m} |\dots p \dots\rangle |\dots p \dots\rangle. \quad (2.73)$$

We can see that the operator \hat{N}_p does not change the ket state. When \hat{N}_p acts on a ket where p is unoccupied we get

$$\hat{N}_p |\dots p \dots\rangle = \hat{X}_p^\dagger \hat{X}_p |\dots p \dots\rangle = 0. \quad (2.74)$$

Thus

$$\hat{N}_p |\dots n_p \dots\rangle = n_p |\dots n_p \dots\rangle. \quad (2.75)$$

The state $|p\rangle$ is an eigenstate of N_p in number occupancy representation with eigenvalue n_p , just as a state with definite position $|x\rangle$ is an eigenstate of the position operator \hat{x} in position space representation. In fact, these eigenkets *define* these representations. For most of this text, we will prefer to use the number occupancy representation of our many-fermion states.

Now we define the total number operator

$$\hat{N} = \sum_p \hat{X}_p^\dagger \hat{X}_p = \sum_p \hat{N}_p, \quad (2.76)$$

$$\hat{N} |\dots n_p \dots\rangle = \overbrace{\left(\sum_k n_k \right)}^A |\dots n_p \dots\rangle, \quad (2.77)$$

where $\sum_k n_k = A$ since we are restricting ourselves to the A -fermion Hilbert space. Thus

$$\hat{N} |\Psi\rangle = A |\Psi\rangle. \quad (2.78)$$

2.6 Anti-commutation relations

The most defining characteristic of the creation and annihilation operators are their anti-commutation rules,

(1)

$$\{\hat{X}_p^\dagger, \hat{X}_q\} = \hat{X}_p^\dagger \hat{X}_q + \hat{X}_q \hat{X}_p^\dagger = \delta_{pq} \mathbb{1}, \quad (2.79)$$

(2)

$$\{\hat{X}_p, \hat{X}_q\} = 0, \quad (2.80)$$

(3)

$$\{\hat{X}_p^\dagger, \hat{X}_q^\dagger\} = 0. \quad (2.81)$$

As an example of a calculation that can be done with second quantization, let's compute the overlap of two Slater determinants. Starting with a pair of two-particle Slater determinants:

$|\Phi_{pq}\rangle = |\{pq\}\rangle$, $|\Phi_{rs}\rangle = |\{rs\}\rangle$, what is $s = \langle\{pq\} | \{rs\}\rangle$?

$$\begin{aligned} s &= \langle\{pq\} | \{rs\}\rangle = \langle 0 | \hat{X}_q \hat{X}_p \hat{X}_r^\dagger \hat{X}_s^\dagger | 0 \rangle \\ &= \langle 0 | \hat{X}_q (\delta_{pr} - \hat{X}_r^\dagger \hat{X}_p) \hat{X}_s^\dagger | 0 \rangle \\ &= \delta_{pr} \langle 0 | \hat{X}_q \hat{X}_s^\dagger | 0 \rangle - \langle 0 | \hat{X}_q \hat{X}_r^\dagger \hat{X}_p \hat{X}_s^\dagger | 0 \rangle \\ &= \delta_{pr} \langle q | s \rangle - \langle 0 | \hat{X}_q \hat{X}_r^\dagger (\delta_{ps} - \hat{X}_s^\dagger \hat{X}_p) | 0 \rangle \\ &= \delta_{pr} \delta_{qs} - \delta_{ps} \langle 0 | \hat{X}_q \hat{X}_r^\dagger | 0 \rangle + \langle 0 | \hat{X}_q \hat{X}_r^\dagger \hat{X}_s^\dagger \hat{X}_p | 0 \rangle \\ &= \delta_{pr} \delta_{qs} - \delta_{ps} \langle q | r \rangle + \langle 0 | \hat{X}_q \hat{X}_r^\dagger \hat{X}_s^\dagger \hat{X}_p | 0 \rangle \\ &= \delta_{pr} \delta_{qs} - \delta_{ps} \delta_{qr}. \end{aligned}$$

Here, the general strategy was to push one of the annihilation operators as far right as possible until it hit the vacuum ket state. Once the annihilation operator acts on the vacuum ket, the state is gone entirely, and the expression simplifies quite a bit to simple Kronecker delta functions which we can more easily deal with. While this is a powerful tool, more efficient tools will be developed later.

2.7 Operators in Second Quantized Form

Let's again take a look at our Hamiltonian with at most three-body operators

$$\hat{H} = \hat{Z} + \hat{V} + \hat{W}, \quad (2.82)$$

where we split it into a 1-body piece

$$\hat{Z} = \sum_{i=1}^A \hat{z}(x_i), \quad (2.83)$$

a two-body piece

$$\hat{V} = \sum_{1 \leq i < j}^A \hat{v}(x_i, x_j), \quad (2.84)$$

and a three-body piece

$$\hat{W} = \sum_{1 \leq i < j < k}^A \hat{w}(x_i, x_j, x_k). \quad (2.85)$$

This is a generic procedure, as any operator can be split into a 0-body piece, 1-body piece, etc.

$$\hat{O} = \sum_{k=0}^A \hat{o}_k, \quad \hat{o}_k = \sum_{1 \leq i_1 < \dots < i_k}^A \hat{o}_k(x_{i_1}, \dots, x_{i_k}). \quad (2.86)$$

The next goal is to develop how these operators act on our many-fermion kets $\hat{O}_k |\{p_1 \dots p_N\}\rangle$. Before we get to generic operators, we need to further develop the second quantized formalism. We are now writing our ket states as strings of operators, and we will use capital pi (II) to represent the product of many of these operators. The new representation is then

$$\prod_{k=1}^A \hat{X}_{p_k}^\dagger |0\rangle \equiv \hat{X}_{p_1}^\dagger \dots \hat{X}_{p_A}^\dagger |0\rangle. \quad (2.87)$$

Acting with an annihilation operator on such a string of operators yields

$$\hat{X}_q \prod_{k=1}^A \hat{X}_{p_k}^\dagger |0\rangle = \sum_{i=1}^A (-1)^{i-1} \delta_{qp_i} \prod_{\substack{k=1 \\ k \neq i}}^A \hat{X}_{p_k}^\dagger |0\rangle. \quad (2.88)$$

To help parse what this chain of symbols means let's break it down. We want to act with an annihilation operator of state q on a ket state, but now our ket state is represented by a chain of creation operators. The result is a sum, where the kronecker delta eliminates any term in the sum that does not correspond to the annihilated state q . Then for each term where $q = p_i$, there is an induced phase $(-1)^{i-1}$ and a new ket with the corresponding missing creation operator.

Now to operators in second quantization. In first quantization, a one-body operator acting on A particles can be written as

$$\hat{O}_1 = \sum_{i=1}^A \hat{o}_1(x_i). \quad (2.89)$$

In second quantization, the one-body operator will look like

$$\hat{O}_1 = \sum_{pq} \langle p|\hat{o}_1|q\rangle \hat{X}_p^\dagger \hat{X}_q, \quad (2.90)$$

where

$$\langle p|\hat{o}_1|q\rangle = \int \psi_p^*(x) \hat{o}_1(x) \psi_q(x) dx, \quad (2.91)$$

where the integral over dx is a symbolic notation, meaning integrate over all 3 spatial dimensions and sum over all internal (spin) degrees of freedom. The two-body operator in first quantization looks like

$$\hat{O}_2 = \sum_{i<j} \hat{o}_2(x_i, x_j). \quad (2.92)$$

And in second quantization the two-body operator looks like

$$\hat{O}_2 = \frac{1}{2} \sum_{pqrs} \langle pq|\hat{o}_2|rs\rangle \hat{X}_p^\dagger \hat{X}_q^\dagger \hat{X}_s \hat{X}_r, \quad (2.93)$$

where

$$\langle pq|\hat{o}_2|rs\rangle = \int \psi_p^*(x_1) \psi_q^*(x_2) \hat{o}_2(x_1, x_2) \psi_r(x_1) \psi_s(x_2) dx_1 dx_2. \quad (2.94)$$

Note the ordering of the annihilation operators. The fact that the indices in the ket are reversed from the indices of the operators is crucial. Also note the sum, we have chosen to sum over the entire range of all of the indices, but due to the symmetries of particle interchange, we do not have to if we do not want to. For a general k -body operator (rank

k), we can write it in second quantization representation in the Goldstone form [32] as

$$\hat{O}_k = \left(\frac{1}{k!}\right) \sum_{\substack{p_1 \dots p_k \\ q_1 \dots q_k}} \langle p_1 \dots p_k | \hat{o}_k | q_1 \dots q_k \rangle \hat{X}_{p_1}^\dagger \dots \hat{X}_{p_k}^\dagger \hat{X}_{q_k} \dots \hat{X}_{q_1}, \quad (2.95)$$

where we notice that we are summing over two times the rank number of indices, and where

$$\langle p_1 \dots p_k | \hat{o}_k | q_1 \dots q_k \rangle = \int \dots \int \psi_{p_1}^*(x_1) \dots \psi_{p_k}^*(x_k) \hat{o}_k(x_1, \dots, x_k) \psi_{q_1}(x_1) \dots \psi_{q_k}(x_k) dx_1 \dots dx_k. \quad (2.96)$$

Alternatively we can write the operator in the Hugenholtz form [33]

$$\hat{O}_k = \left(\frac{1}{k!}\right)^2 \sum_{\substack{p_1 \dots p_k \\ q_1 \dots q_k}} \langle p_1 \dots p_k | \hat{o}_k | q_1 \dots q_k \rangle_{\mathcal{A}} \hat{X}_{p_1}^\dagger \dots \hat{X}_{p_k}^\dagger \hat{X}_{q_k} \dots \hat{X}_{q_1}, \quad (2.97)$$

where we are now using the anti-symmetrized matrix element

$$\langle p_1 \dots p_k | \hat{o}_k | q_1 \dots q_k \rangle_{\mathcal{A}} = \sum_{\hat{R} \in \mathcal{S}_k} (-1)^R \langle p_1 \dots p_k | \hat{o}_k | q_{R_1} \dots q_{R_k} \rangle. \quad (2.98)$$

As an example, let's look at the two-body operator in Hugenholtz form:

$$\hat{O}_2 = \frac{1}{2} \sum_{pqrs} \langle pq | \hat{o}_2 | rs \rangle_{\mathcal{A}} \hat{X}_p^\dagger \hat{X}_q^\dagger \hat{X}_s \hat{X}_r, \quad (2.99)$$

where we have defined the two-body matrix elements as

$$\langle pr | \hat{o}_2 | rs \rangle_{\mathcal{A}} = \langle pq | \hat{o}_2 | rs \rangle - \langle pq | \hat{o}_2 | sr \rangle. \quad (2.100)$$

It is usually the case that writing equations using the antisymmetrized matrix elements is more compact, and so we will be using them frequently.

2.8 Wick's Theorem

The purpose of Wick's theorem [34] is to give us a more concise way of dealing with these huge cumbersome strings of creation and annihilation operators. To deal with the matrix elements of many-body operators, we run into expressions like

$$\begin{aligned} & \langle \Phi_{p_1 \dots p_A} | \hat{O}_k | \Phi_{q_1 \dots q_A} \rangle = \\ & \left(\frac{1}{k!} \right)^2 \sum_{\substack{r_1 \dots r_k \\ s_1 \dots s_k}} \langle r_1 \dots r_k | \hat{O}_k | s_1 \dots s_k \rangle_{\mathcal{A}} \times \\ & \langle 0 | \hat{X}_{p_A} \dots \hat{X}_{p_1} \hat{X}_{r_1}^\dagger \dots \hat{X}_{r_k}^\dagger \hat{X}_{s_k} \dots \hat{X}_{s_1} \hat{X}_{q_1}^\dagger \dots \hat{X}_{q_A}^\dagger | 0 \rangle, \end{aligned}$$

which leads to a very unwieldy chain of operators, especially since our only tool to calculate what this means is by anti-commuting these operators around between each other. Wick's theorem will give us a much more manageable way to deal with such chains of operators. First however, we must develop the tools with which Wick's theorem is expressed. The first thing we do is to become blind to whether an operator is a creation or annihilation operator, and we simply label each of them as a capital \hat{M} . In this new notation, we would write a generic vacuum expectation value of a chain of operators as

$$\langle 0 | \hat{M}_1 \dots \hat{M}_m | 0 \rangle, \quad \hat{M}_i \equiv \hat{X}_{p_i} \text{ or } \hat{X}_{p_i}^\dagger, \quad (2.101)$$

and an operator acting on a Slater determinant would become

$$\hat{O}_k |\Phi_{p_1 \dots p_A}\rangle \rightarrow \hat{M}_1 \dots \hat{M}_m |0\rangle. \quad (2.102)$$

To write down Wick's theorem, we need normal ordered products of operators, contractions of operators, and the normal product with contractions. First, we define normal product n acting on a chain of operators as

$$n[\hat{M}_1 \dots \hat{M}_m] = (-1)^R \hat{X}_{R_1}^\dagger \dots \hat{X}_{R_j}^\dagger \hat{X}_{R_{j+1}} \dots \hat{X}_{R_m}, \quad (2.103)$$

where again, the $(-1)^R$ term is keeping track of if this is an even or odd permutation. The permutation R can be written as

$$R = \begin{pmatrix} 1 & 2 & \dots & j & j+1 & \dots & m \\ R_1 & R_2 & \dots & R_j & R_{j+1} & \dots & R_m \end{pmatrix},$$

where the top row indicates the original ordering of the indices on the left-hand side of the equation, and the second row indicates the final ordering of the indices on the right hand side of the equation. The take away here is that the normal ordering operation on a chain of operators pushes all of the annihilation operators to the right. This is useful, because as we said before, a common strategy in calculations is to push the annihilation operators rightwards so that they annihilate the vacuum state, yielding zeros, which tidy up the algebra. Here are some examples of the normal ordering in action.

Ex:

$$n[\hat{X}_p^\dagger \hat{X}_q \hat{X}_r^\dagger] = -\hat{X}_p^\dagger \hat{X}_r^\dagger \hat{X}_q$$

$$R = \begin{pmatrix} p & q & r \\ p & r & q \end{pmatrix} = (p)(qr) \implies (-1)^R = (+1)(-1) = -1$$

The notation $(p)(qr)$ denotes the *permutation cycles* of the permutation. A permutation cycle is a subset of a permutation whose elements trade places with each other. In the example above, p does not move, so it is a one-cycle, and q and r trade places with each other, so they are a two-cycle. Cycles containing an odd number of elements do not induce a phase, while cycles with an even number induce a phase of (-1) . So to read the equation above, it is saying that the phase of permutation $R = \{p, q, r\} \rightarrow \{p, r, q\}$ is equal to the phase of a one-cycle times the phase of a two-cycle which is (-1) . This is usually the easiest and fastest way to compute the phase of a permutation.

Contraction:

A contraction between two operators tells you how different from a normal ordering they are. A contraction is defined as

$$\hat{M}_1 \hat{M}_2 = \hat{M}_1 \hat{M}_2 - n[\hat{M}_1 \hat{M}_2]. \quad (2.104)$$

Here are the four cases that can arise out of this definition:

(i) $\hat{M}_1 = \hat{X}_p, \hat{M}_2 = \hat{X}_q,$

$$\hat{X}_p \hat{X}_q = \hat{X}_p \hat{X}_q - n[\hat{X}_p \hat{X}_q] = \hat{X}_p \hat{X}_q - \hat{X}_p \hat{X}_q = 0.$$

$$(ii) \hat{M}_1 = \hat{X}_p, \hat{M}_2 = \hat{X}_q^\dagger,$$

$$\hat{X}_p \hat{X}_q^\dagger = \hat{X}_p \hat{X}_q^\dagger - n[\hat{X}_p \hat{X}_q^\dagger] = \hat{X}_p \hat{X}_q + \hat{X}_q^\dagger \hat{X}_p = \delta_{pq}.$$

$$(iii) \hat{M}_1 = \hat{X}_p^\dagger, \hat{M}_2 = \hat{X}_q,$$

$$\hat{X}_p^\dagger \hat{X}_q = \hat{X}_p^\dagger \hat{X}_q - n[\hat{X}_p^\dagger \hat{X}_q] = \hat{X}_p^\dagger \hat{X}_q - \hat{X}_p^\dagger \hat{X}_q = 0.$$

$$(iv) \hat{M}_1 = \hat{X}_p^\dagger, \hat{M}_2 = \hat{X}_q^\dagger,$$

$$\hat{X}_p^\dagger \hat{X}_q^\dagger = \hat{X}_p^\dagger \hat{X}_q^\dagger - n[\hat{X}_p^\dagger \hat{X}_q^\dagger] = \hat{X}_p^\dagger \hat{X}_q^\dagger - \hat{X}_p^\dagger \hat{X}_q^\dagger = 0.$$

Therefore $\hat{M}_1 \hat{M}_2 = 0$ except in the case of $\hat{X}_p \hat{X}_p^\dagger = 1$.

Normal Product with Contractions:

Once two operators are contracted together, they become a simple real number, and thus can be pulled out of the normal product. This can be written as

$$\begin{aligned} & n[\hat{M}_1 \dots \hat{M}_{i_1} \dots \hat{M}_{i_\lambda} \dots \hat{M}_{j_1} \dots \hat{M}_{j_\lambda} \dots \hat{M}_m] \\ &= (-1)^R \hat{M}_{i_1} \hat{M}_{j_1} \dots \hat{M}_{i_\lambda} \hat{M}_{j_\lambda} n[\hat{M}_{k_1} \dots \hat{M}_{k_\mu}] \end{aligned} \quad (2.105)$$

$$R = \begin{pmatrix} 1 & 2 & \dots & (2\lambda - 1) & (2\lambda) & (2\lambda + 1) & \dots & m \\ i_1 & j_1 & \dots & i_\lambda & j_\lambda & k_1 & \dots & k_\mu \end{pmatrix}$$

where $2\lambda + \mu = m$. Here, all of the contracted pairs have been pulled out of the normal product and the phase is kept track in this permutation. When doing these operations, note that $\hat{M}_1 \hat{M}_2 \neq \hat{M}_2 \hat{M}_1$.

Ex: $n[\hat{X}_p \hat{X}_q \hat{X}_r^\dagger] = -\hat{X}_p \hat{X}_r^\dagger n[\hat{X}_q] = -\delta_{pr} \hat{X}_q$

$$R = \begin{pmatrix} p & q & r \\ p & r & q \end{pmatrix} = (p)(qr) \implies (-1)^R = (+1)(-1) = (-1) = -1.$$

Without proof, we will now state some useful properties of contractions and normal ordered operators.

1. $n[\hat{M}_1 \dots \hat{M}_m] |0\rangle = 0$, unless all of the \hat{M} 's are creation operators.
2. $\langle 0|n[\hat{M}_1 \dots \hat{M}_m]|0\rangle = 0$, unless $m = 0$.
3. $n[\hat{M}_1 \dots \hat{M}_{\underbrace{i_1 \dots j_1}}] |0\rangle = 0$, If at least one uncontracted operator \hat{M} is an annihilator.
4. $\langle 0|n[\hat{M}_1 \dots \hat{M}_{\underbrace{i_1 \dots j_1}} \dots \hat{M}_{\underbrace{i_\lambda \dots j_\lambda}} \dots \hat{M}_m]|0\rangle = 0$, unless all operators are contracted.

We now finally write down the definition of Wick's theorem on an arbitrary chain of creation and annihilation operators.

$$\begin{aligned} \hat{M}_1 \dots \hat{M}_m &= n[\hat{M}_1 \dots \hat{M}_m] + \sum_{1 \leq i_1 < j_1 \leq m} n[\hat{M}_1 \dots \hat{M}_{\underbrace{i_1 \dots j_1}} \dots \hat{M}_m] \\ &\quad + \sum_{\substack{1 \leq i_1 < j_1 \leq m \\ 1 \leq i_2 < j_2 \leq m \\ i_1 < i_2, j_1 \neq j_2}} n[\hat{M}_1 \dots \hat{M}_{\underbrace{i_1 \dots j_1}} \dots \hat{M}_{\underbrace{i_2 \dots j_2}} \dots \hat{M}_m] \\ &\quad + \text{sum of all possible 3 contractions} \\ &\quad + \dots \\ &\quad + \text{sum of all possible } N \text{ contractions,} \end{aligned}$$

where N is the maximum number of contractions possible. For an even number of operators, this means they are all contracted, but for an odd number of operators, all but one will be contracted. In words, Wick's theorem is the statement that an arbitrary chain of creation and annihilation operators can be written entirely as the normal product of that chain of operators and the normal product of all possible ways to contract that chain of operators.

2.9 Generalized Wick's Theorem

Wick's theorem is a very powerful tool now at our disposal. However, we would like to be able to tackle objects like $\hat{M}_1 n[\hat{M}_2 \hat{M}_3]$ or $n[\hat{M}_1 \hat{M}_2] n[\hat{M}_3 \hat{M}_4]$. The generalized Wick's theorem accounts for the partially normal product cases for us and is stated as

$$\begin{aligned} & \hat{M}_1 \dots \hat{M}_{k_{\mu-1}} n[\hat{M}_{k_{\mu-1}+1} \dots \hat{M}_{k_{\mu}}] \hat{M}_{k_{\mu}+1} \dots \hat{M}_m \\ &= n[\hat{M}_1 \dots \hat{M}_{k_{\mu-1}} \hat{X}_{p_1}^\dagger \dots \hat{X}_{p_\alpha}^\dagger \hat{X}_{p_{\alpha+1}} \dots \hat{X}_{p_\beta} \hat{M}_{k_{\mu}+1} \dots \hat{M}_m] \\ &+ \sum_{\text{modified}} n[\hat{M}_1 \dots \hat{M}_{k_{\mu-1}} \hat{X}_{p_1}^\dagger \dots \hat{X}_{p_\alpha}^\dagger \hat{X}_{p_{\alpha+1}} \dots \hat{X}_{p_\beta} \hat{M}_{k_{\mu}+1} \dots \hat{M}_m], \end{aligned}$$

where this modified sum excludes contraction terms from the original n product. The purpose of these rules is to speed up tedious pen and paper manipulations.

2.10 Slater-Condon Rules

The Slater-Condon rules [29, 9] give simplified expressions for manipulations of the Hamiltonian in second quantization. To see how they arise let's look at how the Hamiltonian acts on these many-body kets. For this section, we will restrict our Hamiltonian to a one-body

piece and a two-body piece

$$\hat{H} |\Psi\rangle = E |\Psi\rangle, \quad (2.106)$$

$$\hat{H} = \hat{Z} + \hat{V}, \quad (2.107)$$

and we write the solution to the Schrödinger equation as a linear combination of our complete and orthonormal antisymmetrized A body states

$$|\Psi\rangle = \sum C_{p_1 \dots p_A} |\Phi_{p_1 \dots p_A}\rangle. \quad (2.108)$$

In this basis, we can write the Schrödinger equation as a matrix eigenvalue problem, since $|\Psi\rangle$ can be written as the vector of $C_{p_1 \dots p_A}$ coefficients, and the Hamiltonian can be written as a matrix with matrix elements

$$H_{ij} = \langle \Phi_i | \hat{H} | \Phi_j \rangle = \langle \Phi_i | \hat{Z} + \hat{V} | \Phi_j \rangle. \quad (2.109)$$

The Slater rules are rules about the Hamiltonian matrix elements. First, let's look at the matrix elements of the one-body operator

$$\begin{aligned}
& \langle \{p_1 \dots p_A\} | Z | \{q_1 \dots q_A\} \rangle \\
&= \sum_{r,s} \langle 0 | \hat{X}_{p_A} \dots \hat{X}_{p_1} \hat{X}_r^\dagger \hat{X}_s \hat{X}_{q_1}^\dagger \dots \hat{X}_{q_A}^\dagger | 0 \rangle \langle r | \hat{z} | s \rangle \\
&= \sum_{r,s} \langle r | \hat{z} | s \rangle \sum_{F.C.} \langle 0 | \hat{X}_{p_A} \dots \hat{X}_{p_1} \hat{X}_r^\dagger \hat{X}_s \hat{X}_{q_1}^\dagger \dots \hat{X}_{q_A}^\dagger | 0 \rangle \\
&= \sum_{r,s} \langle r | \hat{z} | s \rangle \sum_{F.C.} \langle 0 | n[\hat{X}_{p_A} \dots \hat{X}_{p_1}] n[\hat{X}_r^\dagger \hat{X}_s] n[\hat{X}_{q_1}^\dagger \dots \hat{X}_{q_A}^\dagger] | 0 \rangle.
\end{aligned}$$

Remember that only contractions of the form $\hat{X} \hat{X}^\dagger$ are non-zero. Also remember that the generalized Wick's theorem means we get rid of contraction terms between normal products. This means that \hat{X}_r^\dagger *must* contract with an annihilation operator to its left, and that \hat{X}_s *must* contract with a creation operator to its right. The fully contracted sum must obey these rules, and we get

$$\begin{aligned}
& \sum_{r,s} \langle r | \hat{z} | s \rangle \sum_{F.C.} \langle 0 | n[\hat{X}_{p_A} \dots \hat{X}_{p_1}] n[\hat{X}_r^\dagger \hat{X}_s] n[\hat{X}_{q_1}^\dagger \dots \hat{X}_{q_A}^\dagger] | 0 \rangle \\
&= \sum_{r,s} \langle r | \hat{z} | s \rangle \sum_{F.C.} \langle 0 | \hat{X}_{p_A} \dots \hat{X}_{p_i} \dots \hat{X}_{p_1} \hat{X}_r^\dagger \hat{X}_s \hat{X}_{q_1}^\dagger \dots \hat{X}_{q_j}^\dagger \dots \hat{X}_{q_A}^\dagger | 0 \rangle,
\end{aligned}$$

where the r and s terms are clearly contracted. Note that for \hat{X}_{p_k} , where $k \neq i$, it must be contracted fully with $\hat{X}_{q_l}^\dagger$ where $l \neq j$. This means that these p_k indices must be permutations of the q_l indices. This gives rise to our first Slater rule.

One-body Slater rules: $\langle \{p_1 \dots p_A\} | \hat{Z} | \{q_1 \dots q_A\} \rangle \neq 0$ when:

- (1) $\{p_k\}_{k=1}^A$ and $\{q_l\}_{l=1}^A$ differ by one spin-orbital

(2) $\{p_k\}_{k=1}^A$ and $\{q_l\}_{l=1}^A$ do not differ. (May differ by permutation)

These two non-zero cases lead to different expressions for the one-body matrix elements.

$$p_1 \neq q_1, p_2 = q_2, \dots, p_n = q_n.$$

$$\begin{aligned} & \langle \{p_1 \dots p_A\} | \hat{Z} | \{q_1 \dots q_A\} \rangle \\ &= \sum_{r,s} \langle r | \hat{z} | s \rangle \langle 0 | \underbrace{\hat{X}_{p_A} \dots \hat{X}_{p_2} \hat{X}_{p_1} \hat{X}_r^\dagger \hat{X}_s \hat{X}_{q_1}^\dagger \hat{X}_{q_2}^\dagger \dots \hat{X}_{q_A}^\dagger}_{\text{}} | 0 \rangle \\ &= \sum_{r,s} \langle r | \hat{z} | s \rangle \delta_{rp_1} \delta_{sq_1} \\ &= \langle p_1 | \hat{z} | q_1 \rangle, \end{aligned}$$

where we see the expression for when one basis state differs, is simply the one-body matrix element between these two states. Now we have the case where the two sets of basis states are the same up to a permutation. Without loss of generality, we write this as, $p_1 = q_1, \dots, p_A = q_A$,

$$\begin{aligned} & \langle \{p_1 \dots p_A\} | \hat{Z} | \{p_1 \dots p_A\} \rangle \\ &= \sum_{r,s} \langle r | \hat{z} | s \rangle \sum_{F.C.} \langle 0 | \hat{X}_{p_A} \dots \hat{X}_{p_i} \dots \hat{X}_{p_1} \hat{X}_r^\dagger \hat{X}_s \hat{X}_{p_1}^\dagger \dots \hat{X}_{p_j}^\dagger \dots \hat{X}_{p_A}^\dagger | 0 \rangle. \end{aligned}$$

Notice here that if $p_i \neq p_j$, then there will be a mismatch somewhere with the other contractions. For the next case, we have $p_i = p_j$,

$$\begin{aligned}
& \langle \{p_1 \dots p_A\} | \hat{Z} | \{p_1 \dots p_A\} \rangle \\
&= \sum_{r,s} \langle r | \hat{z} | s \rangle \sum_{i=1}^A \overbrace{\langle 0 | \hat{X}_{p_A} \dots \hat{X}_{p_i} \dots \hat{X}_{p_1} \hat{X}_r^\dagger \hat{X}_s \hat{X}_{p_1}^\dagger \dots \hat{X}_{p_i}^\dagger \dots \hat{X}_{p_A}^\dagger | 0 \rangle}^{\text{Even number of crossings}} \\
&= \sum_{r,s} \sum_{i=1}^A \langle r | \hat{z} | s \rangle \delta_{rp_i} \delta_{sp_i} \\
&= \sum_{i=1}^A \langle p_i | \hat{z} | p_i \rangle,
\end{aligned}$$

where here we sum over all of the single-particle states in the many-body state. In other words, the expectation value of the one-body operator of a many-body state is the sum of single-particle expectation values of the states in the many-body state.

Two-Body Slater Rules:

We want to understand when $\langle \{p_1 \dots p_A\} | \hat{V} | \{q_1 \dots q_A\} \rangle \neq 0$. Writing this out further we obtain

$$\begin{aligned}
& \langle \{p_1 \dots p_A\} | \hat{V} | \{q_1 \dots q_A\} \rangle \\
&= \frac{1}{2} \sum_{rstu} \langle rs | \hat{v} | tu \rangle \langle 0 | \hat{X}_{p_A} \dots \hat{X}_{p_1} \hat{X}_r^\dagger \hat{X}_s^\dagger \hat{X}_u \hat{X}_t \hat{X}_{q_1}^\dagger \dots \hat{X}_{q_A}^\dagger | 0 \rangle.
\end{aligned}$$

Now we play a similar game as we did with the one-body operator. Due to the partial normal-ordering of the $rsut$ operators, the rs creation operators must contract to the left to some p_i, p_j annihilation operators, and the ut annihilation operators must contract to the right

against some q_k, q_l creation operators. After those four have been contracted, the remaining \hat{X}_{p_m} and $\hat{X}_{q_n}^\dagger$ must be contracted, where $m \neq i, j$ and $n \neq k, l$. Thus, these operators cannot differ, and they must be permutations of each other at most. That is, $\{p_m\}_{m \neq i, j}, \{q_n\}_{n \neq k, l}$ must represent permutations. This means that we get $\langle \{p_1 \dots p_A\} | \hat{V} | \{q_1 \dots q_A\} \rangle = 0$ if $\{p_m\}$ and $\{q_n\}$ differ by more than two single-particle basis states. There are three cases where we do not get zero, which will not be proven here. These are (1) $p_1 \neq q_1, p_2 \neq q_2$, with all other $p_m = q_m$ identical,

$$\langle \{p_1 p_2 p_3 \dots p_A\} | \hat{V} | \{q_1 q_2 p_3 \dots p_A\} \rangle = \langle p_1 p_2 | \hat{v} | q_1 q_2 \rangle_{\mathcal{A}}.$$

(2) $p_1 \neq q_1, p_2 = q_2 \dots p_A = q_A$,

$$\langle \{p_1 p_2 \dots p_A\} | \hat{V} | \{q_1 p_2 \dots p_A\} \rangle = \sum_{k=1}^A \langle p_1 p_k | \hat{v} | q_1 p_k \rangle_{\mathcal{A}},$$

where here, starting the sum from $k = 1$ is equally valid, as this corresponds to adding in a zero term in the form of the Pauli exclusion breaking term $\langle p_1 p_1 | \hat{v} | q_1 p_1 \rangle_{\mathcal{A}} = 0$. Finally the last case is (3) $p_1 = q_1, p_2 = q_2 \dots p_A = q_A$

$$\langle \{p_1 \dots p_A\} | \hat{V} | \{p_1 \dots p_A\} \rangle = \frac{1}{2} \sum_{k,l=1}^A \langle p_k p_l | \hat{v} | p_k p_l \rangle_{\mathcal{A}}.$$

It is with expressions like this that the power of second quantization really shines, since we have turned matrix elements in the full many-body basis into simple sums of matrix elements in the one or two-body basis. This is an enormous simplification, and helps with calculations immensely.

2.11 The Fermi Vacuum

As a reminder, once we have settled on our single-particle basis, we can expand any many-fermion ket in terms of our anti-symmetrized Slater determinants,

$$|\Psi\rangle = \sum_{q_1 < \dots < q_A} c_{q_1 \dots q_A} |\{q_1 \dots q_A\}\rangle,$$

for some set of constants $c_{q_1 \dots q_A}$. This sum is organized pretty arbitrarily, with no stress put on what the first item in this sum is. However, depending on the physics of the situation, we can select out a many-body state we determine as important, and organize around how close we are to this “reference state”. We will denote the reference state as $|\Phi\rangle$. For now, let’s say that single-particle states labeled with p ’s are occupied in $|\Phi\rangle$ and states labeled with q ’s are unoccupied,

$$|\Phi\rangle = \hat{X}_{p_1}^\dagger \dots \hat{X}_{p_N}^\dagger |0\rangle = |\{p_1 \dots p_N\}\rangle.$$

We can now write any other N -fermion ket relative to our reference state. For example, a state that differs by one single-particle state from our reference state can be written as

$$\begin{aligned} |\{p_1 \dots p_{\mu-1} q_\mu p_{\mu+1} \dots p_N\}\rangle &= \hat{X}_{q_\mu}^\dagger \hat{X}_{p_\mu} |\{p_1 \dots p_{\mu-1} p_\mu p_{\mu+1} \dots p_N\}\rangle \\ &= \hat{X}_{q_\mu}^\dagger \hat{X}_{p_\mu} |\Phi\rangle, \end{aligned}$$

where now we are only dealing with 2 operators. Or in the case that we want to examine a state that differs by 2 single-particle states

$$\begin{aligned}
& |\{p_1 \dots p_{\mu-1} q_{\mu} p_{\mu+1} \dots p_{\nu-1} q_{\nu} p_{\nu+1} \dots p_N\}\rangle \\
&= \hat{X}_{q_{\mu}}^{\dagger} \hat{X}_{p_{\mu}} \hat{X}_{q_{\nu}}^{\dagger} \hat{X}_{p_{\nu}} |\{p_1 \dots p_{\mu-1} p_{\mu} p_{\mu+1} \dots p_{\nu-1} p_{\nu} p_{\nu+1} \dots p_N\}\rangle \\
&= \hat{X}_{q_{\mu}}^{\dagger} \hat{X}_{p_{\mu}} \hat{X}_{q_{\nu}}^{\dagger} \hat{X}_{p_{\nu}} |\Phi\rangle,
\end{aligned}$$

where we now only have 4 operators. This is a huge simplification from having to deal with the full N creation operators that we would typically have! This pattern continues; every single-particle state different from our reference state that differs costs us one creation and one annihilation operator.

Notation:

We are now going to change our notation a bit. We assign single-particle labels to have a specific meaning in Table 2.1. Note that this notation only makes sense with respect to a

Table 2.1: Single-Particle Index Conventions

$i, j, k, \dots (i_1, i_2, \dots)$	\implies	s.p. state occupied in $ \Phi\rangle$
$a, b, c, \dots (a_1, a_2, \dots)$	\implies	s.p. state unoccupied in $ \Phi\rangle$
$p, q, r, \dots (p_1, p_2, \dots)$	\implies	s.p. state is a generic state $ \Phi\rangle$

particular reference state. We will also define a compressed notation for states that differ from the reference state as

$$\hat{X}_a^{\dagger} \hat{X}_i |\Phi\rangle = |\Phi_i^a\rangle, \tag{2.110}$$

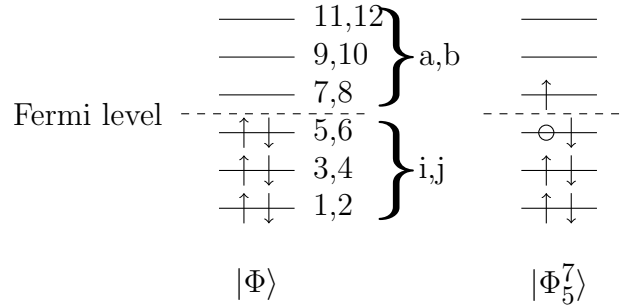
which indicates a one-particles one-hole excitation

$$\hat{X}_a^\dagger \hat{X}_i \hat{X}_b^\dagger \hat{X}_j |\Phi\rangle = |\Phi_{ij}^{ab}\rangle = \hat{X}_a^\dagger \hat{X}_b^\dagger \hat{X}_j \hat{X}_i |\Phi\rangle, \quad (2.111)$$

which indicates a two-particle two-hole excitation, and

$$|\Phi_{i_1 \dots i_n}^{a_1 \dots a_n}\rangle = \hat{X}_{a_1}^\dagger \hat{X}_{i_1} \dots \hat{X}_{a_n}^\dagger \hat{X}_{i_n} |\Phi\rangle = \prod_{\mu=1}^n \hat{X}_{a_\mu}^\dagger \hat{X}_{i_\mu} |\Phi\rangle, \quad (2.112)$$

which indicates an n -particle n -hole excitation. In each of these cases, an occupied index is being annihilated, and replaced by an unoccupied index. Let's look at an example with $N = 6$ spin-1/2 fermion in a basis with 12 spin-orbitals. The Fermi level is defined as the energy where the six particles are occupying the six lowest spin-orbitals.



In this graphic, we have a cartoon of two different many-body states. We have defined the reference state $|\Phi\rangle = |\{123456\}\rangle$ to be filling all of the lowest spin-orbitals up to the Fermi level. This is a very common choice for the reference state. To the right we have $|\Phi_5^7\rangle = \hat{X}_7^\dagger \hat{X}_5 |\Phi\rangle$, which has had one particle under the Fermi level with another particle that is above the Fermi level.

With the definition of a Fermi level we define our ansatz for the ground state, represented by a Slater determinant Φ_0 . Switching notation a bit, the annihilation operator will now be represented as a , where this is a more common symbol in nuclear physics, and we drop the

hat and from context determine that it is an operator. We can rewrite the ansatz for the ground state as

$$|\Phi_0\rangle = \prod_{i \leq F} a_i^\dagger |0\rangle, \quad (2.113)$$

where we have introduced the shorthand labels for states below the Fermi level F as $i, j, \dots \leq F$. For single-particle states above the Fermi level we reserve the labels $a, b, \dots > F$, while the labels p, q, \dots represent any possible single-particle state.

The focus of the work is on infinite systems, where the one-body part of the Hamiltonian is given by the kinetic energy operator only. In second quantization it is defined as

$$\hat{H}_0 = \hat{T} = \sum_{pq} \langle p | \hat{t} | q \rangle a_p^\dagger a_q, \quad (2.114)$$

where the matrix elements $\langle p | \hat{t} | q \rangle$ represent the expectation value of the kinetic energy operator (see the discussion below as well). The two-body interaction reads

$$\hat{H}_I = \hat{V} = \frac{1}{4} \sum_{pqrs} \langle pq | \hat{v} | rs \rangle_{AS} a_p^\dagger a_q^\dagger a_s a_r, \quad (2.115)$$

where we have defined the anti-symmetrized matrix elements

$$\langle pq | \hat{v} | rs \rangle_{AS} = \langle pq | \hat{v} | rs \rangle - \langle pq | \hat{v} | sr \rangle. \quad (2.116)$$

We can also define a three-body operator

$$\hat{W} = \frac{1}{36} \sum_{pqrst} \langle pqr | \hat{w} | stu \rangle_{AS} a_p^\dagger a_q^\dagger a_r^\dagger a_u a_t a_s, \quad (2.117)$$

with the anti-symmetrized matrix element

$$\begin{aligned} \langle pqr|\hat{w}|stu\rangle_{AS} &= \langle pqr|\hat{w}|stu\rangle + \langle pqr|\hat{w}|tus\rangle + \langle pqr|\hat{w}|ust\rangle \\ &\quad - \langle pqr|\hat{w}|sut\rangle - \langle pqr|\hat{w}|tsu\rangle - \langle pqr|\hat{w}|uts\rangle. \end{aligned}$$

In this and the forthcoming chapters we will limit ourselves to two-body interactions at most. Throughout this chapter and the subsequent three we will drop the subscript AS and use only anti-symmetrized matrix elements.

Using the ansatz for the ground state $|\Phi_0\rangle$ as new reference vacuum state, we need to redefine the anticommutation relations to

$$\{a_p^\dagger, a_q\} = \delta_{pq}, \quad p, q \leq F, \quad (2.118)$$

and

$$\{a_p, a_q^\dagger\} = \delta_{pq}, \quad p, q > F. \quad (2.119)$$

It is easy to see that

$$a_i|\Phi_0\rangle = |\Phi_i\rangle \neq 0, \quad a_a^\dagger|\Phi_0\rangle = |\Phi^a\rangle \neq 0, \quad (2.120)$$

and

$$a_i^\dagger|\Phi_0\rangle = 0 \quad a_a|\Phi_0\rangle = 0. \quad (2.121)$$

With the new reference vacuum state the Hamiltonian can be rewritten as,

$$\hat{H} = E_{\text{Ref}} + \hat{H}_N, \quad (2.122)$$

with the reference energy defined as the expectation value of the Hamiltonian using the reference state Φ_0

$$E_{\text{Ref}} = \langle \Phi_0 | \hat{H} | \Phi_0 \rangle = \sum_{i \leq F} \langle i | \hat{h}_0 | i \rangle + \frac{1}{2} \sum_{ij \leq F} \langle ij | \hat{v} | ij \rangle, \quad (2.123)$$

and the new normal-ordered Hamiltonian (all creation operators to the left of the annihilation operators) is defined as

$$\hat{H}_N = \sum_{pq} \langle p | \hat{h}_0 | q \rangle \{ a_p^\dagger a_q \} + \frac{1}{4} \sum_{pqrs} \langle pq | \hat{v} | rs \rangle \{ a_p^\dagger a_q^\dagger a_s a_r \} + \sum_{pq, i \leq F} \langle pi | \hat{v} | qi \rangle \{ a_p^\dagger a_q \}, \quad (2.124)$$

where the curly brackets represent normal-ordering with respect to the new reference vacuum state. The normal-ordered Hamiltonian can be rewritten in terms of a new one-body operator and a two-body operator as

$$\hat{H}_N = \hat{F}_N + \hat{V}_N, \quad (2.125)$$

with

$$\hat{F}_N = \sum_{pq} \langle p | \hat{f} | q \rangle \{ a_p^\dagger a_q \}, \quad (2.126)$$

where

$$\langle p | \hat{f} | q \rangle = \langle p | \hat{h}_0 | q \rangle + \sum_{i \leq F} \langle pi | \hat{v} | qi \rangle. \quad (2.127)$$

The last term on the right hand side represents a medium modification to the single-particle Hamiltonian due to the two-body interaction. Finally, the two-body interaction is given by

$$\hat{V}_N = \frac{1}{4} \sum_{pqrs} \langle pq | \hat{v} | rs \rangle \{ a_p^\dagger a_q^\dagger a_s a_r \}.$$

2.12 Configuration Interaction

With this in place, let's look again at the many-body Schrödinger equation.

$$\hat{H} |\Psi\rangle = E |\Psi\rangle \quad (2.128)$$

and we expand the solution to the Schrödinger equation in the basis of our complete and orthonormal antisymmetrized Slater determinants

$$|\Psi\rangle = \sum_{i \in \text{all SD's}} C_i |\Phi_i\rangle, \quad (2.129)$$

$$\hat{H} \sum_i C_i |\Phi_i\rangle = E \sum_i C_i |\Phi_i\rangle. \quad (2.130)$$

As stated in the Slater rules section, we can project Eqn. (2.128) onto $\langle \Phi_j |$, yielding

$$\langle \Phi_j | \hat{H} \sum_i C_i |\Phi_i\rangle = \langle \Phi_j | E \sum_i C_i |\Phi_i\rangle, \quad (2.131)$$

$$\sum_i H_{ij} C_i = E C_j, \quad (2.132)$$

which is exactly the index notation for $\overleftrightarrow{H} \vec{C} = E \vec{C}$, which is the classic statement of the eigenvalue problem in linear algebra, where the Hamiltonian can be written as a matrix with matrix elements

$$H_{ij} = \langle \Phi_i | \hat{H} | \Phi_j \rangle.$$

To begin solving this equation, first a single-particle basis truncation must be made. Since the many-body basis is built up from a single-particle basis, this ensures there are a finite

number of Slater determinants, and thus a finite number of matrix elements. Once this matrix is finite, the eigenvalues and eigenvectors can be found by diagonalizing this matrix, giving the exact solution within this truncated space. Recomputing this solution for larger and larger single-particle basis set cutoffs will create a series of solutions that can hopefully generate a smooth curve and an infinite basis limit can be extrapolated to. Thus the many-body problem is solved.

Well, not quite. Since the size of the Hamiltonian matrix is $N \times N$ where N is the number of Slater determinants, and since the Slater determinants are generated by creating all permutations in the symmetry group \mathcal{S}_n for n single-particle states which grows factorially, this matrix gets very large, very fast. So computing these matrix diagonalizations with even the largest modern supercomputers quickly becomes impossible even for systems on the order of 10 particles. This means that further approximations are necessary to compute properties of larger quantum systems. Along with the truncation to the single-particle basis, we can truncate the basis of Slater determinants. While it is valid to take the list of Slater determinants and throw a large fraction away so that the Hamiltonian matrix is smaller, not all truncations are equal. This is where the machinery developed in the Fermi level formalism section comes into use. In most many-body problems, not all configurations of particles and states are equally important. For example, the probability of finding all A particles in the A highest lying states in your basis is usually vanishingly small. So the scheme developed in terms of particle and hole configurations with respect to some reference state keep the “important” states at the front of our attention. Then, if truncations need to be made, we can hopefully truncate Slater determinants which do not have much overlap with the ground state. This of course assumes that an “important” reference state can indeed be picked out, and this procedure will be expanded on further in the Hartree-Fock section.

So the complete expansion of a many body state as in Eqn. (2.129) can be rewritten as

$$|\Psi^{FCI}\rangle = C_0 |\Phi_0\rangle + \sum_{i,a} C_i^a |\Phi_i^a\rangle + \sum_{i,j,a,b} C_{ij}^{ab} |\Phi_{ij}^{ab}\rangle + \dots + \sum_{\substack{i_1,i_2,\dots,i_A \\ a_1,a_2,\dots,a_A}} C_{i_1 i_2 \dots i_A}^{a_1 a_2 \dots a_A} |\Phi_{i_1 i_2 \dots i_A}^{a_1 a_2 \dots a_A}\rangle, \quad (2.133)$$

where *FCI* stands for full configuration interaction, meaning that the full spaces of interacting configurations is being used in this expansion. This is a complete A -body basis, just reorganizing the Slater determinants in terms of how many excitations away from the reference state they are. The first approximation is a finite cutoff for the infinite single-particle basis. Once the single-particle basis has been truncated, the above expression gives the exact answer in this subspace, as FCI includes all Slater determinants up to A -body excitations, at which point the series naturally truncates. The next natural approximation, is to not include every Slater determinant. For example, if only singles and doubles excitations are included, then we get the configuration interaction singles doubles (CISD) approximation, which looks like:

$$|\Psi^{CISD}\rangle = C_0 |\Phi_0\rangle + \sum_{i,a} C_i^a |\Phi_i^a\rangle + \sum_{i,j,a,b} C_{ij}^{ab} |\Phi_{ij}^{ab}\rangle. \quad (2.134)$$

While this is a conceptually nice place to truncate the series, it turns to be a pretty poor way to include correlations into the target many-body state for a given computational cost. The various ways to optimize these truncated many-body correlations is a widely studied topic in its own right. Unfortunately, there is no one *many-body method to rule them all*, as each approximation has its own strengths and weaknesses. This spans from FCI which includes every many-body correlation, down to Hartree-Fock which includes only a single

Slater determinant.

2.13 Hartree-Fock Theory

Hartree-Fock (HF) theory [35, 36], is an algorithm for finding an approximative expression for the ground state of a given Hamiltonian. The basic ingredients contain a single-particle basis $\{\psi_\alpha\}$ defined by the solution of the following eigenvalue problem

$$\hat{h}^{\text{HF}}\psi_\alpha = \varepsilon_\alpha\psi_\alpha, \quad (2.135)$$

with the Hartree-Fock Hamiltonian defined as

$$\hat{h}^{\text{HF}} = \hat{t} + \hat{u}_{\text{ext}} + \hat{u}^{\text{HF}}. \quad (2.136)$$

The term \hat{u}^{HF} is a single-particle potential to be determined by the HF algorithm. The HF algorithm means to select \hat{u}^{HF} in order to have

$$\langle \hat{H} \rangle = E^{\text{HF}} = \langle \Phi_0^{\text{HF}} | \hat{H} | \Phi_0^{\text{HF}} \rangle, \quad (2.137)$$

as a local minimum with a Slater determinant Φ_0^{HF} being the ansatz for the ground state. The variational principle ensures that $E^{\text{HF}} \geq E_0$, with E_0 representing the exact ground state energy.

We will show that the Hartree-Fock Hamiltonian \hat{h}^{HF} equals our definition of the operator \hat{f} discussed in connection with the new definition of the normal-ordered Hamiltonian, that

is we have, for a specific matrix element

$$\langle p|\hat{h}^{\text{HF}}|q\rangle = \langle p|\hat{f}|q\rangle = \langle p|\hat{t} + \hat{u}_{\text{ext}}|q\rangle + \sum_{i \leq F} \langle pi|\hat{V}|qi\rangle, \quad (2.138)$$

meaning that

$$\langle p|\hat{u}^{\text{HF}}|q\rangle = \sum_{i \leq F} \langle pi|\hat{V}|qi\rangle. \quad (2.139)$$

The so-called Hartree-Fock potential \hat{u}^{HF} adds an explicit medium dependence due to the summation over all single-particle states below the Fermi level F . It brings also in an explicit dependence on the two-body interaction (in nuclear physics we can also have complicated three- or higher-body forces). The two-body interaction, with its contribution from the other bystander fermions, creates an effective mean field in which a given fermion moves, in addition to the external potential \hat{u}_{ext} which confines the motion of the fermion. For systems like nuclei or infinite nuclear matter, there is no external confining potential. Nuclei and nuclear matter are examples of self-bound systems, where the binding arises due to the intrinsic nature of the strong force. For nuclear systems thus, there would be no external one-body potential in the Hartree-Fock Hamiltonian.

Another possibility is to expand the single-particle functions in a known basis and vary the coefficients, that is, the new single-particle wave function is written as a linear expansion in terms of a fixed chosen orthogonal basis (for example the well-known harmonic oscillator functions or the hydrogen-like functions, etc). We define our new Hartree-Fock single-particle basis by performing a unitary transformation on our previous basis (labelled with Greek indices) as

$$\psi_p^{\text{HF}} = \sum_{\lambda} C_{p\lambda} \phi_{\lambda}. \quad (2.140)$$

In this case we vary the coefficients $C_{p\lambda}$. If the basis has infinitely many terms, we need to truncate the above sum. We assume that the basis ϕ_λ is orthogonal. A unitary transformation keeps the orthogonality, which is desired.

It is normal to choose a single-particle basis defined as the eigenfunctions of parts of the full Hamiltonian. The typical situation consists of the solutions of the one-body part of the Hamiltonian, that is we have

$$\hat{h}_0\phi_\lambda = \epsilon_\lambda\phi_\lambda. \quad (2.141)$$

For infinite nuclear matter, \hat{h}_0 is given by the kinetic energy operator and the states are given by plane wave functions. Due to the translational invariance of the two-body interaction, the Hartree-Fock single-particle eigenstates are also given by the same functions. Thus, for infinite matter it is only the single-particle energies that change when we solve the Hartree-Fock equations.

The single-particle wave functions $\phi_\lambda(\mathbf{r})$, defined by the quantum numbers λ and \mathbf{r} are defined as the overlap

$$\phi_\lambda(\mathbf{r}) = \langle \mathbf{r} | \lambda \rangle. \quad (2.142)$$

In our discussions we will use our definitions of single-particle states above and below the Fermi (F).

We use Greek letters to refer to our original single-particle basis. The expectation value for the energy with the ansatz Φ_0 for the ground state reads

$$E[\Phi_0] = \sum_{\mu \leq F} \langle \mu | h | \mu \rangle + \frac{1}{2} \sum_{\mu, \nu \leq F} \langle \mu\nu | \hat{v} | \mu\nu \rangle. \quad (2.143)$$

Now we are interested in defining a new basis defined in terms of a chosen basis as defined

in Eq. (2.140). We define the energy functional as

$$E[\Phi^{HF}] = \sum_{i \leq F} \langle i|h|i \rangle + \frac{1}{2} \sum_{ij \leq F} \langle ij|\hat{v}|ij \rangle, \quad (2.144)$$

where Φ^{HF} is the new Slater determinant defined by the new basis of Eq. (2.140).

Using Eq. (2.140) we can rewrite Eq. (2.144) as

$$E[\Psi] = \sum_{i \leq F} \sum_{\alpha\beta} C_{i\alpha}^* C_{i\beta} \langle \alpha|h|\beta \rangle + \frac{1}{2} \sum_{ij \leq F} \sum_{\alpha\beta\gamma\delta} C_{i\alpha}^* C_{j\beta}^* C_{i\gamma} C_{j\delta} \langle \alpha\beta|\hat{v}|\gamma\delta \rangle. \quad (2.145)$$

In order to find the variational minimum of the above functional, we introduce a set of Lagrange multipliers, noting that since $\langle i|j \rangle = \delta_{i,j}$ and $\langle \alpha|\beta \rangle = \delta_{\alpha,\beta}$, the coefficients $C_{i\gamma}$ obey the relation

$$\langle i|j \rangle = \delta_{i,j} = \sum_{\alpha\beta} C_{i\alpha}^* C_{i\beta} \langle \alpha|\beta \rangle = \sum_{\alpha} C_{i\alpha}^* C_{i\alpha}, \quad (2.146)$$

which allows us to define a functional to be minimized that reads

$$F[\Phi^{HF}] = E[\Phi^{HF}] - \sum_{i \leq F} \epsilon_i \sum_{\alpha} C_{i\alpha}^* C_{i\alpha}. \quad (2.147)$$

Minimizing with respect to $C_{i\alpha}^*$ (the equations for $C_{i\alpha}^*$ and $C_{i\alpha}$ can be written as two independent equations) we obtain

$$\frac{d}{dC_{i\alpha}^*} \left[E[\Phi^{HF}] - \sum_j \epsilon_j \sum_{\alpha} C_{j\alpha}^* C_{j\alpha} \right] = 0, \quad (2.148)$$

which yields for every single-particle state i and index α (recalling that the coefficients $C_{i\alpha}$ are matrix elements of a unitary matrix, or orthogonal for a real symmetric matrix) the

following Hartree-Fock equations

$$\sum_{\beta} C_{i\beta} \langle \alpha | h | \beta \rangle + \sum_{j \leq F} \sum_{\beta \gamma \delta} C_{j\beta}^* C_{j\delta} C_{i\gamma} \langle \alpha \beta | \hat{v} | \gamma \delta \rangle = \epsilon_i^{HF} C_{i\alpha}. \quad (2.149)$$

We can rewrite this equation as (changing dummy variables)

$$\sum_{\beta} \left\{ \langle \alpha | h | \beta \rangle + \sum_{j \leq F} \sum_{\gamma \delta} C_{j\gamma}^* C_{j\delta} \langle \alpha \gamma | \hat{v} | \beta \delta \rangle \right\} C_{i\beta} = \epsilon_i^{HF} C_{i\alpha}. \quad (2.150)$$

Note that the sums over Greek indices run over the number of basis set functions (in principle an infinite number).

Defining

$$h_{\alpha\beta}^{HF} = \langle \alpha | h | \beta \rangle + \sum_{j \leq F} \sum_{\gamma \delta} C_{j\gamma}^* C_{j\delta} \langle \alpha \gamma | \hat{v} | \beta \delta \rangle, \quad (2.151)$$

we can rewrite the new equations as

$$\sum_{\beta} h_{\alpha\beta}^{HF} C_{i\beta} = \epsilon_i^{HF} C_{i\alpha}. \quad (2.152)$$

The latter is nothing but a standard eigenvalue problem. Our Hartree-Fock matrix is thus

$$\hat{h}_{\alpha\beta}^{HF} = \langle \alpha | \hat{h}_0 | \beta \rangle + \sum_{j \leq F} \sum_{\gamma \delta} C_{j\gamma}^* C_{j\delta} \langle \alpha \gamma | \hat{v} | \beta \delta \rangle. \quad (2.153)$$

The Hartree-Fock equations are solved in an iterative way starting with a guess for the coefficients $C_{j\gamma} = \delta_{j,\gamma}$ and solving the equations by diagonalization till the new single-particle energies ϵ_i^{HF} do not change anymore by a user-defined small quantity.

Normally we assume that the single-particle basis $|\beta\rangle$ forms an eigenbasis for the operator

\hat{h}_0 , meaning that the Hartree-Fock matrix becomes

$$\hat{h}_{\alpha\beta}^{HF} = \epsilon_{\alpha}\delta_{\alpha,\beta} + \sum_{j \leq F} \sum_{\gamma\delta} C_{j\gamma}^* C_{j\delta} \langle \alpha\gamma | \hat{v} | \beta\delta \rangle. \quad (2.154)$$

2.14 Many-Body Perturbation Theory

Hartree-Fock theory is incredibly powerful considering how simple the idea is: transform the single-particle basis to optimize a single Slater determinant. This optimization problem can be thought of as summing the interactions from the surrounding particles to create a sort of external “mean field” that each particle feels. In some cases, this mean field approach is sufficient to answer the physics questions being asked. However, the heart of many-body theory is the correlation between particles that are purely many-body in nature, meaning that they cannot be described in the independent particle picture. Historically, many-body perturbation theory (MBPT) [37, 38, 33, 16] has been a first attempt to build these many-body correlations on top of a reference state. Like perturbation theory in other branches of physics, or in single particle quantum mechanics, it is assumed that the problem at hand is a small “perturbation” away from a reference problem. In the many-body case, starting from a good reference state is essential, as a bad starting point will require many additional corrections, or in some cases adding additional corrections will not work at all. To set the stage for deriving MBPT, we assume here that we are only interested in the non-degenerate ground state of a given system and expand the exact wave function in terms of a series of Slater determinants

$$|\Psi_0\rangle = |\Phi_0\rangle + \sum_{m=1}^{\infty} C_m |\Phi_m\rangle, \quad (2.155)$$

where we have assumed that the true ground state is dominated by the solution of the unperturbed problem, that is

$$\hat{H}_0|\Phi_0\rangle = W_0|\Phi_0\rangle, \quad (2.156)$$

and that the full Hamiltonian is given by this term plus a small interaction term

$$\hat{H} = \hat{H}_0 + \hat{H}_I. \quad (2.157)$$

The state $|\Psi_0\rangle$ is not normalized and we employ again intermediate normalization via $\langle\Phi_0|\Psi_0\rangle = 1$.

The Schrödinger equation is given by

$$\hat{H}|\Psi_0\rangle = E|\Psi_0\rangle, \quad (2.158)$$

and multiplying the latter from the left with $\langle\Phi_0|$ gives

$$\langle\Phi_0|\hat{H}|\Psi_0\rangle = E\langle\Phi_0|\Psi_0\rangle = E, \quad (2.159)$$

and subtracting from this equation

$$\langle\Psi_0|\hat{H}_0|\Phi_0\rangle = W_0\langle\Psi_0|\Phi_0\rangle = W_0, \quad (2.160)$$

and using the fact that the operators \hat{H} and \hat{H}_0 are hermitian results in

$$\Delta E = E - W_0 = \langle\Phi_0|\hat{H}_I|\Psi_0\rangle, \quad (2.161)$$

which is an exact result. The total energy can be separated into two terms

$$E = E_{\text{Ref}} + \Delta E, \quad (2.162)$$

where ΔE is the correlation energy, and the reference energy is given by

$$E_{\text{Ref}} = \langle \Phi_0 | \hat{H} | \Phi_0 \rangle. \quad (2.163)$$

Equation (2.161) forms the starting point for all perturbative derivations. However, as it stands it represents nothing but a mere formal rewriting of Schrödinger's equation and is not of much practical use. The exact wave function $|\Psi_0\rangle$ is unknown. In order to obtain a perturbative expansion, we need to expand the exact wave function in terms of the interaction \hat{H}_I .

Here we have assumed that our model space defined by the operator \hat{P} is one-dimensional, meaning that

$$\hat{P} = |\Phi_0\rangle\langle\Phi_0|, \quad (2.164)$$

and

$$\hat{Q} = \sum_{m=1}^{\infty} |\Phi_m\rangle\langle\Phi_m|. \quad (2.165)$$

We can thus rewrite the exact wave function as

$$|\Psi_0\rangle = (\hat{P} + \hat{Q})|\Psi_0\rangle = |\Phi_0\rangle + \hat{Q}|\Psi_0\rangle. \quad (2.166)$$

Going back to the Schrödinger equation, we can rewrite it, adding and subtracting a term

$\omega|\Psi_0\rangle$ as

$$\left(\omega - \hat{H}_0\right) |\Psi_0\rangle = \left(\omega - E + \hat{H}_I\right) |\Psi_0\rangle, \quad (2.167)$$

where ω is an energy variable to be specified later.

We assume also that the resolvent of $\left(\omega - \hat{H}_0\right)$ exists, that is it has an inverse which defines the unperturbed Green's function as

$$\left(\omega - \hat{H}_0\right)^{-1} = \frac{1}{\left(\omega - \hat{H}_0\right)}. \quad (2.168)$$

We can rewrite Schrödinger's equation as

$$|\Psi_0\rangle = \frac{1}{\omega - \hat{H}_0} \left(\omega - E + \hat{H}_I\right) |\Psi_0\rangle, \quad (2.169)$$

and multiplying from the left with \hat{Q} results in

$$\hat{Q}|\Psi_0\rangle = \frac{\hat{Q}}{\omega - \hat{H}_0} \left(\omega - E + \hat{H}_I\right) |\Psi_0\rangle, \quad (2.170)$$

which is possible since we have defined the operator \hat{Q} in terms of the eigenfunctions of \hat{H}_0 .

Since these operators commute we have

$$\hat{Q} \frac{1}{\left(\omega - \hat{H}_0\right)} \hat{Q} = \hat{Q} \frac{1}{\left(\omega - \hat{H}_0\right)} = \frac{\hat{Q}}{\left(\omega - \hat{H}_0\right)}. \quad (2.171)$$

With these definitions we can in turn define the wave function as

$$|\Psi_0\rangle = |\Phi_0\rangle + \frac{\hat{Q}}{\omega - \hat{H}_0} \left(\omega - E + \hat{H}_I\right) |\Psi_0\rangle. \quad (2.172)$$

So far, this is just a reorganization of the Schrödinger equation. It is a non-linear equation in two unknown quantities, the energy E and the exact wave function $|\Psi_0\rangle$. We can however start with a guess for $|\Psi_0\rangle$ on the right hand side of the last equation.

The most common choice is to start with the function which is expected to exhibit the largest overlap with the wave function we are searching after, namely $|\Phi_0\rangle$. This can again be inserted in the solution for $|\Psi_0\rangle$ in an iterative fashion and if we continue along these lines we end up with

$$|\Psi_0\rangle = \sum_{i=0}^{\infty} \left\{ \frac{\hat{Q}}{\omega - \hat{H}_0} (\omega - E + \hat{H}_I) \right\}^i |\Phi_0\rangle, \quad (2.173)$$

for the wave function and

$$\Delta E = \sum_{i=0}^{\infty} \langle \Phi_0 | \hat{H}_I \left\{ \frac{\hat{Q}}{\omega - \hat{H}_0} (\omega - E + \hat{H}_I) \right\}^i |\Phi_0\rangle, \quad (2.174)$$

which is now a perturbative expansion of the exact energy in terms of the interaction \hat{H}_I and the unperturbed wave function $|\Psi_0\rangle$.

In our equations for $|\Psi_0\rangle$ and ΔE in terms of the unperturbed solutions $|\Phi_i\rangle$ we have still an undetermined parameter ω and a dependency on the exact energy E . Not much has been gained thus from a practical computational point of view.

In Brillouin-Wigner perturbation theory [16, 39] it is customary to set $\omega = E$. This

results in the following perturbative expansion for the energy ΔE

$$\Delta E = \sum_{i=0}^{\infty} \langle \Phi_0 | \hat{H}_I \left\{ \frac{\hat{Q}}{\omega - \hat{H}_0} (\omega - E + \hat{H}_I) \right\}^i | \Phi_0 \rangle = \quad (2.175)$$

$$\langle \Phi_0 | \left(\hat{H}_I + \hat{H}_I \frac{\hat{Q}}{E - \hat{H}_0} \hat{H}_I + \hat{H}_I \frac{\hat{Q}}{E - \hat{H}_0} \hat{H}_I \frac{\hat{Q}}{E - \hat{H}_0} \hat{H}_I + \dots \right) | \Phi_0 \rangle. \quad (2.176)$$

This expression depends however on the exact energy E and is again not very convenient from a practical point of view. It can obviously be solved iteratively, by starting with a guess for E and then solve till some kind of self-consistency criterion has been reached.

Defining $e = E - \hat{H}_0$ and recalling that \hat{H}_0 commutes with \hat{Q} by construction and that \hat{Q} is an idempotent operator $\hat{Q}^2 = \hat{Q}$, we can rewrite the denominator in the above expansion for ΔE as

$$\hat{Q} \frac{1}{e - \hat{Q} \hat{H}_I \hat{Q}} = \hat{Q} \left[\frac{1}{e} + \frac{1}{e} \hat{Q} \hat{H}_I \hat{Q} \frac{1}{e} + \frac{1}{e} \hat{Q} \hat{H}_I \hat{Q} \frac{1}{e} \hat{Q} \hat{H}_I \hat{Q} \frac{1}{e} + \dots \right] \hat{Q}. \quad (2.177)$$

Inserted in the expression for ΔE , we obtain

$$\Delta E = \langle \Phi_0 | \hat{H}_I + \hat{H}_I \hat{Q} \frac{1}{E - \hat{H}_0 - \hat{Q} \hat{H}_I \hat{Q}} \hat{Q} \hat{H}_I | \Phi_0 \rangle. \quad (2.178)$$

In Rayleigh-Schrödinger (RS) perturbation theory [40, 41, 16] we set $\omega = W_0$ and obtain the following expression for the energy difference

$$\Delta E = \sum_{i=0}^{\infty} \langle \Phi_0 | \hat{H}_I \left\{ \frac{\hat{Q}}{W_0 - \hat{H}_0} (\hat{H}_I - \Delta E) \right\}^i | \Phi_0 \rangle \quad (2.179)$$

$$= \langle \Phi_0 | \left(\hat{H}_I + \hat{H}_I \frac{\hat{Q}}{W_0 - \hat{H}_0} (\hat{H}_I - \Delta E) + \dots \right) | \Phi_0 \rangle. \quad (2.180)$$

The operator \hat{Q} commutes with \hat{H}_0 and since ΔE is a constant we obtain that

$$\hat{Q}\Delta E|\Phi_0\rangle = \hat{Q}\Delta E|\hat{Q}\Phi_0\rangle = 0. \quad (2.181)$$

Inserting this result in the expression for the energy gives us

$$\Delta E = \langle\Phi_0|\left(\hat{H}_I + \hat{H}_I\frac{\hat{Q}}{W_0 - \hat{H}_0}\hat{H}_I + \hat{H}_I\frac{\hat{Q}}{W_0 - \hat{H}_0}(\hat{H}_I - \Delta E)\frac{\hat{Q}}{W_0 - \hat{H}_0}\hat{H}_I + \dots\right)|\Phi_0\rangle. \quad (2.182)$$

We can now perturbatively expand this expression in terms of the interaction \hat{H}_I , which is assumed to be small. We obtain then

$$\Delta E = \sum_{i=1}^{\infty} \Delta E^{(i)}, \quad (2.183)$$

with the following expression for $\Delta E^{(i)}$

$$\Delta E^{(1)} = \langle\Phi_0|\hat{H}_I|\Phi_0\rangle, \quad (2.184)$$

which is just the contribution to first order in perturbation theory,

$$\Delta E^{(2)} = \langle\Phi_0|\hat{H}_I\frac{\hat{Q}}{W_0 - \hat{H}_0}\hat{H}_I|\Phi_0\rangle, \quad (2.185)$$

which is the contribution to second order. There exists a formal theory for the calculation of each additional term, see for example Ref. [16], where a diagrammatic method is described to generate any order of MBPT. Inserting in the \hat{Q} space operator and the energy denominators in Eqn. (2.185) we get the expression for MBPT(2), the energy correction for many-body

perturbation theory to second order,

$$\Delta E^{(2)} = \frac{1}{2^2} \sum_{ij \leq F} \sum_{ab > F} \frac{\langle ij | \hat{v} | ab \rangle \langle ab | \hat{v} | ij \rangle}{\varepsilon_i + \varepsilon_j - \varepsilon_a - \varepsilon_b}. \quad (2.186)$$

In the expressions for the various diagrams the quantity ε denotes the single-particle energies defined by H_0 . Many-body perturbation theory is quite powerful, and can provide corrections quite accurately for many systems. Unfortunately, most nuclear physics applications do not fall in this regime where MBPT is accurate due to that large short range correlations of the nucleon-nucleon potential. Any system for which the interactions are too large compared to the non-interacting mean-field model will not be meaningfully captured by MBPT even at high orders of correction. This will be illustrated in Chapter 3, where the simple pairing model is examined.

2.15 In-Medium Similarity Renormalization Group

So far we have covered three important methods in quantum many-body theory. First, was Full configuration interaction (FCI), where the only approximation is the necessary truncation to the single-particle basis. The many-body basis is then constructed from the single-particle basis, but FCI does not make any additional truncations to the many-body space. Next, was Hartree-Fock (HF) mean field theory, which optimizes the many-body ground state energy in a single Slater determinant by performing a unitary transformation on the single-particle basis. Last, was many-body perturbation theory (MBPT), which exists between a simple mean field model and the full many-body solution. This is the regime where the vast majority of many-body physics is done, as many interesting problems are

too computationally expensive for FCI, but too correlated for Hartree-Fock to be sufficient. As a result, many different approximations to the many-body problem have been developed with various strengths and weaknesses to target different applications. The strength of *ab initio* many-body methods is that by maintaining the essential degrees of freedom, all of the approximations can be extended to recover the full solution. Of course the trade-off is then that these extensions towards the exact solutions again become prohibitively expensive, but this allows for a choice in the trade-off between accuracy in computational cost. Additionally, in nuclear physics the nuclear potentials can be developed in a similar way that allows for increased accuracy (at increasing computational cost), but this work will focus on various approximations to the many-body methods rather than the input potentials. In particular, most of the calculations in this work are done with an *ab initio* many-body method called coupled cluster (CC) theory, which is explained in detail in Chapter 4. Another *ab initio* many-body method similar to coupled cluster is in-medium similarity renormalization group (IM-SRG) [42, 43, 44, 45, 46, 47, 48, 3].

The renormalization group is a tool that has been used in physics for many decades, which allows physical quantities of interest to be examined at different distance or energy scales and has been essential in the development of quantum electrodynamics and quantum chromodynamics. In nuclear physics most realistic nuclear potentials have a sharp repulsive core which can lead to divergences in calculating matrix elements, generating strong off-diagonal contributions as low momentum modes are coupled to high momentum modes. However for certain physical quantities, like the ground state energy of an atomic nucleus, the low energy of the system indicates that the nucleons should not probe the very short range distance scales of this repulsive core. Similarity renormalization group (SRG) has had success in “softening” the repulsive of the nuclear potential, by driving the momentum

space interaction matrix to a band diagonal form, decoupling the high momentum from low momentum modes while maintaining accuracy of the target observables [4, 5].

In-medium similarity renormalization group (IM-SRG) takes this philosophy of decoupling distance scales and applies it to the “medium” of a particular reference state. The idea is that for a matrix problem in the many-body basis, transforming the matrix to a form where the ground state is decoupled from the rest of the matrix will give the ground state eigenvalue. In the case of IM-SRG, the Hamiltonian is normal ordered with respect to a reference state and the ground state energy is isolated by a continuous unitary transformation.

A unitary transformation U is an isomorphism between two Hilbert spaces H_1, H_2 that preserves the inner product,

$$U : H_1 \rightarrow H_2, \tag{2.187}$$

$$\langle Ux, Uy \rangle_{H_1} = \langle x, y \rangle_{H_2}, \tag{2.188}$$

$\forall x, y \in H_1$. Similarly, for an antiunitary transformation,

$$\langle Ux, Uy \rangle = \langle x, y \rangle^* = \langle y, x \rangle. \tag{2.189}$$

Thus for a unitary transformation, in bra-ket notation,

$$\langle Ux|Uy \rangle = \langle x|U^\dagger U|y \rangle = \langle x|y \rangle, \tag{2.190}$$

$$\implies U^\dagger U = UU^\dagger = \mathbb{1}. \tag{2.191}$$

A continuous unitary transformation is a unitary transformation parametrized by some continuous parameter s , such that $U(s)U(s)^\dagger = \mathbb{1}$. This generates a unitarily transformed Hamiltonian for all points s ,

$$H(s) = U^\dagger(s)HU(s). \quad (2.192)$$

The transformation is implemented by solving a coupled set of flow equations for the matrix elements for the Hamiltonian, which we can find by taking the derivative of Eqn. (2.192),

$$\frac{dH(s)}{ds} = \frac{dU^\dagger(s)}{ds}HU(s) + U^\dagger(s)H\frac{dU(s)}{ds}, \quad (2.193)$$

and the derivative of Eqn. (2.191)

$$\frac{dU^\dagger(s)}{ds}U(s) + U^\dagger(s)\frac{dU(s)}{ds} = 0. \quad (2.194)$$

From here, we write down the generator of the transformation η as

$$\eta(s) = \frac{dU^\dagger(s)}{ds}U(s) = -U^\dagger(s)\frac{dU(s)}{ds}, \quad (2.195)$$

which leads to the flow equations as

$$\frac{dH(s)}{ds} = [\eta(s), H(s)]. \quad (2.196)$$

For actual calculations, an explicit expression from the transformation $U(s)$ is rarely written out. Instead, the generator η defines the unitary transformation. To actually implement

this, we partition the Hamiltonian as

$$H(s) = H^d(s) + H^{od}(s), \quad (2.197)$$

where these are the diagonal and off-diagonal components of the matrix. The evolution with the continuous flow parameter s is again The choice of the generator first suggested by Wegner [49],

$$\eta(s) = [H^d(s), H(s)] = [H^d(s), H^{od}(s)], \quad (2.198)$$

guarantees

$$\frac{d}{ds} \text{Tr} \left((H^{od})^2 \right) = 2 \text{Tr}(\eta^2) = -2 \text{Tr}(\eta^\dagger \eta) \leq 0, \quad (2.199)$$

which demonstrates that H^{od} decays with increasing s which is precisely what is needed to decouple the high and low momentum modes[50]. Analyzing the flow equations in the eigenbasis of $H^d(s)$ and defining $H_{ii}^d(s) \equiv \epsilon_i$ one can show that

$$H_{ij}^{od}(s) \sim e^{-s(\epsilon_i - \epsilon_j)^2} H_{ij}^{od}(0). \quad (2.200)$$

However, this can lead to stiff ODE's, so a more common generator is the White generator [51]

$$\eta_{ij}(s) = \frac{H_{ij}^{od}(s)}{\epsilon_i - \epsilon_j}, \quad (2.201)$$

which gives uniform suppression

$$H_{ij}^{od}(s) \sim e^{-s} H_{ij}^{od}(0). \quad (2.202)$$

While SRG is typically used to soften nuclear potentials with a repulsive core, an alternative is to perform the SRG evolution in-medium (IM-SRG) for each A-body system of interest. Starting from a general second-quantized Hamiltonian with two- and three-body interactions

$$H = \sum_{qr} T_{qr} a_q^\dagger a_r + \frac{1}{2!2} \sum_{qrst} V_{qrst}^{(2)} a_q^\dagger a_r^\dagger a_t a_s + \frac{1}{3!2} \sum_{qrstuv} V_{qrstuv}^{(3)} a_q^\dagger a_r^\dagger a_s^\dagger a_v a_u a_t + \dots \quad (2.203)$$

All operators can be normal-ordered with respect to a finite-density Fermi vacuum $|\Phi\rangle$ (e.g. the Hartree-Fock ground state), as opposed to the zero particle vacuum. Wick's theorem can then be used to exactly write H as

$$H = E + \sum_{qr} f_{qr} \{a_q^\dagger a_r\} + \frac{1}{4} \sum_{qrst} \Gamma_{qrst} \{a_q^\dagger a_r^\dagger a_t a_s\} + \frac{1}{36} \sum_{qrstuv} W_{qrstuv} \{a_q^\dagger a_r^\dagger a_s^\dagger a_v a_u a_t\}, \quad (2.204)$$

where strings of normal ordered operators obey

$$\langle \Phi | \{a_q^\dagger \dots a_r\} | \Phi \rangle = 0, \quad (2.205)$$

and the terms in (2.204) are given by

$$E = \sum_q T_{qq} n_q + \frac{1}{2} \sum_{qr} V_{qrqr}^{(2)} n_q n_r + \frac{1}{6} \sum_{qrs} V_{qrsqrs}^{(3)} n_q n_r n_s, \quad (2.206)$$

$$f_{qr} = T_{qr} + \sum_s V_{qsrs}^{(2)} n_s + \frac{1}{2} \sum_{st} V_{qstrst}^{(3)} n_s n_t, \quad (2.207)$$

$$\Gamma_{qrst} = V_{qrst}^{(2)} + \sum_u V_{qrustu}^{(3)} n_u, \quad (2.208)$$

$$W_{qrtsuv} = V_{qrstuv}^{(3)}, \quad (2.209)$$

where $n_q = \theta(\epsilon_F - \epsilon_q)$ are the occupation numbers in the reference state $|\Phi\rangle$. Notice that the normal ordered 0-,1-, and 2-body terms include contributions from the three-body interaction $V^{(3)}$ through sums over the occupied single-particle states in the reference state $|\Phi\rangle$. Neglecting the residual three-body interaction leads to the normal-ordered two-body approximation (NO2B) which has shown to be an excellent approximation in nuclear systems. Truncating the in-medium SRG equations to normal-ordered two-body operators is denoted IM-SRG(2). Using this normal ordered Hamiltonian and using Wick's theorem on Eqn. (2.196) with $H(s) = E_0(s) + f(s) + \Gamma(s)$ and truncating $\eta(s) = \eta^{(1)}(s) + \eta^{(2)}(s)$ to two-body yields the coupled IM-SRG(2) equations

$$\frac{dE_0}{ds} = \sum_{qr} \eta_{qr} f_{rq} (n_q - n_r) + \frac{1}{2} \sum_{qrst} \eta_{qrst} \Gamma_{stqr} n_q n_r \bar{n}_s \bar{n}_t, \quad (2.210)$$

$$\begin{aligned} \frac{df_{qr}}{ds} = & \sum_s (1 + P_{qr}) \eta_{qs} f_{sr} + \sum_{st} (n_s - n_t) (\eta_{st} \Gamma_{tqsr} - f_{st} \eta_{tqsr}) \\ & + \sum_{stu} (n_s n_t \bar{n}_u + \bar{n}_s \bar{n}_t n_u) (1 + P_{qr}) \eta_{uqst} \Gamma_{stur}, \end{aligned} \quad (2.211)$$

$$\begin{aligned} \frac{d\Gamma_{qrst}}{ds} = & \sum_u (1 - P_{qr}) (\eta_{qu} \Gamma_{urst} - f_{qu} \eta_{urst}) \\ & - \sum_u (1 - P_{st}) (\eta_{us} \Gamma_{qrut} - f_{us} \eta_{qrut}) \\ & + \frac{1}{2} \sum_{uv} (1 - n_u - n_v) (\eta_{qrv} \Gamma_{uvst} - \Gamma_{qrv} \eta_{uvst}) \\ & - \sum_{uv} (n_u - n_v) (1 - P_{qr}) (1 - P_{st}) \eta_{vrut} \Gamma_{uqvs}, \end{aligned} \quad (2.212)$$

where the $\bar{n}_r \equiv (1 - n_r)$, P_{qr} is the permutation operator and s dependence has been made implicit to clear up visual clutter. The White generator is then

$$\eta = \sum_{ai} \frac{f_{ai}}{f_a - f_i} \{a_a^\dagger a_i\} + \frac{1}{4} \sum_{abij} \frac{\Gamma_{abij}}{f_a + f_b - f_i - f_j} \{a_a^\dagger a_b^\dagger a_j a_i\} - \text{H.c.}, \quad (2.213)$$

where $f_a = f_{aa}$ are the Møller-Plesset energy denominators. Unfortunately, these equations can be very sensitive, as small amounts of numerical error can break the unitarity of the transformation. This means that to solve these equations, a high-order differential equation solver is typically needed. These solvers need to store many copies of the solution vector to maintain accuracy, and these copies rapidly increase the storage requirements. Fortunately, the Magnus expansion can help out here, ensuring that unitarity is preserved at every step in the differential equation.

2.16 The Magnus Formulation of IM-SRG

The starting point of the Magnus formulation [50] of IM-SRG is once again taking the derivative of the unitarity condition $U(s)U^\dagger(s) = U^\dagger(s)U(s) = \mathbb{1}$,

$$\frac{dU(s)}{ds} U^\dagger(s) = -U(s) \frac{dU^\dagger(s)}{ds}. \quad (2.214)$$

Now define $\eta \equiv U(s) \frac{dU^\dagger(s)}{ds}$ and multiply Eqn. (2.214) on the right by $U(s)$ to yield the differential equation

$$\frac{dU(s)}{ds} U^\dagger(s) U(s) = -U(s) \frac{dU^\dagger(s)}{ds} U(s), \quad (2.215)$$

$$\implies \frac{dU(s)}{ds} = -\eta(s) U(s), \quad (2.216)$$

with the boundary condition $U(0) = 1$. To get some intuition for this differential equation, we look to a familiar unitary transformation, like the time evolution operator, the Hamiltonian.

$$U(t) = e^{-iHt}. \quad (2.217)$$

Taking the time derivative yields

$$\frac{dU(t)}{dt} = -iHe^{-iHt} = -iHU(t). \quad (2.218)$$

This is true when H is independent of t and explains why the solution is so compact. If we look at $U(s) = e^{-\eta s}$, the derivative would be

$$\frac{dU(s)}{ds} = -\eta e^{-\eta s} = -\eta U(s), \quad (2.219)$$

which would be a nice solution to the differential equation. So it becomes clear that the s dependence in $\eta(s)$ makes things more complicated. If we had $U(s) = e^{-\eta(s)}$, then the derivative would be

$$\frac{dU(s)}{ds} = -\frac{d\eta(s)}{ds} e^{-\eta(s)}. \quad (2.220)$$

Thus to get the solution we want, we need the anti-derivative of $\eta(s)$ to be exponentiated; so something like $\text{Exp}(-\int_0^s \eta(s') ds')$. But here, there are all sorts of issues since this is a matrix exponential, which is really just short hand for the polynomial series. So terms like

$$\frac{1}{n!} \int_0^s \cdots \int_0^s \eta(s'_1) \cdots \eta(s'_n) ds_1 \cdots ds_n, \quad (2.221)$$

arise. And here, unless all of the η terms at any value of s commute, the order matters. This can be formally integrated as the time-ordered exponential

$$U(s) = T_s \left\{ e^{-\int_0^s \eta(s') ds'} \right\} \equiv 1 - \int_0^s ds' \eta(s') + \int_0^s ds' \int_0^{ds'} ds'' \eta(s') \eta(s'') + \dots \quad (2.222)$$

This is not useful from a practical point of view. The Magnus expansion [52] is the statement that given a few technical requirements on $\eta(s)$, a solution of the form

$$U(s) = e^{\Omega(s)} \quad (2.223)$$

exists, where $\Omega^\dagger(s) = -\Omega(s)$ and $\Omega(0) = 0$. This lines up with the previously stated boundary condition of $U(0) = 1$, which is satisfied by $\Omega(0) = 0$. The anti-Hermitian property of Ω is necessary since for any unitary operator U to be expressed as exponentiated operator Ω requires that the exponentiated operator Ω be anti-Hermitian,

$$UU^\dagger = \mathbb{1} \stackrel{?}{=} e^\Omega e^{\Omega^\dagger} = e^{\Omega + \Omega^\dagger} e^{[\Omega, \Omega^\dagger]}. \quad (2.224)$$

This expression will be satisfied as long as $\Omega^\dagger = -\Omega$, since

$$[\Omega, \Omega^\dagger] = \Omega \Omega^\dagger - \Omega^\dagger \Omega = -\Omega^2 + \Omega^2 = 0 \quad (2.225)$$

$$\implies e^{\Omega + \Omega^\dagger} e^{[\Omega, \Omega^\dagger]} = e^0 e^0 = \mathbb{1}.$$

This is why the time evolution operator e^{iHt} has the characteristic phase i . Since H is Hermitian, the i is needed in the exponential to make the exponent anti-Hermitian overall to ensure the unitarity of the transformation.

In previous applications of the Magnus expansion, $\Omega(s)$ is expanded in powers of $\eta(s)$ as

$$\Omega = \sum_{n=1}^{\infty} \Omega_n \quad (2.226)$$

where

$$\Omega_1(s) = - \int_0^s ds_1 \eta(s_1) \quad (2.227)$$

$$\Omega_2(s) = \frac{1}{2} \int_0^s ds_1 \int_0^{s_1} ds_2 [\eta(s_1), \eta(s_2)]. \quad (2.228)$$

$$\vdots \quad (2.229)$$

Here, the complications of the time-ordered exponential are moved inside the exponential. The advantage of this is that truncating Ω at any order will still be anti-Hermitian, and thus result in a unitary transformation. This is unlike truncating (2.222) which is not guaranteed to be unitary if any truncations are made. Let's quickly check that truncating Ω will still be anti-Hermitian. First, check that η is anti-Hermitian. Starting from $U(s) \frac{dU^\dagger(s)}{ds} = -\frac{dU(s)}{ds} U^\dagger(s)$ with the fact that $(AB)^\dagger = B^\dagger A^\dagger$

$$\eta^\dagger(s) = \left(U(s) \frac{dU^\dagger(s)}{ds} \right)^\dagger = \frac{dU(s)}{ds} U^\dagger(s) = -\eta(s) \quad (2.230)$$

which shows that η is indeed anti-Hermitian. To check that the commutators in a term like

Ω_2 are anti-Hermitian, let's call $A = [\eta(s_1), \eta(s_2)]$. Then

$$\begin{aligned}
A^\dagger &= [\eta(s_1), \eta(s_2)]^\dagger = \left(\eta(s_1)\eta(s_2) - \eta(s_2)\eta(s_1) \right)^\dagger & (2.231) \\
&= \eta(s_2)^\dagger \eta(s_1)^\dagger - \eta(s_1)^\dagger \eta(s_2)^\dagger \\
&= (-1)^2 \eta(s_2)\eta(s_1) - (-1)^2 \eta(s_1)\eta(s_2) \\
&= -(\eta(s_1)\eta(s_2) - \eta(s_2)\eta(s_1)) \\
&= -A. & (2.232)
\end{aligned}$$

This proves that the commutator of any two anti-Hermitian operators is itself anti-Hermitian. Therefore, every term of the Magnus expansion is anti-Hermitian, so truncating at any level ensures that Ω is anti-Hermitian.

To demonstrate the SRG, let's consider a small two-level system, represented by the initial Hamiltonian

$$H = T + V = \begin{pmatrix} 1 & 1 \\ 1 & -1 \end{pmatrix}. \quad (2.233)$$

Let's try to diagonalize H using the Wegner generator $\eta(s) = [T, H(s)]$,

$$\begin{aligned}
\eta(0) &= TH - HT \\
&= \begin{pmatrix} 1 & 0 \\ 0 & -1 \end{pmatrix} \begin{pmatrix} 1 & 1 \\ 1 & -1 \end{pmatrix} - \begin{pmatrix} 1 & 1 \\ 1 & -1 \end{pmatrix} \begin{pmatrix} 1 & 0 \\ 0 & -1 \end{pmatrix} \\
&= \begin{pmatrix} 1 & 1 \\ -1 & 1 \end{pmatrix} - \begin{pmatrix} 1 & -1 \\ 1 & 1 \end{pmatrix} \\
&= \begin{pmatrix} 0 & 2 \\ -2 & 0 \end{pmatrix} \\
&= 2i\sigma_2,
\end{aligned} \tag{2.234}$$

and by definition, $\Omega(0) = 0$. Looking at the recursively defined derivative of Ω

$$\begin{aligned}
\frac{d\Omega}{ds} &= \sum_{k=0}^{\infty} \frac{B_k}{k!} ad_{\Omega}^k(\eta), \\
ad_{\Omega}^0(\eta) &= \eta, \\
ad_{\Omega}^k(\eta) &= [\Omega, ad_{\Omega}^{k-1}(\eta)].
\end{aligned} \tag{2.235}$$

At $s = 0$ we have $\frac{d\Omega}{ds}|_{s=0} = \eta(0)$, since $ad_{\Omega}^1 = [0, \eta(0)] = 0$. In general, the next step is to calculate $\Omega(s)$ by integrating Eqn. (2.235), and then find the transformed Hamiltonian as

$$H(s) = e^{\Omega(s)} H(0) e^{-\Omega(s)} \tag{2.236}$$

by using the Baker-Campbell-Hausdorff expansion. However, in this simple model, we can just take the exponential of the Pauli matrices rather than doing a truncated BCH expansion.

With this example η and Ω truncate after one term, and will always be antisymmetric matrices, that is

$$\eta(s) = ig_{\eta}(s)\sigma_2 \tag{2.237}$$

$$\Omega(s) = ig_{\Omega}(s)\sigma_2. \tag{2.238}$$

With this form for Ω , we can look at the exact BCH expansion for $H(0) = \sigma_1 + \sigma_3$, using the matrix exponential of a Pauli matrix. In the case where $\vec{a} = a\hat{n}$, we have

$$e^{ia(\hat{n}\cdot\vec{\sigma})} = \mathbb{1}\cos(a) + i(\hat{n}\cdot\vec{\sigma})\sin(a). \tag{2.239}$$

In our case, we want $e^{\Omega} = e^{ig\sigma_2}$ so to get this, $ia(\hat{n}\cdot\vec{\sigma}) = ig\sigma_2$, therefore $a = g$ and $\hat{n} = \hat{y}$.

This leads to

$$e^{ig\sigma_2} = \mathbb{1}\cos(g) + i\sigma_2\sin(g) \tag{2.240}$$

and for $e^{-\Omega}$ just take $g \rightarrow -g$. Then use $\cos(-g) = \cos(g)$ and $\sin(-g) = -\sin(g)$. Thus the

transformed Hamiltonian is

$$\begin{aligned}
H(s) &= e^{ig\sigma_2}(\sigma_1 + \sigma_3)e^{-ig\sigma_2} \\
&= [\mathbb{1}\cos(g) + i\sigma_2\sin(g)] [\sigma_1 + \sigma_3](\mathbb{1}\cos(g) - i\sigma_2\sin(g)) \\
&= [\mathbb{1}\cos(g) + i\sigma_2\sin(g)] [\sigma_1\cos(g) - i\sigma_1\sigma_2\sin(g) + \sigma_3\cos(g) - i\sigma_3\sigma_2\sin(g)] \\
&= [\mathbb{1}\cos(g) + i\sigma_2\sin(g)] [\sigma_1\cos(g) - i^2\sigma_3\sin(g) + \sigma_3\cos(g) + i^2\sigma_1\sin(g)] \\
&= [\mathbb{1}\cos(g) + i\sigma_2\sin(g)] [\sigma_1(\cos(g) - \sin(g)) + \sigma_3(\cos(g) + \sin(g))] \\
&= \sigma_1(\cos(g) - \sin(g))\cos(g) + \sigma_3(\cos(g) + \sin(g))\cos(g) \\
&\quad + i\sigma_2\sigma_1(\cos(g) - \sin(g))\sin(g) + i\sigma_2\sigma_3(\cos(g) + \sin(g))\sin(g) \\
&= \sigma_1(\cos(g) - \sin(g))\cos(g) + \sigma_3(\cos(g) + \sin(g))\cos(g) \\
&\quad - i^2\sigma_3(\cos(g) - \sin(g))\sin(g) + i^2\sigma_1(\cos(g) + \sin(g))\sin(g) \\
&= \sigma_1[\cos^2(g) - \sin^2(g) - 2\cos(g)\sin(g)] \\
&\quad + \sigma_3[\cos^2(g) - \sin^2(g) + 2\cos(g)\sin(g)] \\
&= \sigma_1[\cos(2g) - \sin(2g)] + \sigma_3[\cos(2g) + \sin(2g)],
\end{aligned}$$

where we used $\sigma_a\sigma_b = \delta_{ab}\mathbb{1} + i\varepsilon_{abc}\sigma_c$ as well as the trig identity $\cos^2(g) - \sin^2(g) = \cos(2g)$ and $\sin(2g) = 2\sin(g)\cos(g)$. This can be generalized slightly for a Hamiltonian of the form

$H(0) = d\sigma_3 + v\sigma_1$, where the full transformed Hamiltonian is

$$\begin{aligned}
H(s) &= e^{ig\sigma_2}(v\sigma_1 + d\sigma_3)e^{-ig\sigma_2} \\
&= [\mathbb{1}\cos(g) + i\sigma_2\sin(g)](v\sigma_1 + d\sigma_3)[\mathbb{1}\cos(g) - i\sigma_2\sin(g)] \\
&= [\mathbb{1}\cos(g) + i\sigma_2\sin(g)] [v\sigma_1\cos(g) - iv\sigma_1\sigma_2\sin(g) + d\sigma_3\cos(g) - id\sigma_3\sigma_2\sin(g)] \\
&= [\mathbb{1}\cos(g) + i\sigma_2\sin(g)] [v\sigma_1\cos(g) - i^2v\sigma_3\sin(g) + d\sigma_3\cos(g) + i^2d\sigma_1\sin(g)] \\
&= [\mathbb{1}\cos(g) + i\sigma_2\sin(g)] [\sigma_1(v\cos(g) - d\sin(g)) + \sigma_3(d\cos(g) + v\sin(g))] \\
&= \sigma_1(v * \cos(g) - d * \sin(g))\cos(g) + \sigma_3(d * \cos(g) + v * \sin(g))\cos(g) \\
&\quad + i\sigma_2\sigma_1(v * \cos(g) - d * \sin(g))\sin(g) + i\sigma_2\sigma_3(d * \cos(g) + v * \sin(g))\sin(g) \\
&= \sigma_1(v * \cos(g) - d * \sin(g))\cos(g) + \sigma_3(d * \cos(g) + v * \sin(g))\cos(g) \\
&\quad - i^2\sigma_3(v * \cos(g) - d * \sin(g))\sin(g) + i^2\sigma_1(d * \cos(g) + v * \sin(g))\sin(g) \\
&= \sigma_1[v * \cos^2(g) - v * \sin^2(g) - 2d * \cos(g)\sin(g)] \\
&\quad + \sigma_3[d * \cos^2(g) - d * \sin^2(g) + 2v * \cos(g)\sin(g)] \\
&= \sigma_1[v * \cos(2g) - d * \sin(2g)] + \sigma_3[d * \cos(2g) + v * \sin(2g)]. \tag{2.241}
\end{aligned}$$

With these exact results derived, we can compare the direct SRG integration against the Magnus formulation. This is shown in figure 2.1, and it is clear how much numerical stability is gained from ensuring the unitarity each step with the Magnus expansion. The Magnus formulation relatively quickly reaches the “machine precision” of the finite precision floating point variables in the calculation, while the direct integration method has error that is highly dependent on the “time step” δs of the integration.

This 2×2 toy example hides two sources of error that would exist in an actual calculation. This first is that the expressions truncate naturally for η and Ω , which will not happen in

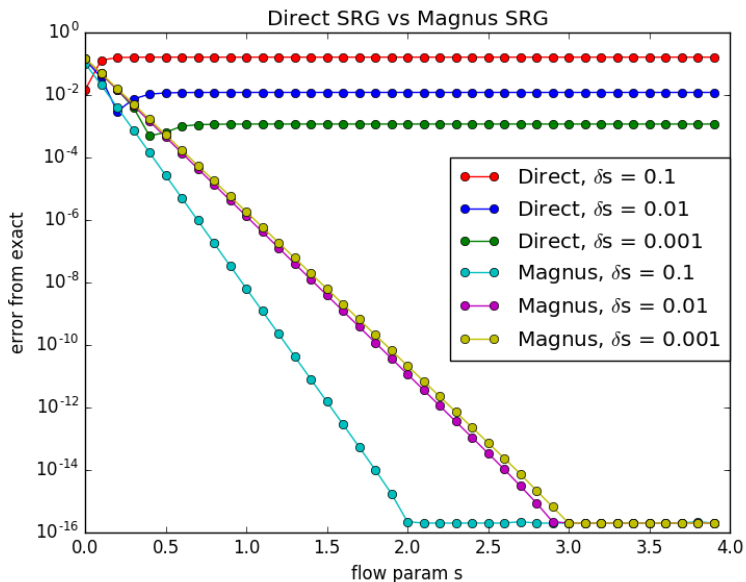


Figure 2.1: SRG with direct integration and with the Magnus expansion.

a many-body physics problem, and the second source of error is that the BCH expansion is done to infinite order in Eqn. (2.241). In a realistic many-body calculation, the terms in these series are observed to decrease monotonically, and a cutoff tolerance can be used to minimize the numerical error from truncation. To gain insight into the error generated from the BCH expansion truncation, the nested commutators can be compared against the exact expression derived in Eqn. (2.241). In figure 2.2 this source of truncation error goes back down to machine precision after about 20 terms, which is pretty substantial, although machine precision is rarely necessary.

Rather than setting a fixed number of terms in the expansion, it is more typical to specify an error tolerance so that the BCH expansion can be assuredly not the primary source of error. This is what is done in figure 2.3, where the tolerance ϵ here is defined to be greater than the row 0 column 0 element of the next term in the BCH expansion.

By setting $\epsilon = 10^{-8}$, we are asserting that we want the smallest eigenvalue (the (0,0) element of the matrix) to be changing by not more than 10^{-8} for the next term in the BCH

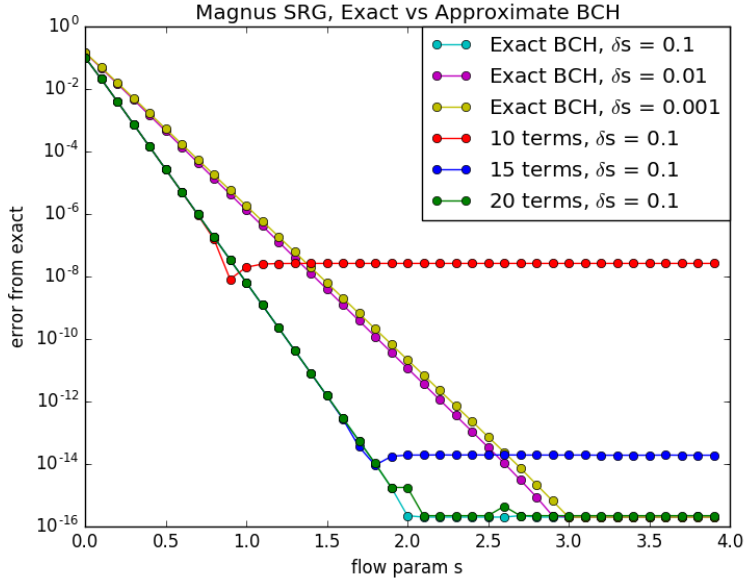


Figure 2.2: Magnus SRG with the exact unitary transformation and with a BCH expansion truncated after a fixed number of terms

series. There are other tolerances that can be chosen, but looking at the plot, it seems to work well. As a note, the three tolerances of $(10^{-8}, 10^{-12}, 10^{-16})$ used (12, 15, 18) terms in their expansions.

The Magnus expansion has shown to be a great tool for these calculations, but potentially the greatest gain from this is that any operator can also be computed after the flow. Once the flow has finished, it only costs an exact BCH to compute $O(s) = e^{\Omega} O e^{\Omega^\dagger}$ along with $H(s) = e^{\Omega} H e^{\Omega^\dagger}$.

While the 2x2 example was not an exercise in many-body physics, IM-SRG and the use of the Magnus expansion have seen great success in the calculation of many interesting nuclear systems [42, 43, 44, 45, 46, 47, 48, 3]. The many-body physics results of this work will focus on the use of coupled cluster theory which is detailed in Chapter 4.

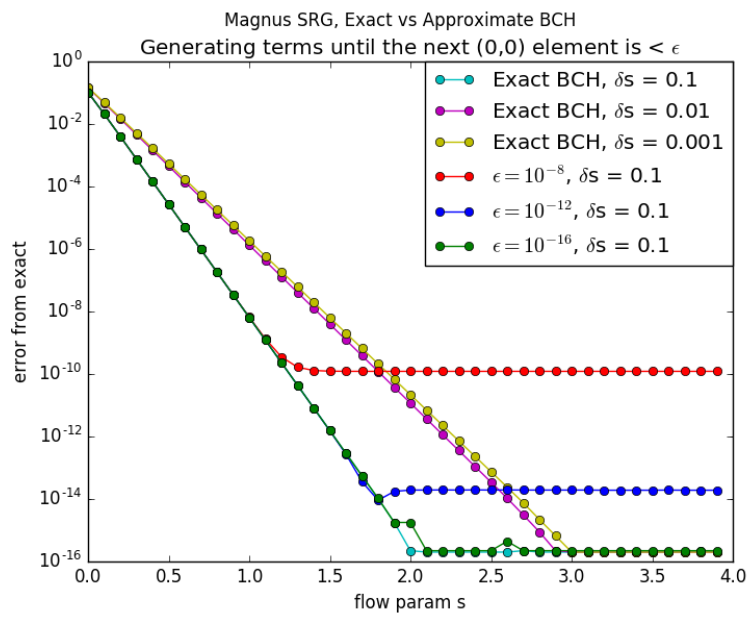


Figure 2.3: Magnus SRG with the exact unitary transformation and with a BCH expansion truncated after a fixed tolerance is met

Chapter 3

Physical Systems

With the mathematical framework of quantum many-body theory as a foundation any quantum system can be investigated numerically. The many-body Schrödinger equation has proven to be an excellent model for studying nearly any physical system for which the particles are traveling sufficiently slower than the speed of light. A wide range of fields including atomic physics, quantum chemistry, materials science, and nuclear physics greatly benefit from these theoretical tools, which make studying the mathematical and computational methods surrounding many-body physics a worthwhile endeavor *per se*. While the physical systems introduced in this chapter have applications in answering real world questions, much of the interest in these systems is theoretical. The pairing model is a simple quantum system which can be studied analytically and exactly. It is therefore an excellent testing ground for properties of various many-body methods, and as a system to validate numerical implementations. Infinite fermionic matter is important for studying valence electrons in metals [23], and also for studying the volumetric bulk of neutrons thought to constitute the crust of neutron stars, or as a model for dense nuclear matter [2, 1, 22].

3.1 Pairing Model

The pairing model Hamiltonian $\hat{H} = \hat{H}_0 + \hat{V}$ is defined as

$$\hat{H}_0 = \delta \sum_{p\sigma} (p-1) a_{p\sigma}^\dagger a_{p\sigma} \quad (3.1)$$

$$\hat{V} = -\frac{1}{2}g \sum_{pq} a_{p+}^\dagger a_{p-}^\dagger, a_{q-} a_{q+} \quad (3.2)$$

which represents a quantum system with p levels, each having a spin degeneracy of two. A common choice for single-particle states are eigenstates of the Hartree-Fock operator, $(\hat{u} + \hat{u}_{\text{HF}}) |p\rangle = \epsilon_p |p\rangle$. In the pairing model, this condition is already fulfilled. We define the states below the Fermi level as holes and redefine the single-particle energies,

$$\epsilon_q = h_{qq} + \sum_i \langle qi | \hat{v} | qi \rangle. \quad (3.3)$$

To be more specific, let us look at the pairing model with four particles and eight single-particle states. These states (with $\delta = 1.0$) could be labeled as shown in Table 3.1. The Hamiltonian matrix for this four-particle problem with no broken pairs is defined by six possible Slater determinants, one representing the ground state and zero-particle-zero-hole excitations $0p-0h$, four representing various $2p-2h$ excitations and finally one representing a $4p-4h$ excitation. Ignoring Slater determinants with broken pairs, this problem is then

Table 3.1: Single-particle states and their quantum numbers and their energies from Eq. (3.3). The degeneracy for every quantum number p is equal to two due to the two possible spin values.

State Label	p	$2s_z$	E	type
0	1	1	$-g/2$	hole
1	1	-1	$-g/2$	hole
2	2	1	$1-g/2$	hole
3	2	-1	$1-g/2$	hole
4	3	1	2	particle
5	3	-1	2	particle
6	4	1	3	particle
7	4	-1	3	particle

represented by the Hamiltonian matrix

$$H = \begin{bmatrix} 2\delta - g & -g/2 & -g/2 & -g/2 & -g/2 & 0 \\ -g/2 & 4\delta - g & -g/2 & -g/2 & -0 & -g/2 \\ -g/2 & -g/2 & 6\delta - g & 0 & -g/2 & -g/2 \\ -g/2 & -g/2 & 0 & 6\delta - g & -g/2 & -g/2 \\ -g/2 & 0 & -g/2 & -g/2 & 8\delta - g & -g/2 \\ 0 & -g/2 & -g/2 & -g/2 & -g/2 & 10\delta - g \end{bmatrix}. \quad (3.4)$$

Here, the exact eigenvalues can be found by diagonalizing this small matrix. Additionally, it is easy to calculate low orders of many-body perturbation theory analytically. This is a very useful check of the numerical implementation since this analytical expression can also be used to check our coupled cluster implementation as described in Chapter 4. As a reminder, the expression for the correlation energy for MBPT(2) is

$$\Delta E_{MBPT2} = \frac{1}{4} \sum_{abij} \frac{\langle ij|\hat{v}|ab\rangle \langle ab|\hat{v}|ij\rangle}{\epsilon_{ij}^{ab}} = \sum_{a<b, i<j} \frac{\langle ij|\hat{v}|ab\rangle \langle ab|\hat{v}|ij\rangle}{\epsilon_{ij}^{ab}}. \quad (3.5)$$

Additionally, we look at many-body perturbation theory at third order (MBPT(3)) which is given by the expression

$$\Delta E_{MBPT3} = \Delta E_{MBPT2} + \frac{1}{8} \sum_{abcdij} \frac{\langle ij|\hat{v}|ab\rangle \langle ab|\hat{v}|cd\rangle \langle cd|\hat{v}|ij\rangle}{\epsilon_{ij}^{ab} \epsilon_{ij}^{cd}} + \frac{1}{8} \sum_{abijkl} \frac{\langle ab|\hat{v}|kl\rangle \langle kl|\hat{v}|ij\rangle \langle ij|\hat{v}|ab\rangle}{\epsilon_{ij}^{ab} \epsilon_{kl}^{ab}}. \quad (3.6)$$

For our pairing example we obtain the following result

$$\Delta E_{MBPT2} = \frac{\langle 01|\hat{v}|45\rangle^2}{\epsilon_{01}^{45}} + \frac{\langle 01|\hat{v}|67\rangle^2}{\epsilon_{01}^{67}} + \frac{\langle 23|\hat{v}|45\rangle^2}{\epsilon_{23}^{45}} + \frac{\langle 23|\hat{v}|67\rangle^2}{\epsilon_{23}^{67}}, \quad (3.7)$$

which translates into

$$\Delta E_{MBPT2} = -\frac{g^2}{4} \left(\frac{1}{4+g} + \frac{1}{6+g} + \frac{1}{2+g} + \frac{1}{4+g} \right). \quad (3.8)$$

Figure 3.1 shows the resulting correlation energies for the exact case, MBPT2 and MBPT3. In Fig. 3.1 we see that the approximation to both second and third order are very good when the interaction strength is small and contained in the interval $g \in [-0.5, 0.5]$, but as the interaction gets stronger in absolute value the agreement with the exact reference energy for MBPT2 and MBPT3 worsens. We also note that the third-order result is actually worse than the second order result for larger values of the interaction strength, indicating that there is no guarantee that higher orders in many-body perturbation theory may reduce the relative error in a systematic way. The disagreement when the interaction strength increases hints at the possibility that many-body perturbation theory may not converge order by order. Also note the non-variational character of many-body perturbation theory, with results at different levels of many-body perturbation theory either overshooting or undershooting the

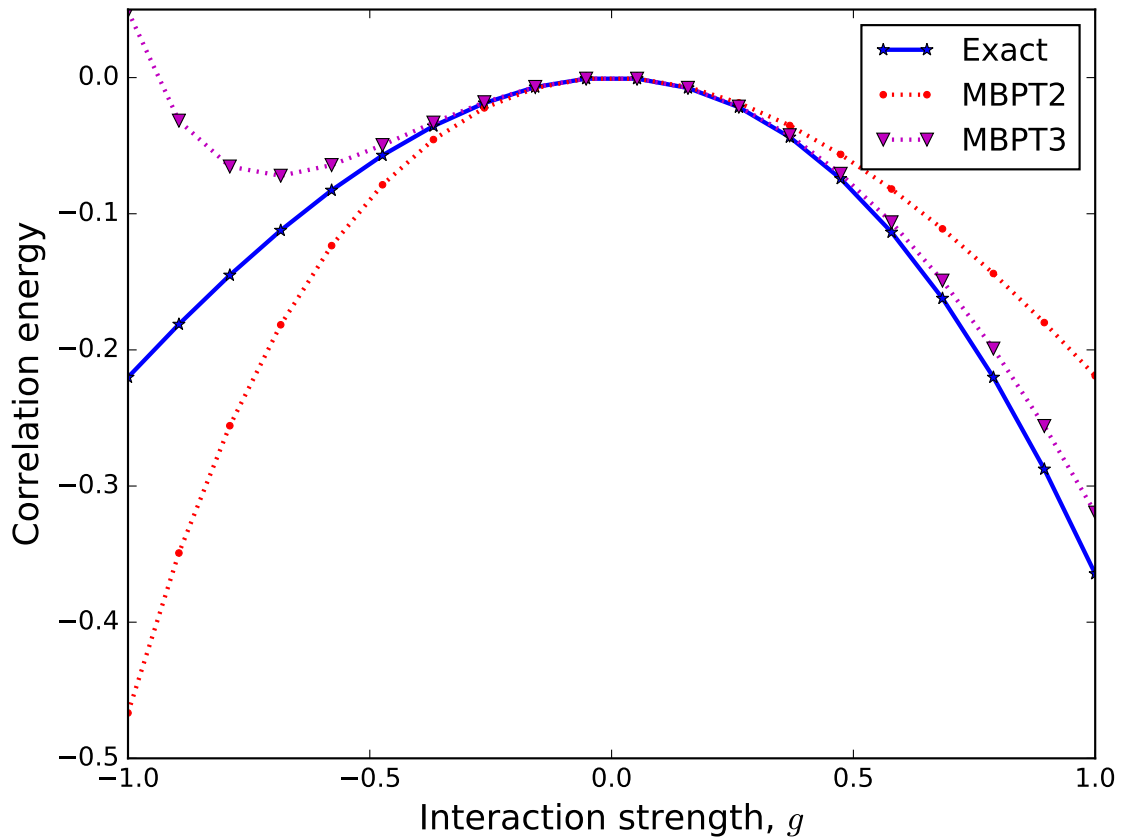


Figure 3.1: Correlation energy for the pairing model with exact diagonalization, MBPT2 and perturbation theory to third order MBPT3 for a range of interaction values. A canonical Hartree-Fock basis has been employed in all MBPT calculations.

true ground state correlation energy.

3.2 Single-Particle Basis for Infinite Fermionic Matter

Neutron stars are several kilometers across, but supported by the purely quantum phenomenon of Fermi statistics. Studying systems that span from 10^4m to 10^{-15}m [1] is a task that is certainly impossible from an *ab initio* perspective. However, the short range of the nucleon-nucleon interaction allows us to study a small slab of this matter to determine properties of the bulk. This matter is self bound, but unlike atomic nuclei, the nucleons are bound gravitationally which presents a considerable problem as a quantum theory of gravity is debatably the largest unsolved problem in physics. However, we can work around this problem by forcing the nucleons together via an external density (ρ) parameter. Once the neutrons are fixed to a particular density to simulate the gravitational environment, there is no external potential. This means that the one-body piece of the Hamiltonian is just the kinetic energy operator $\hat{p}^2/2m$, for which the eigenstates are free particles, represented mathematically by plane waves. These basis states are infinite in their spatial extent, making them difficult to work with, so the plane waves are put into a finite box, discretizing the spectrum. These one-particle wave functions are normalized to a volume Ω for a box with length L (the limit $L \rightarrow \infty$ is to be taken after we have computed various expectation values)

$$\psi_{\mathbf{k}\sigma}(\mathbf{r}) = \frac{1}{\sqrt{\Omega}} \exp(i\mathbf{k}\mathbf{r})\xi_{\sigma}, \quad (3.9)$$

where \mathbf{k} is the wave number and ξ_σ is the spin function for either spin up or down nucleons

$$\xi_{\sigma=+1/2} = \begin{pmatrix} 1 \\ 0 \end{pmatrix} \quad \xi_{\sigma=-1/2} = \begin{pmatrix} 0 \\ 1 \end{pmatrix}. \quad (3.10)$$

We assume that we have periodic boundary conditions ($\Psi(0) = e^{i\theta}\Psi(L)$) which limit the allowed wave numbers to

$$k_i = \frac{2\pi n_i}{L}, \quad i = x, y, z, \quad n_i \in \mathbb{Z}. \quad (3.11)$$

The operator for the kinetic energy can be written as

$$\hat{T} = \sum_{\mathbf{p}\sigma_p} \frac{\hbar^2 k_p^2}{2m} a_{\mathbf{p}\sigma_p}^\dagger a_{\mathbf{p}\sigma_p}. \quad (3.12)$$

When using periodic boundary conditions, the discrete-momentum single-particle basis functions (excluding spin and/or isospin degrees of freedom) result in the following single-particle energy

$$\varepsilon_{n_x, n_y, n_z} = \frac{\hbar^2}{2m} \left(\frac{2\pi}{L} \right)^2 (n_x^2 + n_y^2 + n_z^2) = \frac{\hbar^2}{2m} (k_{n_x}^2 + k_{n_y}^2 + k_{n_z}^2),$$

for a three-dimensional system with

$$k_{n_i} = \frac{2\pi n_i}{L}, \quad n_i \in \mathbb{Z}. \quad (3.13)$$

We will select the single-particle basis such that both the occupied and unoccupied single-particle states have a closed-shell structure. This means that all single-particle states cor-

responding to energies below a chosen cutoff are included in the basis. With the kinetic energy rewritten in terms of the discretized momenta we can set up a list (assuming identical particles and including spin up and spin down solutions) of single-particle energies with momentum quantum numbers such that $n_x^2 + n_y^2 + n_z^2 \leq 3$, as shown, for example, in Table 3.2.

Continuing in this way we get for $n_x^2 + n_y^2 + n_z^2 = 4$ a total of 12 additional states, resulting in 66 as a new magic number. For the lowest six energy values the degeneracy in energy gives us 2, 14, 38, 54, 66 and 114 as magic numbers. Each many-body calculation has an energy cutoff and a magic number determining how many particles are in the simulation, and a second magic number determining how many unoccupied single-particles states span the finite Hilbert space. If we wish to study infinite nuclear matter with both protons and neutrons, the above magic numbers become 4, 28, 76, 108, 132, 228, \dots .

Once the number of particles in the simulation are determined and a density ρ has been selected the Fermi momentum k_F of the system is determined via

$$\rho = g \frac{k_F^3}{6\pi^2}, \quad (3.14)$$

where g is the degeneracy, which is two for one type of spin-1/2 particles and four for symmetric nuclear matter. From here we can define the length L of the box used with periodic boundary contributions via the relation

$$V = L^3 = \frac{A}{\rho}, \quad (3.15)$$

where A is the number of nucleons. If we deal with the electron gas only, this needs to be

Table 3.2: Total number of particle filling $N_{\uparrow\downarrow}$ for various $n_x^2+n_y^2+n_z^2$ values for one spin-1/2 fermion species. Borrowing from nuclear shell-model terminology, filled shells correspond to all single-particle states for one $n_x^2+n_y^2+n_z^2$ value being occupied. For matter with both protons and neutrons, the filling degree increased with a factor of 2.

$n_x^2+n_y^2+n_z^2$	n_x	n_y	n_z	$N_{\uparrow\downarrow}$
0	0	0	0	2
1	-1	0	0	
1	1	0	0	
1	0	-1	0	
1	0	1	0	
1	0	0	-1	
1	0	0	1	14
2	-1	-1	0	
2	-1	1	0	
2	1	-1	0	
2	1	1	0	
2	-1	0	-1	
2	-1	0	1	
2	1	0	-1	
2	1	0	1	
2	0	-1	-1	
2	0	-1	1	
2	0	1	-1	
2	0	1	1	38
3	-1	-1	-1	
3	-1	-1	1	
3	-1	1	-1	
3	-1	1	1	
3	1	-1	-1	
3	1	-1	1	
3	1	1	-1	
3	1	1	1	54

replaced by the number of electrons N .

3.3 Two-Nucleon Interaction

As mentioned above, we will employ a plane wave basis for our calculations of infinite matter properties. With a Cartesian basis we can directly calculate the various matrix elements. However, a discrete and finite Cartesian basis represents an approximation to the thermodynamical limit. In order to compare the stability of our basis with results from the thermodynamical limit, it is convenient to rewrite the nucleon-nucleon interaction in terms of a partial wave expansion. This will allow us to compute the Hartree-Fock energy of the ground state in the thermodynamical limit (with the caveat that we need to limit the number of partial waves). In order to find the expressions for the Hartree-Fock energy in a partial wave basis, we will find it convenient to rewrite our two-body force in terms of the relative and center-of-mass motion momenta.

The direct matrix element, with single-particle three-dimensional momenta \mathbf{k}_p , spin σ_p and isospin τ_p , is defined as

$$\langle \mathbf{k}_p \sigma_p \tau_p \mathbf{k}_q \sigma_q \tau_q | \hat{v} | \mathbf{k}_r \sigma_r \tau_r \mathbf{k}_s \sigma_s \tau_s \rangle, \quad (3.16)$$

or in a more compact form as $\langle \mathbf{p} \mathbf{q} | \hat{v} | \mathbf{r} \mathbf{s} \rangle$ where the boldfaced letters \mathbf{p} etc represent the relevant quantum numbers, here momentum, spin and isospin. Introducing the relative momentum

$$\mathbf{k} = \frac{1}{2} (\mathbf{k}_p - \mathbf{k}_q), \quad (3.17)$$

and the center-of-mass momentum

$$\mathbf{K} = \mathbf{k}_p + \mathbf{k}_q, \quad (3.18)$$

we have

$$\langle \mathbf{k}_p \sigma_p \tau_p \mathbf{k}_q \sigma_q \tau_q | \hat{v} | \mathbf{k}_r \sigma_r \tau_r \mathbf{k}_s \sigma_s \tau_s \rangle = \langle \mathbf{k} \mathbf{K} \sigma_p \tau_p \sigma_q \tau_q | \hat{v} | \mathbf{k}' \mathbf{K}' \sigma_r \tau_r \sigma_s \tau_s \rangle. \quad (3.19)$$

The nucleon-nucleon interaction conserves the total momentum and charge, implying that the above uncoupled matrix element reads

$$\langle \mathbf{k} \mathbf{K} \sigma_p \tau_p \sigma_q \tau_q | \hat{v} | \mathbf{k}' \mathbf{K}' \sigma_r \tau_r \sigma_s \tau_s \rangle = \delta_{T_z, T'_z} \delta(\mathbf{K} - \mathbf{K}') \langle \mathbf{k} T_z S_z = (\sigma_a + \sigma_b) | \hat{v} | \mathbf{k}' T_z S'_z = (\sigma_c + \sigma_d) \rangle, \quad (3.20)$$

where we have defined the isospin projections $T_z = \tau_p + \tau_q$ and $T'_z = \tau_r + \tau_s$. Defining $\hat{v} = \hat{v}(\mathbf{k}, \mathbf{k}')$, we can rewrite the previous equation in a more compact form as

$$\delta_{T_z, T'_z} \delta(\mathbf{K} - \mathbf{K}') \langle \mathbf{k} T_z S_z = (\sigma_p + \sigma_q) | \hat{v} | \mathbf{k}' T_z S'_z = (\sigma_r + \sigma_s) \rangle = \delta_{T_z, T'_z} \delta(\mathbf{K} - \mathbf{K}') \langle T_z S_z | \hat{v}(\mathbf{k}, \mathbf{k}') | T_z S'_z \rangle. \quad (3.21)$$

These matrix elements can in turn be rewritten in terms of the total two-body quantum numbers for the spin S of two spin-1/2 fermions as

$$\langle \mathbf{k} T_z S_z | \hat{v}(\mathbf{k}, \mathbf{k}') | \mathbf{k}' T_z S'_z \rangle = \sum_{SS'} \langle \frac{1}{2} \sigma_p \frac{1}{2} \sigma_q | S S_z \rangle \langle \frac{1}{2} \sigma_r \frac{1}{2} \sigma_s | S' S'_z \rangle \langle \mathbf{k} T_z S S_z | \hat{v}(\mathbf{k}, \mathbf{k}') | \mathbf{k} T_z S' S'_z \rangle. \quad (3.22)$$

The coefficients $\langle \frac{1}{2} \sigma_p \frac{1}{2} \sigma_q | S S_z \rangle$ are so-called Clebsch-Gordan recoupling coefficients. We will assume that our interactions conserve charge. We will refer to $T_z = 0$ as the pn (proton-

neutron) channel, $T_z = -1$ as the pp (proton-proton) channel and $T_z = 1$ as the nn (neutron-neutron) channel.

The nucleon-nucleon force is often derived and analyzed theoretically in terms of a partial wave expansion. A state with linear momentum \mathbf{k} can be written in terms of spherical harmonics Y_{lm} as

$$|\mathbf{k}\rangle = \sum_{l=0}^{\infty} \sum_{m=-l}^l i^l Y_{lm}(\hat{\mathbf{k}}|klm_l\rangle. \quad (3.23)$$

In terms of the relative and center-of-mass momenta \mathbf{k} and \mathbf{K} , the potential in momentum space is related to the nonlocal operator $V(\mathbf{r}, \mathbf{r}')$ by

$$\langle \mathbf{k}'\mathbf{K}'|\hat{v}|\mathbf{k}\mathbf{K}\rangle = \int d\mathbf{r}d\mathbf{r}' e^{-i\mathbf{k}'\mathbf{r}'} V(\mathbf{r}', \mathbf{r}) e^{i\mathbf{k}\mathbf{r}} \delta(\mathbf{K}, \mathbf{K}'). \quad (3.24)$$

We will assume that the interaction is spherically symmetric and use the partial wave expansion of the plane waves in terms of spherical harmonics. This means that we can separate the radial part of the wave function from its angular dependence. The wave function of the relative motion is described in terms of plane waves as

$$e^{i\mathbf{k}\mathbf{r}} = \langle \mathbf{r}|\mathbf{k}\rangle = 4\pi \sum_{lm} i^l j_l(kr) Y_{lm}^*(\hat{\mathbf{k}}) Y_{lm}(\hat{\mathbf{r}}), \quad (3.25)$$

where j_l is a spherical Bessel function and Y_{lm} the spherical harmonic. This partial wave basis is useful for defining the operator for the nucleon-nucleon interaction, which is symmetric with respect to rotations, parity and isospin transformations. These symmetries imply that the interaction is diagonal with respect to the quantum numbers of total angular momentum J , spin S and isospin T . Using the above plane wave expansion, and coupling to final J, S

and T we get

$$\langle \mathbf{k}' | V | \mathbf{k} \rangle = (4\pi)^2 \sum_{JM} \sum_{lm} \sum_{l'm'} i^{l+l'} Y_{lm}^*(\hat{\mathbf{k}}) Y_{l'm'}(\hat{\mathbf{k}}') C_{m'M_{SM}}^{l'SJ} C_{mM_{SM}}^{lSJ} \langle k'l'STJM | V | klSTJM \rangle, \quad (3.26)$$

where we have defined

$$\langle k'l'STJM | V | klSTJM \rangle = \int j_{\nu}(k'r') \langle l'STJM | V(r', r) | lSTJM \rangle j_l(kr) r'^2 dr' r^2 dr. \quad (3.27)$$

We have omitted the momentum of the center-of-mass motion \mathbf{K} and the corresponding orbital momentum L , since the interaction is diagonal in these variables.

The interaction we will use for these calculations is a semirealistic nucleon-nucleon potential known as the Minnesota potential [53] which has the form, $V_{\alpha}(r) = V_{\alpha} \exp(-\alpha r^2)$.

The spin and isospin dependence of the Minnesota potential is given by,

$$V(r) = \frac{1}{2} \left(V_R + \frac{1}{2} (1 + P_{12}^{\sigma}) V_T + \frac{1}{2} (1 - P_{12}^{\sigma}) V_S \right) (1 - P_{12}^{\sigma} P_{12}^{\tau}), \quad (3.28)$$

where $P_{12}^{\sigma} = \frac{1}{2} (1 + \sigma_1 \cdot \sigma_2)$ and $P_{12}^{\tau} = \frac{1}{2} (1 + \tau_1 \cdot \tau_2)$ are the spin and isospin exchange operators, respectively. A Fourier transform to momentum space of the radial part $V_{\alpha}(r)$ is rather simple, since the radial depends only on the magnitude of the relative distance and thereby the relative momentum $\vec{q} = \frac{1}{2} (\vec{k}_p - \vec{k}_q - \vec{k}_r + \vec{k}_s)$. Omitting spin and isospin dependencies, the momentum space version of the interaction reads

$$\langle \mathbf{k}_p \mathbf{k}_q | V_{\alpha} | \mathbf{k}_r \mathbf{k}_s \rangle = \frac{V_{\alpha}}{L^3} \left(\frac{\pi}{\alpha} \right)^{3/2} \exp\left(\frac{-q^2}{4\alpha}\right) \delta_{\vec{k}_p + \vec{k}_q, \vec{k}_r + \vec{k}_s}. \quad (3.29)$$

The various parameters defining the interaction model used in this work are listed in Table

Table 3.3: Parameters used to define the Minnesota interaction model [53].

α	V_α in MeV	κ_α in fm^{-2}
R	200	1.487
T	178	0.639
S	91.85	0.465

3.3.

3.4 Homogeneous Electron Gas

From a numerical calculation perspective, once the tools have been developed to compute properties it is not too difficult to compute properties of other infinite matter systems. In this case, properties of the homogeneous electron gas (HEG) can be examined using a similar prescription as infinite nuclear matter. The plane wave basis and periodic boundary conditions can once again be used to simulate an infinite gas of electrons interacting in a uniform positive background charge to keep the system charge neutral on average. There are a few differences, the first of which is that the mass of the particles is different and so the single particle energies will differ. Next is more of a cultural shift, in that it is typical to describe the density of electrons in terms of the dimensionless Wigner-Seitz radius r_s as an input parameter defined by

$$r_s = \frac{r_0}{r_b}, \quad (3.30)$$

where $r_b = \hbar / m_e c \alpha$ is the Bohr radius and r_0 can be used to define the box size L by

$$\frac{4}{3}\pi r_0^3 = \frac{N}{L^3}. \quad (3.31)$$

The electron-electron interaction is given by the Coulomb interaction which conserves total linear momentum and total spin projection such that

$$\vec{q} = \vec{k}_p + \vec{k}_q = \vec{k}_r + \vec{k}_s, \quad s_{z_p} + s_{z_q} = s_{z_r} + s_{z_s}. \quad (3.32)$$

Any matrix element which breaks these symmetries must be zero, otherwise the matrix elements expressed in momentum space are given by

$$\langle pq|\hat{v}|rs\rangle = \frac{e^2}{L^3} \frac{1}{q^2}. \quad (3.33)$$

The divergence at $q = 0$ is avoided by clever cancellation with the energy of the uniform positive background charge, as shown in reference [30].

Chapter 4

Coupled Cluster

4.1 Prologue to Coupled Cluster

The previous chapter laid out much of the machinery that is useful for quantum many-body theory, and a few many-body methods like full configuration interaction (FCI)[8, 9, 10, 11], Hartree-Fock (HF) [35, 36], and in-medium similarity renormalization group (IM-SRG) [50, 42, 43, 44, 45]. With this groundwork laid we are in a good position to derivate coupled cluster (CC) theory. Coupled cluster theory is another approach to solving the many-body Schrödinger equation in the same vein as configuration interaction from the previous chapter, except with a different scheme for organizing the excitations. In the FCI scheme, any many-body state can be written with respect to a reference state as:

$$|\Psi^{FCI}\rangle = C_0 |\Phi_0\rangle + \sum_{i,a} C_i^a |\Phi_i^a\rangle + \sum_{i,j,a,b} C_{ij}^{ab} |\Phi_{ij}^{ab}\rangle + \cdots + \sum_{\substack{i_1, i_2, \dots, i_A \\ a_1, a_2, \dots, a_A}} C_{i_1 i_2 \dots i_A}^{a_1 a_2 \dots a_A} |\Phi_{i_1 i_2 \dots i_A}^{a_1 a_2 \dots a_A}\rangle, \quad (4.1)$$

where the overlap coefficients are defined as

$$C_{i_1 i_2 \dots i_A}^{a_1 a_2 \dots a_A} = \langle \Psi^{FCI} | \Phi_{i_1 i_2 \dots i_A}^{a_1 a_2 \dots a_A} \rangle. \quad (4.2)$$

This is really just the statement that any state can be represented as a linear combination of Slater determinants, which is a complete A -body basis as discussed last chapter. The first approximation to this complete solution is to find a finite cutoff M for the infinite single-particle basis. This must always be done, as there is no way to finish this calculation on a computer if the particle state index a is summing to infinity. Once the single-particle basis has been truncated, the above expression gives the exact answer in this subspace, as FCI includes all Slater determinants up to A -body excitations, at which point the series naturally truncates. However, this is prohibitively expensive, scaling factorially with respect to the single-particle basis since there are $\binom{M}{A}$ Slater determinants in this many-body basis. The next natural approximation is to start excluding certain Slater determinants. For example, if only singles and doubles excitations are included, then we get the configuration interaction singles doubles (CISD) approximation, which is expressed as

$$|\Psi^{CISD}\rangle = C_0 |\Phi_0\rangle + \sum_{i,a} C_i^a |\Phi_i^a\rangle + \sum_{i,j,a,b} C_{ij}^{ab} |\Phi_{ij}^{ab}\rangle. \quad (4.3)$$

While this is a conceptually nice place to truncate the series, it turns to be a pretty poor way to include correlations into the target many-body state. This is where coupled cluster (CC) theory has made its mark in the many-body community. Coupled cluster theory is a way to organize the many-body basis such that the natural truncations lead to very accurate calculations for relatively low computational cost. Originally developed in the 1950's by Coester [17, 18] and Kümmel [19], CC saw some success solving problems for nuclear physics. Unfortunately, the nucleon-nucleon interactions of the 50's required large single-particle bases to converge, and the computers of the day weren't powerful enough for CC to find much success. However, CC was reformulated in the 60's by Čížek *et al.*, for use in

electronic systems [12, 13, 14]. This proved to work magnificently, as coupled cluster theory saw enormous success with the interaction of electrons and underwent rapid development over the next several decades [54, 55, 15]. Fast forward to today, CC is referred to as the “gold standard” for precise quantum chemistry calculations.

After the developmental boom in quantum chemistry, nucleon-nucleon interactions gradually became more suitable to *ab initio* methods leading to its readoption in nuclear physics in the early to mid-2000’s [56, 57, 58, 59]. Today, improved nuclear forces softened by similarity renormalization group (SRG) [4, 5], greater computational power, and improved many-body techniques have created an environment for CC theory to thrive in nuclear physics.

To first understand coupled cluster theory, it might help to first look at the Thouless theorem. The Thouless theorem states that any Slater determinant $|\Phi_0\rangle$ can be transformed to any other Slater determinant $|\Phi\rangle$ that isn’t orthogonal to the original by

$$|\Phi\rangle = e^{\hat{T}_1} |\Phi_0\rangle \quad (4.4)$$

$$\hat{T}_1 = \sum_{i,a} t_i^a \hat{a}^\dagger \hat{i}, \quad (4.5)$$

where the coefficients t_i^a are uniquely determined [60]. The exponential of this one-particle one-hole operator \hat{T}_1 is referred to as the operator exponential, and is written out as the infinite series

$$e^{\hat{T}_1} = \sum_{k=0}^{\infty} \frac{1}{k!} \hat{T}_1^k = 1 + \hat{T}_1 + \frac{1}{2} \hat{T}_1^2 + \dots, \quad (4.6)$$

where $\hat{T}_1^2 = \hat{T}_1 \hat{T}_1$ is just the repeated action of the operator on a state. As a notational remark, in this chapter ket states with the capital Greek letter $|\Phi\rangle$ will refer only to a single Slater determinant, but ket states with the capital Greek letter $|\Psi\rangle$ can refer to any many-

body state. Also, matrix elements will be written both as t_i^a and $\langle a|\hat{t}|i\rangle$ whenever either is more convenient, but they refer to the same object.

The Thouless theorem is very powerful, but is limited in that this exponentiated operator can only take a single product state to another product state. If we expand this operator to take into account higher order excitations, we can generate higher order correlations. This is the famous exponential ansatz of coupled cluster theory:

$$|\Psi\rangle = e^{\hat{T}} |\Phi\rangle \quad (4.7)$$

$$\hat{T}^{(A)} = \sum_{n=1}^A \hat{T}_n \quad (4.8)$$

$$\hat{T}_n = \frac{1}{(A!)^2} \sum_{\substack{i_1, i_2, \dots, i_A \\ a_1, a_2, \dots, a_A}} t_{i_1 i_2 \dots i_A}^{a_1 a_2 \dots a_A} \hat{a}_1^\dagger \hat{a}_2^\dagger \dots \hat{a}_A^\dagger \hat{i}_A \dots \hat{i}_2 \hat{i}_1. \quad (4.9)$$

By including every excitation up to A -body excitations, any many-body state $|\Psi\rangle$ can be generated by finding the appropriate operator coefficients t applied to a reference state $|\Phi\rangle$ which is non-orthogonal to the target state. If any non-orthogonal many-body state can be found, then this must be quite similar to the FCI statement which is similarly just a linear combination of excitations of some reference state. Since this is just another complete many-body space, it is natural to ask why this formulation is any better than FCI. The answer lies in the fact that truncating CC theory at a given order brings in many additional many-body correlations for a similar cost than FCI at the corresponding CI truncation. This is due to the rich structure generated by the cross terms of the exponential,

$$\begin{aligned} e^{\hat{T}} &= 1 + (\hat{T}_1 + \hat{T}_2 + \dots) + \frac{1}{2}(\hat{T}_1 + \hat{T}_2 + \dots)^2 + \dots \\ &= 1 + \hat{T}_1 + \hat{T}_2 + \dots + \frac{1}{2}\hat{T}_1^2 + \hat{T}_1\hat{T}_2 + \frac{1}{2}\hat{T}_2^2 + \dots \end{aligned}$$

where terms like $\hat{T}_1\hat{T}_2$ do not appear in CI with only singles and doubles excitations. By comparing excitation levels, we can write down what various levels of CI equal in CC theory

$$\hat{C}_1 = \hat{T}_1, \quad (4.10)$$

$$\hat{C}_2 = \hat{T}_2 + \frac{1}{2}\hat{T}_1^2, \quad (4.11)$$

$$\hat{C}_3 = \hat{T}_3 + \hat{T}_1\hat{T}_2 + \frac{1}{6}\hat{T}_1^3. \quad (4.12)$$

This shows which terms of CC theory CISDT (single, doubles and triples excitations) recovers, whereas just CCD accounts for $\hat{T}_2, \hat{T}_2^3, \hat{T}_2^4 \dots$ excitations up to infinite order. These non-linear contributions of the excitation operators generally leads CC (for example CCSD) to recover more correlations than CI at the same level of excitation (for example CISD). The full details of how coupled cluster theory works will not be explained in this chapter, but given a few assumptions, we can derive a working set of equations with which to calculate properties of many-body systems [16].

4.2 Coupled Cluster Theory

The normal-ordered many-body Schrödinger equation can be expressed using the exponential ansatz as

$$\hat{H}_N |\Psi\rangle = \hat{H}_N e^{\hat{T}} |\Phi_0\rangle = \Delta E e^{\hat{T}} |\Phi_0\rangle, \quad (4.13)$$

where $|\Phi_0\rangle$ again is our reference Slater determinant, and $|\Psi\rangle$ is the ground state eigenstate of an A -body Hamiltonian of interest. Then we can get the ground state energy by projecting

Eqn. (4.13) onto $\langle \Psi |$ which gives

$$\Delta E_0 = \langle \Psi | \hat{H}_N | \Psi \rangle = \langle \Phi_0 | e^{-\hat{T}} \hat{H}_N e^{\hat{T}} | \Phi_0 \rangle = \langle \Phi_0 | \bar{H}_N | \Phi_0 \rangle, \quad (4.14)$$

where we have defined the normal-ordered *coupled cluster effective Hamiltonian*

$$\bar{H} \equiv e^{-\hat{T}} \hat{H}_N e^{\hat{T}}. \quad (4.15)$$

If we can find a way to determine the coefficients of \hat{T} , then we immediately have a prescription for finding the group state energy. An important aspect of CC theory is that the excitation operator \hat{T} , is not Hermitian, which as explained in Chapter 2 ensures that $e^{\hat{T}}$ is not a unitary operator. This means that Eqn. (4.15) describes a non-unitary similarity transformation. This has some inconvenient consequences, such that CC theory is not variational (where the approximate ground state energy always approaches the true ground state energy from above), but for much of the work presented here, this is not a problem, as a similarity transformation preserves the eigenvalue spectrum of the operator, which is what we are after.

We can apply the Baker-Campbell-Hausdorff expansion to the similarity transform to gain an explicit expression for \bar{H} as

$$\bar{H} = e^{-\hat{T}} \hat{H}_N e^{\hat{T}} = \hat{H}_N + [\hat{H}_N, \hat{T}] + \frac{1}{2} [[\hat{H}_N, \hat{T}], \hat{T}] + \frac{1}{3!} [[[[\hat{H}_N, \hat{T}], \hat{T}], \hat{T}], \hat{T}] + \dots \quad (4.16)$$

One can show that this series naturally terminates [16]. The basic reason is that applying the generalized Wick's theorem to this expression cancels out the vast majority of the terms.

Only terms which start with \hat{H}_N on the left, and are contracted with this term survive.

$$\begin{aligned}
\bar{H} &= e^{-\hat{T}} \hat{H}_N e^{\hat{T}} \\
&= \hat{H}_N + \overbrace{\hat{H}_N \hat{T}} + \overbrace{\hat{H}_N \hat{T} \hat{T}} + \overbrace{\hat{H}_N \hat{T} \hat{T} \hat{T}} + \overbrace{\hat{H}_N \hat{T} \hat{T} \hat{T} \hat{T}} \\
&= \left(\hat{H}_N e^{\hat{T}} \right)_C,
\end{aligned} \tag{4.17}$$

where the contraction symbol represents the sum over all the ways each of the operators can be contracted together and the C subscript stands for “connected”, meaning that only terms which connect to \hat{H}_N via a contraction survive. The reason that this expression terminates at four contractions, is that we are assuming the Hamiltonian to have at most two-body forces, and thus only two creation and two annihilation operators. This leaves only four operators to contract with, so there can be no further terms. However, in nuclear theory, three-body and higher-body forces are often needed, which will add to the amount of contractions available. This is quite amazing, since the exponential of the excitation operator has contributions up to infinite order of powers of \hat{T} , and naturally terminates without any approximation. Other approximations will need to be made down the road, but this fact is where much of the power of CC theory resides.

We can now write the CC correlation energy as the connected form of the Schrödinger equation

$$\langle \Phi_0 | (\hat{H}_N e^{\hat{T}})_C | \Phi_0 \rangle = \Delta E, \tag{4.18}$$

by projecting onto the reference state $\langle \Phi_0 |$. We can also project the Schrödinger equation onto any of the orthogonal excitations from the reference state

$$\langle \Phi_{ij\dots}^{ab\dots} | (\hat{H}_N e^{\hat{T}})_C | \Phi_0 \rangle = 0. \tag{4.19}$$

Since we need the t -amplitudes of the excitation operator to calculate the correlation energy, we can project onto as many excitations as necessary to generate as many equations as we have unknowns.

4.3 Coupled Cluster Diagrams

To actually generate the CC equations from Eqn. (4.18) and Eqn. (4.19) would require an enormous amount of algebra. Even with the incredible reduction in complexity of the generalized Wick's theorem, carrying out these operations is very time consuming and prone to error. In Quantum Field Theory, the use of pictorial Feynman diagrams are an essential tool for handling otherwise unwieldy algebraic expressions of Wick's theorem in a time-dependent framework. In CC theory, the use of time-independent Bradow diagrams are used in a similar way to handle the Wick's theorem expressions necessary to generate the CC equations.

Plugging in a normal-ordered one and two-body force for the Hamiltonian $\hat{H}_N = \hat{F}_N + \hat{V}_N$ into the energy equation (4.18) yields

$$\Delta E = \langle \Phi_0 | (F_N T_1)_c | \Phi_0 \rangle + \langle \Phi_0 | (V_N T_2)_c | \Phi_0 \rangle + \frac{1}{2} \langle \Phi_0 | (V_N T_1^2)_c | \Phi_0 \rangle. \quad (4.20)$$

To represent these expressions diagrammatically, we start with the reference state $|\Phi_0\rangle$ as our blank canvas since all of the necessary expressions are being applied to this state. Next, excitations applied to the reference state are drawn as lines, with upward lines representing particle states and downward lines representing hole states

$$|\Phi_i^a\rangle = \begin{array}{c} \uparrow a \quad i \downarrow \\ | \\ | \end{array} \quad |\Phi_{ij}^{ab}\rangle = \begin{array}{c} \uparrow a i \downarrow \quad \uparrow b j \downarrow \\ | \quad | \quad | \quad | \end{array} \quad (4.21)$$

where these diagrams are read from bottom to top. So the reference state $|\Phi_0\rangle$ is at the bottom, and undergoes a one-particle one-hole excitation moving towards the top of the diagram. The notation of the arrows is borrowed from Quantum Field Theory where anti-particles can be thought of as the time-reversal form of their corresponding particle, and so move backwards in time. Here, the hole states can be thought of as the anti-particle to the particle states, and the arrow direction is reversed. Next, the one-body excitation operator \hat{T}_1 is drawn as a one-particle one-hole excitation originating from an open circle, and the two-body two-hole excitation operator \hat{T}_2 is drawn as black line from which the particle and hole lines come from

$$\hat{T}_1 = \sum_{i,a} \langle a|\hat{t}|i\rangle \hat{a}^\dagger \hat{i} : \quad \hat{T}_2 = \sum_{ijab} \langle ab|\hat{t}|ij\rangle \hat{a}^\dagger \hat{b}^\dagger \hat{j} \hat{i} : \quad (4.22)$$

These lines that extend from an operator and exit via the top of the diagram are called “external” lines, and indicate “live” operators which can be connected (contracted) against other operators above them. The fact that the \hat{T} operator’s lines only point up is capturing the fact that this is an excitation operator, and thus can only connect to operators above

it in the diagram, or algebraically, can only contract with operators applied after it (like $\widehat{H}_N \widehat{T}$). First, let's look at the one-body piece of the Hamiltonian \widehat{F}_N . Since this operator has one creation operator and one annihilation operator, it must have two lines associated with it. The diagrammatic symbol for the one-body operator will be two lines attached to a dark X by a dotted line

$$\widehat{F}_N = \sum_{pq} \langle p|\widehat{f}|q\rangle \{\widehat{p}^\dagger \widehat{q}\} = \begin{array}{c} | \\ \bullet \text{---} \times \end{array} . \quad (4.23)$$

The lines here do not have arrows, since p and q do not have a fixed particle or hole natures. This means that there are four different orientations of this diagram.

$$\sum_{ab} \langle a|\widehat{f}|b\rangle \{\widehat{a}^\dagger \widehat{b}\} = \begin{array}{c} \swarrow a \\ \bullet \text{---} \times \\ \searrow b \end{array} \quad \sum_{ij} \langle i|\widehat{f}|j\rangle \{\widehat{i}^\dagger \widehat{j}\} = \begin{array}{c} \swarrow j \\ \bullet \text{---} \times \\ \searrow i \end{array} \quad (4.24)$$

$$\sum_{ai} \langle a|\widehat{f}|i\rangle \{\widehat{a}^\dagger \widehat{i}\} = \begin{array}{c} \swarrow a \\ \swarrow i \\ \bullet \text{---} \times \end{array} \quad \sum_{ai} \langle i|\widehat{f}|a\rangle \{\widehat{i}^\dagger \widehat{a}\} = \begin{array}{c} \bullet \text{---} \times \\ \swarrow a \\ \searrow i \end{array} . \quad (4.25)$$

Only looking at the diagram, it might seem difficult to recover the algebraic expression, but there is a unique mapping looking at how the lines enter and exit the vertex. The matrix element associated with the one-body vertex will always be written as

$$\langle \text{index exiting} | \widehat{f} | \text{index entering} \rangle \quad (4.26)$$

and the corresponding operators are

$$\left\{ (\text{index exiting})^\dagger (\text{index entering}) \right\} \quad (4.27)$$

which provides a unique description of the operator. The sums are implied via the normal Einstein summation rules for repeated indices. Note that these terms can be described by whether they are an excitation, a de-excitation, or neither. The two terms in Eqn. (4.24) are neither excitations or de-excitations since the creation and annihilation operators do not change the particle-hole nature of the state. The first term in Eqn. (4.25) is an excitation operator, with lines extending out of the top of the diagram (like \hat{T}_1), and the second term is a de-excitation operator, with lines extending out of the bottom of the diagram.

The last operator we need is the two-body piece of the Hamiltonian \hat{V}_N , which is expressed diagrammatically as two vertices connected via a dotted line, with each vertex having one creation and one annihilation operator

$$\hat{V}_N = \sum_{pqrs} \langle pq|\hat{v}|rs\rangle \hat{p}^\dagger \hat{q}^\dagger \hat{s} \hat{r} = \begin{array}{c} | \quad | \\ \bullet \text{---} \bullet \\ | \quad | \end{array} . \quad (4.28)$$

The rules of this operator are very similar to \hat{F}_N , except now for four indices, they are uniquely mapped based on whether the lines are attached to the left vertex or the right vertex as

$$\langle \text{left-out right-out}|\hat{v}|\text{left-in right-out}\rangle . \quad (4.29)$$

Similarly, the operators are

$$\left\{ (\text{left-out})^\dagger (\text{right-out})^\dagger (\text{right-in}) (\text{left-in}) \right\}. \quad (4.30)$$

The last ingredient needed to diagrammatically perform Wick's theorem, is that of a contraction operation. Diagrammatically, this corresponds to joining the line from one diagram with a line from another diagram. This leads to a very intuitive set of consequences that exactly match up with Wick's theorem. Lines of opposite orientation cannot be joined, and an operator with k external lines can at most contract k times with other operators. Diagrams can be stretched and manipulated, while the indices and the entering and exiting line rules above keep track of just about everything. The part which is not so intuitive, which will not be derived here, is how to keep track of phases and weights. This will be detailed in a table below.

Let's look at a quick example of how to perform a contraction between the operators \hat{F}_N and \hat{T}_1 . Since \hat{T}_1 only has lines from above (due to it being an excitation operator), the operator \hat{F}_N must be placed above the operator. This corresponds algebraically to this operator being placed afterwards as $\hat{F}_N \overline{\hat{T}_1}$. Since these operators both have two external lines, either one or two connections can be made, corresponding to how only one or two contractions can be made between their creation and annihilation operators. There are

three topologically distinct ways in total to do this

(4.31)

Here, the first two terms would have the same topology if the orientation of the lines was not fixed by the particle or hole arrow. Regardless of how the arrows are oriented, the third term produces the same expression. In general, these techniques refer to what are called non-oriented Hugenholtz diagrams, and the oriented Brandow diagrams [33, 32, 61]. The Hugenholtz diagrams are useful for getting a grasp on the unique topologies available by connecting lines. From there, all of the various particle-hole orientations can be drawn to find the actual algebraic expressions.

Now that we have established a rough intuition for the operators and how to connect them, we list a consistent set of rules for reading the algebraic expressions generated from the diagrammatic expressions for Wick's theorem [16]:

1. Label external lines with hole (i, j, k) and particle (a, b, c) target indices. These correspond to the bra state indices.
2. Label internal lines with hole (l, m, n, \dots) and particle (d, e, f, \dots) and sum over these indices.
3. Every one-body interaction vertex picks up a factor of $\langle \text{out} | \hat{f} | \text{in} \rangle = f_{\text{in}}^{\text{out}}$.
4. Every two-body interaction vertex picks up a factor of $\langle \text{left-out right-out} | \hat{v} | \text{left-in right-in} \rangle$.
5. Every \hat{T}_m vertex picks up an amplitude $t_{ij\dots}^{ab\dots}$

6. Each pair of equivalent internal lines picks up a factor of $\frac{1}{2}$. Two lines are considered equivalent if they have the same starting and ending vertices.
7. Each pair of equivalent \hat{T}_m vertices picks up a factor of $\frac{1}{2}$. Two \hat{T}_m vertices are considered equivalent if they connect to the interaction vertex in the same way.
8. The sign (\pm) of a diagram term is $(-1)^{h+l}$, where h is the number of hole lines and l is the number of loops.
9. Each pair of unique external particle (or hole) lines not connected to the same interaction adds a permutation factor $\hat{P}(l_1, l_2)$, where l_1 and l_2 refer to the labels of the equivalent lines.

While working with just a two-body force, \hat{H}_N only has four legs, and thus can connect to a maximum of four other \hat{T}_m diagrams. To keep track of all of the ways that the diagrams can connect, we will use the sign table method. In this method, each interaction and cluster operator is assigned a set of plus signs and minus signs. These assignments label the number of lines extending below interaction vertices, and lines above cluster operators. A plus sign is used for each particle line and a minus sign for each hole line. Let us list out the relevant operators for CCD. First, \hat{F}_N :

$$\begin{array}{cccc}
 \begin{array}{c} | \\ \bullet \\ \uparrow \\ \times \end{array} & \begin{array}{c} | \\ \bullet \\ \downarrow \\ \times \end{array} & \begin{array}{c} \vee \\ \bullet \\ \times \end{array} & \begin{array}{c} \bullet \\ \uparrow \downarrow \\ \times \end{array} \\
 + & - & 0 & +- \\
 \end{array} \tag{4.32}$$

Next, \hat{V}_N :

$$\begin{array}{ccccc}
\begin{array}{c} | \\ \bullet \\ \hline \bullet \\ | \quad \diagup \\ \uparrow \end{array} & \begin{array}{c} | \\ \bullet \\ \hline \bullet \\ | \quad \diagup \\ \downarrow \end{array} & \begin{array}{c} | \\ \bullet \\ \hline \bullet \\ | \quad | \\ \uparrow \quad \uparrow \end{array} & \begin{array}{c} | \\ \bullet \\ \hline \bullet \\ | \quad | \\ \downarrow \quad \downarrow \end{array} & \begin{array}{c} | \\ \bullet \\ \hline \bullet \\ | \quad | \\ \uparrow \quad \downarrow \end{array} \\
+ & - & ++ & -- & +- \\
\begin{array}{c} | \\ \bullet \\ \hline \bullet \\ | \quad \diagdown \\ \uparrow \quad \diagdown \end{array} & \begin{array}{c} | \\ \bullet \\ \hline \bullet \\ | \quad \diagdown \\ \downarrow \quad \diagdown \end{array} & \begin{array}{c} | \\ \bullet \\ \hline \bullet \\ | \quad \diagdown \\ \uparrow \quad \diagdown \end{array} & \begin{array}{c} | \\ \bullet \\ \hline \bullet \\ | \quad \diagdown \\ \uparrow \quad \diagdown \end{array} & \begin{array}{c} | \\ \bullet \\ \hline \bullet \\ | \quad \diagdown \\ \uparrow \quad \diagdown \end{array} \\
++- & +-- & ++-- & 0 &
\end{array} \tag{4.33}$$

Lastly, the cluster operators can only connect upwards, so \hat{T}_2 and \hat{T}_3 :

$$\begin{array}{cc}
\begin{array}{c} \diagup \quad \diagdown \\ \hline \diagup \quad \diagdown \end{array} & \begin{array}{c} \diagup \quad \diagdown \quad \diagup \quad \diagdown \\ \hline \diagup \quad \diagdown \quad \diagup \quad \diagdown \end{array} \\
++-- & +++--- \\
\end{array} \tag{4.34}$$

Repeated cluster operators are separated by a vertical line:

$$\begin{array}{cc}
\begin{array}{c} \diagup \quad \diagdown \\ \hline \diagup \quad \diagdown \end{array} & \begin{array}{c} \diagup \quad \diagdown \\ \hline \diagup \quad \diagdown \end{array} \\
++-- \mid ++-- &
\end{array} \tag{4.35}$$

Let's look at an example term of the form $(\hat{V}_N \hat{T}_2^2)_C$, which would arise from the equation

$$\langle \Phi_{ij}^{ab} | (\hat{H}_N e^{\hat{T}})_C | \Phi_0 \rangle. \quad (4.36)$$

To carry this out, we set up the interaction vertices \hat{V}_N above two \hat{T}_2 operators like so

$$\begin{array}{c}
 \text{---} \\
 \diagup \quad \diagdown \\
 \diagdown \quad \diagup \\
 \text{---} \\
 + + - - \\
 \diagdown \quad \diagup \quad \diagdown \quad \diagup \\
 \text{---} \quad \text{---} \\
 + + - - \mid + + - -
 \end{array} \quad (4.37)$$

The C subscript is a reminder that any disconnected terms vanish, so these three operators must all be connected. Lastly, to project onto the doubly excited bra state $\langle \Phi_{ij}^{ab} |$ we need to connect the operators with two external hole lines and two external particle lines remaining. The sign table method helps us determine how many unique diagrams we have, and which diagrams are left with the four external lines that are needed. They must come from the cluster operators, as if one of the lines of the interaction matrix is an external line, there will be no way to connect the diagrams and have only four external lines total. However, even with this constraint, there are several ways to do so. These four external lines correspond to two $+$ and two $-$ labels. To ensure the diagram is connected, each \hat{T}_2 can only connect 1,

2, or 3 of its lines to \hat{V}_N , as 0 would create leave it disconnected, and 4 would use up all of \hat{V}_N 's lines, leaving the other \hat{T}_2 operator disconnected. In the sign table notation, these are written as

$$++|- - \quad +-|+- \quad +-+|- \quad +--|+$$

which is organized into Table 4.1. Since the order of + and - is irrelevant, we choose to

Table 4.1: Sign table for the four terms of eq. (4.37).

\hat{T}_2	\hat{T}_2
+-	+-
+	+--
-	++-
++	--

always list + signs first. Secondly, since the two \hat{T}_2 operators are equivalent, we do not need to list terms that are symmetric about the bar. For example, $++|- -$ is equivalent to $--|++$, and $+--|+$ is equivalent to $+|+--$. Using the sign table, we generate the

following four diagrams and their algebraic expressions

$$\begin{aligned}
 \left(\frac{1}{2}\hat{V}_N\hat{T}_2^2\right)_C \rightarrow & \text{Diagram 1} + \text{Diagram 2} \\
 & + \text{Diagram 3} + \text{Diagram 4}
 \end{aligned}
 \tag{4.38}$$

$$\begin{aligned}
 & = \hat{P}(ij)\hat{P}(ab)\frac{1}{2}\sum_{lmde}\langle lm|\hat{v}|de\rangle t_{il}^{ad}t_{mj}^{eb} + \hat{P}(ab)\frac{1}{2}\sum_{lmde}\langle lm|\hat{v}|de\rangle t_{ij}^{ad}t_{lm}^{eb} \\
 & + \hat{P}(ij)\frac{1}{2}\sum_{lmde}\langle lm|\hat{v}|de\rangle t_{il}^{de}t_{mj}^{ab} + \frac{1}{4}\sum_{lmde}\langle lm|\hat{v}|de\rangle t_{ij}^{de}t_{lm}^{ab}.
 \end{aligned}$$

One may note how the two \hat{T}_2 operators are counted as equivalent, omitting configurations that already exist if we were to switch place between the two operators, i.e. $++|--$ is the same as $--|++$, thus counted only once. Also, once the particle-hole orientation of the arrows has been selected, the assignment of the index labels can vary, but will always generate equivalent expressions. For this reason, it is common to omit the labels in the diagrams.

4.4 Diagrammatic Derivation of the Coupled Cluster Equations

All of the ingredients are now in place to derive the coupled cluster equations. As a reminder the general expressions for coupled cluster equations are generated by projecting the coupled cluster effective Hamiltonian onto the reference state, and onto an excitation of the reference state,

$$\langle \Phi_0 | (\hat{H}_N e^{\hat{T}})_C | \Phi_0 \rangle = \Delta E,$$

$$\langle \Phi_{ij\dots}^{ab\dots} | (\hat{H}_N e^{\hat{T}})_C | \Phi_0 \rangle = 0.$$

Starting with the energy equation, projecting onto the reference state is equivalent to finding the connected diagrams with no external lines. Truncating the Hamiltonian to only two-body forces again, and expanding the exponential yields

$$\Delta E = \langle \Phi_0 | [\hat{F}_N (1 + \hat{T}_1 + \dots)]_C | \Phi_0 \rangle + \langle \Phi_0 | [\hat{V}_N (1 + \hat{T}_1 + \dots)]_C | \Phi_0 \rangle. \quad (4.39)$$

We see that even though the exponential in general has infinite terms, the only ways to generate connected closed diagrams are the one-body force \hat{F}_N connected with a singles excitation \hat{T}_1 , the two-body interaction \hat{V}_N connected with a doubles excitation \hat{T}_2 , and the two-body interaction connected with two singles excitations. Let's first look at the unique topologies via non-oriented Hugenholtz diagrams [33].

$$\begin{aligned}
(\hat{F}_N \hat{T}_1)_C : & \quad \begin{array}{c} \times \text{---} \\ \bullet \\ \text{---} \\ \circ \end{array} \\
(\hat{V}_N \hat{T}_2)_C : & \quad \begin{array}{c} \bullet \\ \text{---} \\ \circ \end{array} \\
(\hat{V}_N \hat{T}_1^2)_C : & \quad \begin{array}{c} \bullet \\ \text{---} \\ \circ \end{array}
\end{aligned} \tag{4.40}$$

It turns out orienting these lines to have particle-hole character only generates one Brandow diagram [61] for each of them. The diagrams and their corresponding expressions are

$$\begin{aligned}
(\hat{F}_N \hat{T}_1)_C : & \quad \begin{array}{c} \times \text{---} \\ \bullet \\ \text{---} \\ \circ \end{array} \begin{array}{c} i \\ \downarrow \\ \uparrow \\ a \end{array} = \sum_{i,a} \langle i | \hat{f} | a \rangle \langle a | \hat{t}_1 | i \rangle
\end{aligned} \tag{4.41}$$

$$\begin{aligned}
(\hat{V}_N \hat{T}_2)_C : & \quad \begin{array}{c} \text{---} \\ \bullet \\ \text{---} \\ \circ \end{array} \begin{array}{c} i \\ \downarrow \\ \uparrow \\ a \end{array} \begin{array}{c} j \\ \downarrow \\ \uparrow \\ b \end{array} = \frac{1}{4} \sum_{i,j,a,b} \langle ij | \hat{v} | ab \rangle \langle ab | \hat{t}_2 | ij \rangle
\end{aligned} \tag{4.42}$$

$$\begin{aligned}
\frac{1}{2} (\hat{V}_N \hat{T}_1^2)_C : & \quad \begin{array}{c} \text{---} \\ \bullet \\ \text{---} \\ \circ \end{array} \begin{array}{c} i \\ \downarrow \\ \uparrow \\ a \end{array} \begin{array}{c} j \\ \downarrow \\ \uparrow \\ b \end{array} = \frac{1}{2} \sum_{i,j,a,b} \langle ij | \hat{v} | ab \rangle \langle a | \hat{t}_1 | i \rangle \langle b | \hat{t}_1 | j \rangle
\end{aligned} \tag{4.43}$$

At long last we have derived the expression for the CC correlation energy for a Hamiltonian with one and two-body forces

$$\Delta E_{CC} = f_a^i t_i^a + \frac{1}{4} v_{ab}^{ij} t_{ij}^{ab} + \frac{1}{2} v_{ab}^{ij} t_i^a t_j^b, \tag{4.44}$$

where the line labels in this case are all arbitrary indices since they are completely summed over. The positions of the labels in the algebraic expressions are determined by the indices of the incoming and outgoing lines. For bra-ket notation, $\langle \text{out}_1 \text{out}_2 | \hat{v} | \text{in}_1 \text{in}_2 \rangle$ for tensor notation, $v_{\text{in}_1 \text{in}_2}^{\text{out}_1 \text{out}_2}$ becomes an unambiguous mapping. This expression for the coupled cluster correlation energy can be further simplified. For the near future, we will assume that we are working in a Hartree-Fock basis which by construction zeros out all of the hole-particle one-body terms $\langle i | \hat{f} | a \rangle = 0$. The next assumption we will make is that we are using the CCD approximation of coupled cluster. In this approximation, $\hat{T} \approx \hat{T}_2$. This is the first non-trivial approximation to CC, since CCS would just recover a single optimized Slater determinant as shown by the Thouless theorem. As a note, the next approximation would be CCSD, but for the pairing model with no broken pairs and infinite matter systems, there are no singles excitations and so for the systems in this work CCSD is equal to CCD.

These assumptions allow us to discard terms with f_a^i and terms with singles excitations, and we arrive at the expression for the CCD correlation energy,

$$\Delta E_{CCD} = \frac{1}{4} v_{ab}^{ij} t_{ij}^{ab}. \quad (4.45)$$

Since \hat{V}_N is an input from the Hamiltonian, we only need to find the t_{ij}^{ab} amplitudes to calculate the CCD correlation energy. This means we have $N_p^2 N_h^2$ unknowns, and so we need an equivalent amount of constraints to pin these values down. This is typically done by projecting onto the excited reference state

$$\langle \Phi_{i_1 \dots i_n}^{a_1 \dots a_n} | (H_N e^T)_c | \Phi_0 \rangle = 0 \quad (4.46)$$

or in the case of CCD:

$$\langle \Phi_{ij}^{ab} | (\hat{H}_N e^{\hat{T}_2})_C | \Phi_0 \rangle = 0. \quad (4.47)$$

Projecting on the bra state $\langle \Phi_{ij}^{ab} |$ means that we need to find all of the connected diagrams with four external lines a, b, i, j . Since \hat{F}_N only has two lines to connect, and \hat{H}_N only has four lines to connect, the only possible connected diagrams are given by

$$\langle \Phi_{ij}^{ab} | (\hat{F}_N \hat{T}_2)_C | \Phi_0 \rangle + \langle \Phi_{ij}^{ab} | \left[\hat{V}_N (1 + \hat{T}_2 + \frac{1}{2} \hat{T}_2^2) \right]_C | \Phi_0 \rangle = 0. \quad (4.48)$$

Anything beyond \hat{T}_2^2 would have too many lines to be able to fully contract with \hat{H}_N . Let's go through this expression term by term.

First, the contribution from the one-body operator

$$(\hat{F}_N \hat{T}_2)_C \rightarrow \begin{array}{c} \text{Diagram 1: A vertex with four external lines. Two lines on the left have arrows pointing down, and two lines on the right have arrows pointing up. A dashed line with an 'x' at the end extends from the right vertex to the right.} \\ \text{Diagram 2: A vertex with four external lines. Two lines on the left have arrows pointing up, and two lines on the right have arrows pointing down. A dashed line with an 'x' at the end extends from the left vertex to the left.} \end{array} + \quad (4.49)$$

$$= \hat{P}(ab) \sum_d \langle b | \hat{f} | d \rangle t_{ij}^{ad} - \hat{P}(ij) \sum_l \langle l | \hat{f} | i \rangle t_{lj}^{ab},$$

where as a reminder, in the first term, the $\hat{P}(ab)$ operator is the permutation operator $1 - \hat{P}_{ab}$, which comes from the fact that the two external particle lines in the first term connect to different operators, and thus the permutation operator is necessary to recover the antisymmetry of $\langle \Phi_{ij}^{ab} |$.

notation,

$$\begin{aligned}
0 &= v_{ij}^{ab} + \hat{P}(ab) \sum_d f_{bd} t_{ij}^{ad} - \hat{P}(ij) \sum_l f_{kl} t_{il}^{ab} \\
&+ \frac{1}{2} \sum_{de} v_{de}^{ab} t_{ij}^{de} + \frac{1}{2} \sum_{lm} v_{ij}^{lm} t_{lm}^{ab} + \hat{P}(ab|ij) \sum_{ld} v_{dj}^{lb} t_{il}^{ad} \\
&+ \frac{1}{4} \sum_{lmde} v_{de}^{lm} t_{ij}^{de} t_{lm}^{ab} + \hat{P}(ij) \sum_{lmde} v_{de}^{lm} t_{il}^{ad} t_{jm}^{be} \\
&- \frac{1}{2} \hat{P}(ij) \sum_{lmde} v_{de}^{lm} t_{il}^{ed} t_{mj}^{ab} - \frac{1}{2} \hat{P}(ab) \sum_{lmde} v_{de}^{lm} t_{ml}^{ad} t_{ij}^{eb}, \tag{4.52}
\end{aligned}$$

where $\hat{P}(ab|ij) \equiv \hat{P}(ab)\hat{P}(ij)$. Finding the set of amplitudes t_{ij}^{ab} for which this equation is satisfied may seem challenging at first, but we can see a path forward after rewriting these equations a little more. These calculations are frequently done in the Hartree-Fock basis, in which case the one-body terms are diagonal $f_{pq} = f_{pp}\delta_{pq}$, where $f_{pp} = \varepsilon_p$. This assumption is not necessary, however the general CC strategy is more clear if we take this as true for now. This simplification, along with the antisymmetry of t_{ij}^{ab} means we can rewrite the terms which include f_{pq} as

$$\begin{aligned}
&\hat{P}(ab) \sum_d f_{bd} \delta_{bd} t_{ij}^{ad} - \hat{P}(ij) \sum_l f_{lj} \delta_{lj} t_{il}^{ab} \\
&= \hat{P}(ab) f_{bb} t_{ij}^{ab} - \hat{P}(ij) f_{jj} t_{ij}^{ab} \\
&= \hat{P}(ab) \varepsilon_b t_{ij}^{ab} - \hat{P}(ij) \varepsilon_j t_{ij}^{ab} \\
&= \varepsilon_b t_{ij}^{ab} - \varepsilon_a t_{ij}^{ba} - \varepsilon_j t_{ij}^{ab} + \varepsilon_i t_{ji}^{ab} \\
&= \varepsilon_b t_{ij}^{ab} + \varepsilon_a t_{ij}^{ab} - \varepsilon_j t_{ij}^{ab} - \varepsilon_i t_{ij}^{ab} \\
&= t_{ij}^{ab} (\varepsilon_a + \varepsilon_b - \varepsilon_i - \varepsilon_j) \tag{4.53}
\end{aligned}$$

If we rewrite the CCD equations, Eqn. (4.52), subtracting these terms to the left hand side, and defining $\varepsilon_{ij}^{ab} = \varepsilon_i + \varepsilon_j - \varepsilon_a - \varepsilon_b$ we get:

$$\begin{aligned}
t_{ij}^{ab(new)} \varepsilon_{ij}^{ab} &= v_{ij}^{ab} + \frac{1}{2} \sum_{de} v_{de}^{ab} t_{ij}^{de(old)} \\
&+ \frac{1}{2} \sum_{lm} v_{ij}^{lm} t_{lm}^{ab(old)} + \hat{P}(ab|ij) \sum_{ld} v_{dj}^{lb} t_{il}^{ad(old)} \\
&+ \frac{1}{4} \sum_{lmde} v_{de}^{lm} t_{ij}^{de(old)} t_{lm}^{ab(old)} + \hat{P}(ij) \sum_{lmde} v_{de}^{lm} t_{il}^{ad(old)} t_{jm}^{be(old)} \\
&- \frac{1}{2} \hat{P}(ij) \sum_{lmde} v_{de}^{lm} t_{il}^{ed(old)} t_{mj}^{ab(old)} - \frac{1}{2} \hat{P}(ab) \sum_{lmde} v_{de}^{lm} t_{ml}^{ad(old)} t_{ij}^{eb(old)}. \quad (4.54)
\end{aligned}$$

Here the (*new*) and (*old*) superscripts have been added to show that the CCD equations can be solved iteratively. Starting with some guess for t_{ij}^{ab} in the right hand side of Eqn. (4.54), the sums are carried out and stored as $t_{ij}^{ab(new)}$, which can then be used as the guess for the next iteration. This process is solved iteratively, and in most cases converges. The conditions for stability of the convergence can be jeopardized when the gap between the unoccupied and occupied single-particles states is small, causing the energy denominator ε_{ij}^{ab} to approach zero [62]. This manifests for systems with strong many-body correlations, and low order truncations of CC theory are insufficient to capture the physics. To check convergence, after each iteration the new t -amplitudes can be plugged into the ΔE_{CCD} equation to see how much the energy has changed compared to the previous iteration. Numerically, an iteration tolerance can be set, ending the iteration loop once the energy is changing by amounts smaller than the tolerance.

Iterative convergence for CC has been studied in detail providing sophisticated ways to accelerate convergence [63], but for now we will keep this iteration simple. One small change that can be made is to add a linear mixing parameter α , such that the new t -amplitudes for

the i -th iteration are

$$t_{\text{mixing}}^{(i)} = \alpha t^{(i)} + (1 - \alpha)t^{(i-1)}. \quad (4.55)$$

For $\alpha = 0.5$, this means that the next iteration will only use half of the t -amplitudes just calculated, and half from the previous iteration. This can help convergence, especially in situations where the iterations oscillate back and forth between two values. Adding in the mixing parameter can help damp out these large steps in the wrong direction.

All iterative methods need a starting point, so the initial guess of $t_{ij}^{ab} = 0$ is typically used. This actually leads to a second iteration that is $t_{ij}^{ab} = v_{ij}^{ab}/\varepsilon_{ij}^{ab}$, which when plugged into the energy equation gives

$$\Delta E = \frac{1}{4} \frac{|v_{ij}^{ab}|^2}{\varepsilon_{ij}^{ab}},$$

which is the MBPT(2) result. This is quite exciting, as we have recovered another many-body method with CC theory, and all iterations beyond the first add more and more many-body correlations into the t -amplitudes.

Despite $\hat{T} \approx \hat{T}_2$ seeming like a harsh approximation truncating many terms, CCD turns out to provide surprisingly accurate results for many systems. The application of CCD to quantum many-body systems can be seen in Chapters 5 and 6, where for some small models the CCD results can be compared to the exact result. Of course CCD has its limitations. Many systems, especially systems for which the reference state is a poor starting point, CCD can fail to converge. Additional correlations can be included, but this quickly increases the computational scaling of CC theory.

For infinite matter calculations, there are no many-body contributions from the single excitations, therefore the next level of correlations to include are the triples excitations $\hat{T} \approx \hat{T}_2 + \hat{T}_3$. This addition does not change the CC energy expression, but the doubles

where again we are going to assume that we have Hartree-Fock single-particle states which gives the condition $\langle m|\hat{f}|e\rangle = 0$ and so the term in Eqn. (4.58) is zero.

Next, are the equations for the triples amplitudes. The full triples equations are not the focus of this thesis, but we will examine the terms which contribute at leading order to the CC energy. They correspond to

$$\begin{aligned}
 (\hat{V}_N \hat{T}_2)_C \rightarrow & \text{[Diagram 1]} + \text{[Diagram 2]} \\
 & = \hat{P}(k/ij|a/bc) \sum_d \langle bc|\hat{v}|dk\rangle t_{ij}^{ad} - \hat{P}(i/jk|c/ab) \sum_l \langle lc|\hat{v}|jk\rangle t_{il}^{ab}
 \end{aligned}
 \tag{4.60}$$

and

$$\begin{aligned}
 (\hat{F}_N \hat{T}_3)_C \rightarrow & \text{[Diagram 3]} + \text{[Diagram 4]} \\
 & = \hat{P}(c/ab) \sum_d \langle c|\hat{f}|d\rangle t_{ijk}^{abd} - \hat{P}(k/ij) \sum_l \langle l|\hat{f}|k\rangle t_{ijl}^{abc}
 \end{aligned}
 \tag{4.61}$$

where we have a new type of permutation operation $\hat{P}(a/bc) = 1 - P_{ab} - P_{ac}$. Were again we assume that we are in the Hartree-Fock basis $\langle p|\hat{f}|q\rangle = \varepsilon_p \delta_{pq}$ is diagonal, and as in Eqn.

(4.53), we rewrite Eqn. (4.61) as

$$\hat{P}(c/ab) \sum_d \langle c|\hat{f}|d\rangle t_{ijk}^{abd} - \hat{P}(k/ij) \sum_l \langle l|\hat{f}|k\rangle t_{ijl}^{abc} = -\varepsilon_{ijk}^{abc} t_{ijk}^{abc}. \quad (4.62)$$

Just as in the CCD equations, we can move this term to the left-hand side, and divide by the single-particle energy denominator ε_{ijk}^{abc} . In doing so, we now have a minimal set of diagrams for triples excitations in CC theory. We can set up the iterative equations as

$$\varepsilon_{ijk}^{abc} t_{ijk}^{abc} = \hat{P}(k/ij|a/bc) \sum_d \langle bc|\hat{v}|dk\rangle t_{ij}^{ad} - \hat{P}(i/jk|c/ab) \sum_l \langle lc|\hat{v}|jk\rangle t_{il}^{ab}, \quad (4.63)$$

and an initial guess for the t_2 -amplitudes of zero on the right-hand side will generate an initial guess for the t_3 -amplitudes on the right-hand side. These t_3 -amplitudes on the left-hand side of Eqn. (4.63) are then plugged back into the double excitation equations in Eqn. (4.59), completing the iterative scheme. This is referred to as the CCDT-1 approximation to the full CCDT [64].

4.5 Computational Scaling of Coupled Cluster Theory

Now that the equations have been derived, let's look at the computational effort required for a single CCD iteration in Eqn. (4.54). Due to the symmetries of the t -amplitudes, the CCD equations must be solved for $(i > j)$ and $(a > b)$, however it is often convenient to just compute these for all i, j, a, b for reasons that will be explained later. For now, let's just get a handle on the scaling. If these equations are solved for i, j, a, b that already brings a computation complexity of $\mathcal{O}(N_h^2 N_p^2)$ to just loop through the entries of t_{ij}^{ab} , where N_h is the number of occupied single-particle states (holes) relative to the Fermi energy, and N_p is the

number of unoccupied single-particle states. This “big O” notation is used to get a handle on the scaling of the most expensive term, without worrying about constants of multiplication or non-leading terms. Within each t -amplitude equation there are some heavy sums, like

$$\frac{1}{4} \sum_{lmde} v_{de}^{lm} t_{ij}^{de} t_{lm}^{ab}, \quad (4.64)$$

which brings an additional $\mathcal{O}(N_h^2 N_p^2)$ leading to a cost of $\mathcal{O}(N_h^4 N_p^4)$. With the big O notation, it is common to ignore the difference between the number of hole states and particle states and to just use $N \approx N_h \approx N_p$, and to say that CCD written in this form is an $\mathcal{O}(N^8)$ theory for calculating the ground state energy.

For memory requirements, the primary objects that need to be stored are t_{ij}^{ab} and v_{cd}^{ab} , which require $N_h^2 N_p^2$ and N_p^4 number of elements to be stored. In many realistic calculations, $N_p \approx 10 * N_h$ or even $N_p \approx 100 * N_h$, meaning that v_{cd}^{ab} with four particle state indices is by far the largest object that needs to be stored in this theory. If there are three-body forces in the calculation, the object w_{def}^{abc} needs to be stored as well, placing some serious memory requirements on the calculation. A discussion of the memory requirements and data structures to handle the requirements of CC are explained in detail in Chapter 5.

It turns out that by reorganizing some terms, we can reduce the computational complexity of the CCD equations. For example, if we define the intermediate term

$$X_{ij}^{lm} = \sum_{de} v_{de}^{lm} t_{ij}^{de} \quad (4.65)$$

the term in Eqn. (4.64) can be rewritten with the intermediate term as

$$\frac{1}{4} \sum_{lm} X_{ij}^{lm} t_{lm}^{ab} = \frac{1}{4} \sum_{lmde} v_{de}^{lm} t_{ij}^{de} t_{lm}^{ab}. \quad (4.66)$$

By computing the sum over the de indices first, storing the intermediate result, then afterwards computing the sum over the lm indices, we have gone from a scaling of $O(N_h^2 N_p^2)$ to $O(N_h^2 + N_p^2)$, which is a huge advantage! The only downside to this is that extra storage must be used to store X , but this is typically small compared to the other storage requirements. This means that using intermediates, CCD is actually only a $\mathcal{O}(N^6)$ theory, which is extremely cheap for the accuracy it brings. A systematic way of generating these intermediates is to follow the development of diagrams for the coupled cluster effective Hamiltonian $\bar{H} \equiv (\hat{H}_N e^{\hat{T}})_C$ as outlined by Shavitt and Bartlett [16].

Any term which is quadratic in t can be done in two steps with an intermediate. However, by examining which terms can be grouped into their own operators in the CC effective Hamiltonian, we can occasionally reuse terms for additional efficiency. We define the intermediates as

$$X_b^a = f_b^a - \frac{1}{2} \sum_{lmd} v_{bd}^{lm} t_{lm}^{ad}, \quad (4.67)$$

$$X_j^i = f_j^i + \frac{1}{2} \sum_{del} v_{de}^{il} t_{jl}^{de}, \quad (4.68)$$

$$X_{kl}^{ij} = v_{kl}^{ij} + \frac{1}{2} \sum_{de} v_{de}^{ij} t_{kl}^{de}, \quad (4.69)$$

$$X_{jb}^{ia} = v_{jb}^{ia} - \frac{1}{2} \sum_{dl} v_{db}^{il} t_{jl}^{da}, \quad (4.70)$$

and then we can rewrite the CCD equation as

$$\begin{aligned}
0 = & v_{ij}^{ab} + \hat{P}(ab) \sum_d X_d^{at_{ij}db} - \hat{P}(ij) \sum_l X_i^{lt_{lj}ab} \\
& - \frac{1}{2} \sum_{de} v_{de}^{ab} t_{ij}^{de} + \frac{1}{2} \sum_{lm} X_{ij}^{lm} t_{lm}^{ab} - \hat{P}(ab|ij) \sum_{ld} X_{id}^{lb} t_{lj}^{ad},
\end{aligned} \tag{4.71}$$

which is exactly equivalent to the $\mathcal{O}(N^8)$ equations, but reduced down to $\mathcal{O}(N^6)$ operations with minimal additional memory requirements.

The computational details for quantum many-body methods is the primary focus of this work and specifically Chapter 5. As a method with polynomial scaling coupled cluster theory is a great method to investigate computational challenges, since improvements in the data structures and algorithms implementing these equations can greatly expand what can be calculated with the method. This is in contrast to exact methods like full configuration interaction, where it will never outrun the factorial scaling as the problem size increases. Calculations with a large number of particles ($N_h \sim 100$), and a very large basis ($N_p \sim 10^4 - 10^5$) are frequently needed for calculations of interesting physical systems, which require great care in the performance of the CC implementation. Alternatively, for systems without as extreme basis size requirements, it may be necessary to use triples (CCDT) $\hat{T} \approx \hat{T}_2 + \hat{T}_3$ or three-body forces \hat{W}_N to achieve the accuracy desired for a calculation, but these bring a heavy cost.

For a calculation of CCDT with three-body forces, one term for the $\langle \Phi_{ijk}^{abc} |$ projected equations is

$$\frac{1}{8} \sum_{efg} w_{efg}^{abc} t_{ijk}^{efg}, \tag{4.72}$$

which will result in an $\mathcal{O}(N^9)$ scaling theory. This is simply too expensive for anything but

the smallest systems. Three-body forces are brought up here to bring attention to other ways which CC theory can grow prohibitively expensive along with increasing basis size N . This is a pattern in any many-body method, that increasing the accuracy of a calculation always has a cost, which dictates which physical systems can be studied and which cannot. Big O notation can show asymptotically how CC theory will grow, but to consider how expensive a particular calculation will be, it lacks predictive power. Here the multiplicative constants ($c * N^9$) and non-leading terms can be quite important. Chapter 5 will show how the implementation of the CC equations into a code can vary the multiplicative constant by up to five orders of magnitude. This swing in cost is nearly impossible to see just from the CC equations alone, and so great care should be taken when writing a computer program as it can determine the viability of a many-body method.

Chapter 5

Computational Methodology

The previous chapters have stressed how large and unwieldy a many-body calculation can be. Even for a modest single-particle basis, the factorial growth of the full Slater determinant basis becomes quickly impossible for even the largest computers in the world. It was shown in Chapter 4 that coupled cluster (CC) theory generates expressions for the approximate ground state energy which have polynomial scaling. This allows CC theory to compute properties of much larger systems by sacrificing some accuracy of the solution. However, even with efficient implementations of these equations with intermediate diagrams [65], coupled cluster theory is still computationally expensive and runs into computational limits for all but very small physical systems. Modern many-body physics necessarily becomes a computationally challenging field just by the very scale of the problems at hand. This chapter will detail how the same mathematical expressions on paper can take centuries to compute or seconds to compute depending on the choice of data structures and algorithms implemented in the code.

5.1 Code Validation

Before these optimizations are implemented, it is useful to first implement the many-body method equations into code in the most direct translation from mathematics as possible. Optimizing the code to run faster and compute larger basis sets will increase the number

of lines of code substantially, increasing the chance of human error. Once an inefficient, but correct version of the code is finished, incremental optimizations moving forward can be compared to the previously validated solution.

5.1.1 Pairing Model

Here, a simple system like the pairing model described in Chapter 3 is an excellent small system to check the numerical results. In the case of the simple pairing model it is easy to calculate ΔE_{MBPT2} analytically from Eqn. (2.186), where MBPT2 refers to many-body perturbation theory that was described in Chapter 2. This is a very useful check of our codes since this analytical expression can also be used to check our first CCD iteration. We restate this expression here but restrict the sums over single-particle states

$$\Delta E_{MBPT2} = \frac{1}{4} \sum_{abij} \frac{\langle ij|\hat{v}|ab\rangle \langle ab|\hat{v}|ij\rangle}{\epsilon_{ij}^{ab}} = \sum_{a<b, i<j} \frac{\langle ij|\hat{v}|ab\rangle \langle ab|\hat{v}|ij\rangle}{\epsilon_{ij}^{ab}}.$$

For our pairing example we obtain the following result

$$\Delta E_{MBPT2} = \frac{\langle 01|\hat{v}|45\rangle^2}{\epsilon_{01}^{45}} + \frac{\langle 01|\hat{v}|67\rangle^2}{\epsilon_{01}^{67}} + \frac{\langle 23|\hat{v}|45\rangle^2}{\epsilon_{23}^{45}} + \frac{\langle 23|\hat{v}|67\rangle^2}{\epsilon_{23}^{67}},$$

which translates into

$$\Delta E_{MBPT2} = -\frac{g^2}{4} \left(\frac{1}{4+g} + \frac{1}{6+g} + \frac{1}{2+g} + \frac{1}{4+g} \right).$$

This expression can be used to check the results for any value of g and therefore provides an important test of our codes. In Table 5.1, five significant figures are listed to compare MBPT2 and CCD. The MBPT2 results were checked against the analytical results to ensure

that they could be reproduced numerically. Next, the CCD results can be checked against the MBPT2 results. While these are two very different methods, they should give results that are reasonably close to one another, especially at small values of the interaction strength g . At $g = 0$, the particles are no longer interacting, so a first simple check of a code is

Table 5.1: Coupled cluster and MBPT2 results for the simple pairing model with eight single-particle levels and four spin-1/2 fermions for different values of the interaction strength g .

g	E_{ref}	ΔE_{MBPT2}	ΔE_{CCD}
-1.0	3	-0.46667	-0.21895*
-0.5	2.5	-0.08874	-0.06306
0.0	2	0	0
0.5	1.5	-0.06239	-0.08336
1.0	1	-0.21905	-0.36956

that the correlation energy drops to 0. Also note that the $g = -1.0$ case diverges without implementing iterative mixing. Iterative mixing is defined by

$$t^{(i)} = \alpha t_{no_mixing}^{(i)} + (1 - \alpha)t^{(i-1)}, \quad (5.1)$$

where $t^{(i-1)}$ is the t -amplitude from the previous iteration, $t_{no_mixing}^{(i)}$ is the updated amplitude. By choosing a mixing parameter α , we create a simple linear combination of the current iteration and the previous iteration to use in the next iteration. This can help the CC iterations converge faster, or in some cases prevent oscillating or diverging iterations.

In Fig. 5.1 we can see that CCD compares quite well to the exact calculation of FCI in this range of interaction strength g . Also plotted are higher orders of many-body perturbation theory, MBPT3 and MBPT4, which are higher order corrections to the many-body perturbation theory correlation energy. Coupled cluster doubles does not start diverging until larger values of interaction strength, as this method includes significantly more many-

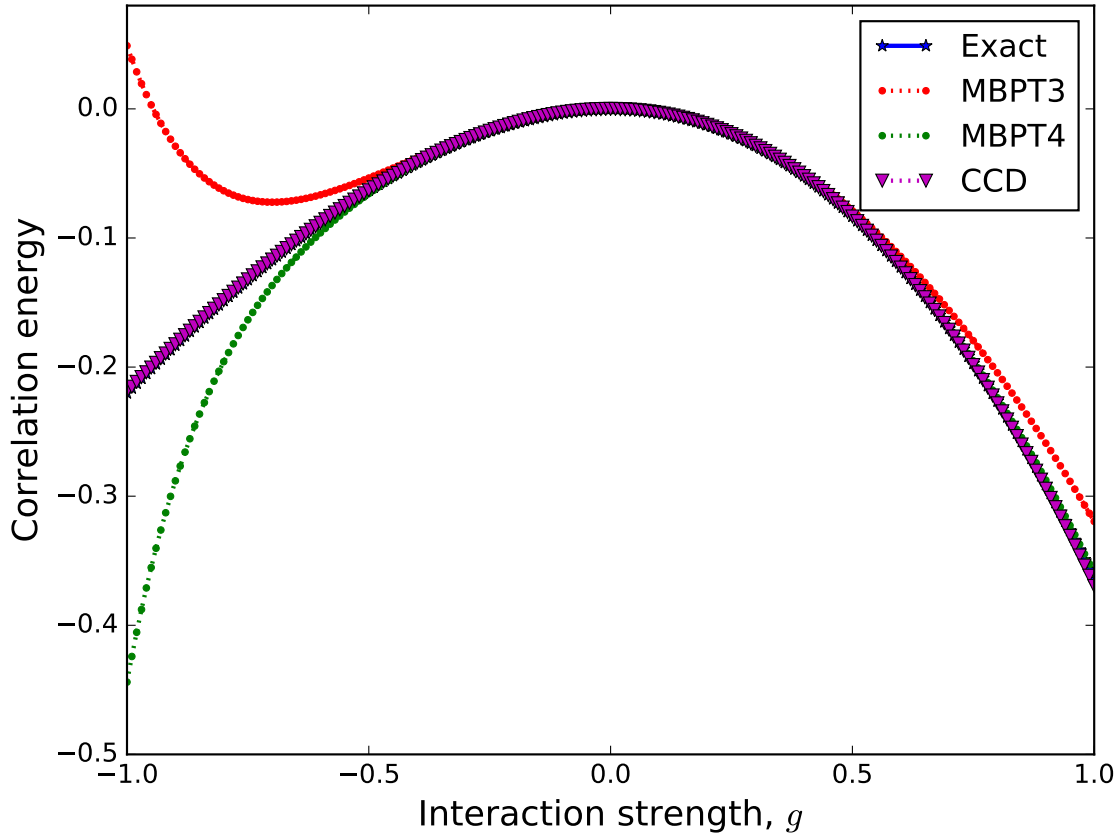


Figure 5.1: Correlation energy for the pairing model with exact diagonalization, CCD and perturbation theory to third (MBPT3) and fourth order (MBPT4) for a range of interaction values.

body correlations. We can say CCD looks good “by eye”, but when validating numerical results, it is necessary to print out several digits and make sure the code is validated to a set level of precision.

5.1.2 Infinite Neutron Matter

Once the pairing model is numerically handled, it is good to benchmark against a more realistic system. By writing the computer program that solves these equations in a modular way, it is not too difficult to add in new physical systems to calculate via their own module

to plug in. To calculate properties of infinite neutron matter, only a few parameters are needed for the system. The number of neutrons in the box, the density of these neutrons, and the number of basis states above the Fermi surface. To get an idea of how the system behaves, it is typical to calculate the ground state energies at different densities, particle numbers and basis sizes. Here we present some calculations for a system of neutrons using many-body perturbation theory (MBPT) and coupled cluster doubles (CCD). Table 5.2 lists a set of numerical values to check the infinite matter basis with the Minnesota potential [53] described in Chapter 3. While this is not a very realistic nuclear force, it has enough of the right symmetries and properties for code validation purposes.

Table 5.2: CCD and MBPT2 results for infinite neutron matter with $N = 66$ neutrons and a maximum number of single-particle states constrained by $N_{max} = 36$ (36 plane wave energy shells).

Density ρ fm ⁻³	E_{MBPT2}	E_{CCD}
0.04	6.472	6.468
0.06	7.919	7.932
0.08	9.075	9.136
1.0	9.577	10.074
1.2	10.430	10.885
1.4	11.212	11.565
1.6	11.853	12.136
1.8	12.377	12.612
2.0	12.799	13.004

5.2 Taming the Two-Body Basis

The first of many computational considerations that will be examined here is how to get a grasp on the two-body basis. As was explained in Chapter 2, the full many-body basis built from Slater determinants is a factorially growing problem with respect to the

single particle basis. This motivated the need for more efficient methods like CC theory and in-medium similarity renormalization group (IM-SRG). However, even in the world of polynomially scaling methods, the size of the problem is still enormous. Let's first look at the memory demands of CC with a two-body force. The two-body force has antisymmetrized matrix elements $\langle pq|\hat{v}|rs\rangle$. If we have a calculation using 10^3 single particle states (common in nuclear matter), then we would need to store 10^{12} matrix elements, which are usually complex numbers of double precision. A double precision floating point number, commonly called a double, holds 8 bytes of data. A complex double needs 16 bytes, a double for the real part and a double for the imaginary part. With this in mind the full two-body matrix requires 16,000 gigabytes of memory. Now, this is not impossibly large for modern supercomputers, but is inaccessible to anyone attempting this calculation on a laptop.

To reduce the storage requirements of the two-body force, we first look to the CC equations. In any particular diagram in the CCD equations, full unrestricted single-particle indices (p, q, r, s) are never used, only terms of indices of a fixed particle (a, b, c, d) or hole (i, j, k, l) nature. We can organize the matrix in terms of groups of particles and holes. For example v_{pp-pp} represents the two-body piece in terms where all of the sums are over particle indices $v_{cd}^{ab} := \langle ab|\hat{v}|cd\rangle$ appear. Following this notation, the interaction can be grouped into $2^4 = 16$ different sectors $v_{pp-ph}, v_{pp-hh}, \dots$. Due to symmetries of the interaction, not every particle-hole sector has to be stored, as these symmetries mean that some of the information is redundant up to a phase as seen in Table 5.3, where all of the terms in parentheses are previously listed. Looking at the symmetries of the two-body operator, these are the only subsections that need to be stored, since by antisymmetry: $\langle pq|\hat{v}|rs\rangle = -\langle qp|\hat{v}|rs\rangle = -\langle pq|\hat{v}|sr\rangle = \langle qp|\hat{v}|sr\rangle$, and by Hermiticity, so $\langle pq|\hat{v}|rs\rangle = \langle rs|\hat{v}|pq\rangle^*$.

Table 5.3: All possible particle-hole sectors are listed in the left column. In the right column are 6 particle hole sectors which contain all of the information of the whole matrix, plus how the other 10 can be equivalently expressed.

Sector	Equivalent Sector
v_{pp-pp}	v_{pp-pp}
v_{pp-ph}	v_{pp-ph}
v_{pp-hh}	v_{pp-hh}
v_{ph-hh}	v_{ph-hh}
v_{hh-hh}	v_{hh-hh}
v_{ph-ph}	v_{ph-ph}
v_{pp-hp}	$-(v_{pp-ph})$
v_{hh-pp}	$(v_{pp-hh})^*$
v_{hh-hp}	$-(v_{ph-hh})^*$
v_{hp-pp}	$-(v_{pp-ph})^*$
v_{hp-hp}	(v_{ph-ph})
v_{ph-pp}	$(v_{pp-ph})^*$
v_{hp-ph}	$-(v_{ph-ph})$
v_{ph-hp}	$-(v_{ph-ph})$
v_{hp-hh}	$-(v_{ph-hh})$
v_{hh-ph}	$(v_{ph-hh})^*$

These two facts let us reproduce any matrix element while only storing six sectors. Since the number of occupied states (hole states) is typically much less than the unoccupied states (particle states) $n_h \ll n_p$, the largest term, v_{pp-pp} comprises the vast majority of memory requirements. The storage of the large amount of matrix elements receives some relief by only storing the non-redundant matrix elements, but the size of v_{pp-pp} alone grows large enough to make many calculations impossible.

Fortunately for most two-body interactions, this matrix is incredibly sparse. To write the two-body interaction as a matrix, all of the two-body states need to be organized. One multi-index scheme maps two single-particle indices i, j which run from 0 to N to a single column index can be written as: Column Index = $(N + 1) * i + j$ as shown in Table 5.4.

While this is a simple way to organize the two-body interaction matrix, it has some

Table 5.4: A straight forward scheme to organize the two-body basis in columns.

Column Number	0	1	2	...	$N + 1$	$N + 2$...	N^2
Two-Body State	$ 00\rangle$	$ 01\rangle$	$ 02\rangle$...	$ 10\rangle$	$ 11\rangle$...	$ NN\rangle$

serious drawbacks. In this scheme, the matrix appears very sparse, but the non-zero matrix elements are organized essentially randomly throughout the matrix. There has been much study of sparse matrices, the underlying physics of the problem serves as a guide to a custom compressed data structure. To look at how to get some more significant reductions, we look at the symmetries of the Hamiltonian.

We know that the quantum numbers of the eigenstates of a Hamiltonian describe the values of the conserved quantities of that Hamiltonian. So it is natural to try and select a single-particle basis for a calculation that is labeled by relevant quantum numbers for the problem. This way, even the approximate solutions that are computed are assured to have the correct symmetries. This is almost always done in CC calculations, although the field of symmetry broken reference states is very active in many-body theory [66]. The advantage here is that the bra and ket states of a Hamiltonian matrix element must have the same conserved quantities. That is, we know *a priori* that any matrix element for which the bra and ket states do not have the same conserved quantities, *must* be zero. This is the fundamental fact that guides the compressed data structure frequently used in many-body theory. We can use the symmetries of the single-particle basis that are unbroken by the Hamiltonian to throw away vast amounts of zeroed matrix elements. Looking back to the two-body force, we want a way to categorize the matrix elements that we know are going to be zero by symmetry arguments. This is done by organizing the two-body basis into “blocks”, where a block is uniquely determined by the conserved quantities of the two body states $|pq\rangle$.

For example, the proton and neutron plane wave basis described in Chapter 3 has single particle states with the quantum numbers $\{p_x, p_y, p_z, s_z, t_z\}$. A particular two-body state $|ij\rangle$ would be sorted into a block with $\xi_{ij} = \{p_{x_i}+p_{x_j}, p_{y_i}+p_{y_j}, p_{z_i}+p_{z_j}, s_{z_i}+s_{z_j}, t_{z_i}+t_{z_j}\}$, where ξ_{ij} is a compact notation for the set of summed quantum numbers. Now we have a convenient system for finding symmetry excluded matrix elements. For example, if two basis states $|13\rangle, |46\rangle$ such that $\xi_{13} \neq \xi_{46}$, then $\langle 13|v|46\rangle = 0$. The goal now is to sort through the whole two-body basis $|pq\rangle, \forall p, q$, and group each state into a symmetry block. Then only two-body states in the same block will produce non-zero matrix elements, and we can ignore all of the rest. In many bases, like the plane wave basis, this yields an enormous reduction in the number of matrix elements that need to be stored. The reason these are called blocks, is because they show that the matrix can be organized into a block diagonal structure. Figure 5.2 shows this block diagonal structure, as well as just how sparse v_{pppp} is.

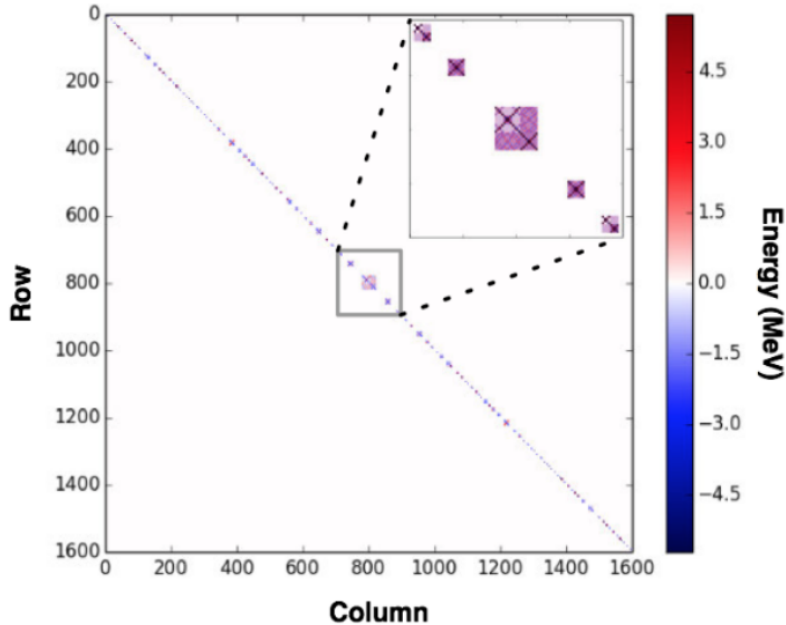


Figure 5.2: The pp-pp sector of a two-body interaction matrix for a simple neutron matter system with 40 single-particle states above the Fermi level.

Figure 5.2 is a case with 54 single-particle basis states and 14 particles, yielding 14 hole

states and 40 particle states. Even in this modest basis size, we can see just how sparse the matrix is. In a more realistic calculation with 1000 single-particle states, a factor of about 1000 can be saved, going from 16Tb of storage needed down to 16Gb, which plenty of laptops nowadays have. This particular matrix in the figure is the two-body matrix for a pure neutron matter calculation with the Minnesota potential with 54 states in the single-particle basis. This was used for visualization, since showing off larger matrices would contain almost entirely white space in this plot. Along with greatly reducing the memory needs of the calculation, this also yields enormous speed improvements, since we can now skip multiplying by zero millions of times.

5.3 Performance Testing Matrix-Matrix Multiplication

Matrix-matrix multiplication, which is frequently used in many-body calculations, is a nice case study for computational speedup. For three matrices A, B, C with matrix elements a_{pq} , the product of $C = A * B$ is written as:

$$c_{pq} = \sum_r a_{pr} * b_{rq} \quad \forall p, q. \quad (5.2)$$

Counting operations, each element c_{pq} is calculated with about r addition operations and r multiplication operations. This must be done for all p, q elements in C . For notational consistency, let's say that the first index p is the row index, and the second index q is the column index. If A, B, C are all $N \times N$ square matrices, this would mean the calculation of C would require $\mathcal{O}(N^3)$ operations. There are mathematical speedups like the Strassen algorithm [67], which scales as $\mathcal{O}(N^{2.8})$, and algorithms which can further lower this computational

complexity, but let's first just look at this simple sum in Eqn. (5.2). While mathematical complexity is very important as better scaling is almost always favorable, they leave out important details, such as potentially large (or small) coefficients in front of these polynomial powers. These coefficients can manifest themselves in unexpected ways if you haven't examined how the mathematics is actually carried out on a low level. To show this, let's introduce two algorithms that are mathematically equivalent. First, when selecting which matrix element c_{pq} to compute, we will first loop over p , the rows of C , followed by q , the columns. In the second algorithm, we will loop over the columns first, then the rows. Importantly, the innermost loop over the summed index is unchanged, so on paper this looks identical.

```

for row  $p$  in  $C$  do
  |
  for col  $q$  in  $C$  do
    |
     $c[p][q] = 0.0;$ 
    for col  $r$  in  $A$  do
      |  $c[p][q] += a[p][r] * b[r][q]$ 
    end
  end
end

```

Algorithm 1: Basic matrix-matrix multiplication, looping over rows then columns

```

for col  $q$  in  $C$  do
  |
  for row  $p$  in  $C$  do
    |
     $c[p][q] = 0.0;$ 
    for col  $r$  in  $A$  do
      |  $c[p][q] += a[p][r] * b[r][q]$ 
    end
  end
end

```

Algorithm 2: Basic matrix-matrix multiplication, looping over columns then rows

Now, in Figure 5.3 is a timing plot, showing how the cpu timings of these algorithms compare, with an optimized routine (dgemm) included as well. The results are pretty dramatic. As the size of the matrix gets larger, algorithm 2 becomes substantially faster than algorithm 1. This is largely due to how data are moved from memory to the processor, but the exact details of this are saved for a later section. The major takeaway is that considerations of how data are accessed in matrices, or tensors in the CC case, is of considerable importance. The red dotted line labeled “dgemm” is a BLAS (Basic Linear Algebra Subprograms) routine

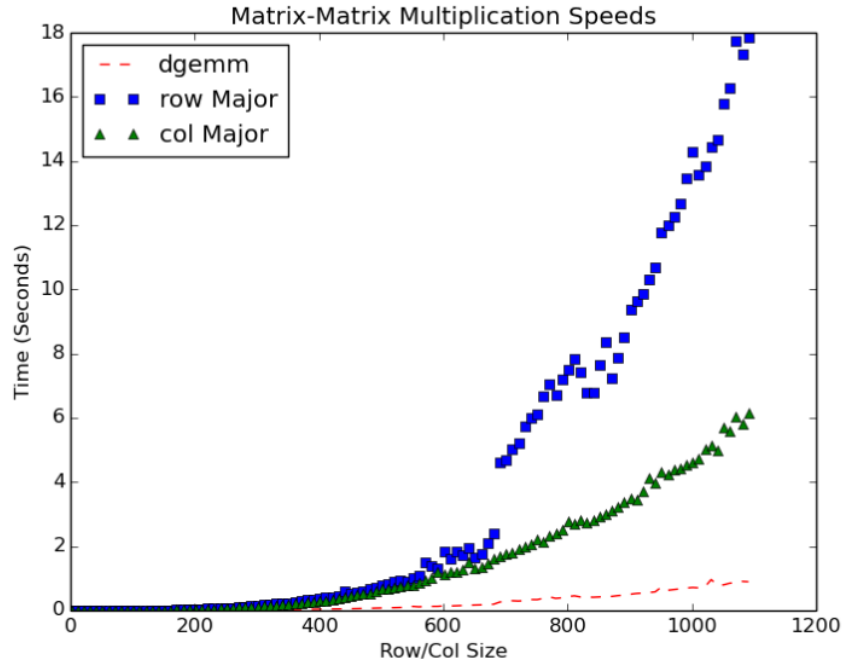


Figure 5.3: Implementation of the same mathematics can have very different run times.

which computes a general matrix-matrix multiplication. The name comes from the fact that the matrices are double precision (d) of general structure (ge), meaning not symmetric, and it is matrix-matrix (mm) multiplication, and not matrix-vector or anything else. Looking at the dgemm speeds where many layers of optimizations have been made, we can see that even for small matrices of size 1000×1000 , full order of magnitude savings can be made. This implementation of dgemm comes from OpenBLAS, which is an open source package [68]. This is not a one-off example, but just a glimpse at how important computational details are. Many-body theory is becoming an increasingly interdisciplinary field, as expertise in physics, applied mathematics, and computational science are all often needed in equal importance to access interesting questions in nature.

5.4 Tensor Contractions as Matrix Multiplication

Let's look at a particularly expensive CC diagram. We can find very expensive terms for a CCDT calculation which includes the full normal-ordered three-body force W_N . In this case, there will be terms that look like $\langle \Phi_{ijk}^{abc} | (\hat{W}_N \hat{T}_3)_C | \Phi_0 \rangle$. In the triples equation, we will have

$$\frac{1}{8} \sum_{def} w_{def}^{abc} t_{ijk}^{def}. \quad (5.3)$$

This triple sum over particle states must be computed for all a, b, c, i, j, k which means that the scaling cost is $\mathcal{O}(n_h^3 n_p^6) = \mathcal{O}(n^9)$. So even for modest single-particle basis sizes, this will be costly to compute. Similar to how the two-body basis was organized in terms of symmetry blocks, we can do the same for the three-body basis. This has two-fold benefits. The first is an enormous reduction in the memory required to store them, which is shown in Chapter 6. The second is that this three-body basis creates a mapping from the three single particle indices into one three-body index $\{a, b, c\} \rightarrow \{A\}$. This way, we can write the n^9 diagram as

$$\frac{1}{8} \sum_B w_B^{A} t_I^B, \quad (5.4)$$

where the inner index that is being summed over. This shows that with this index remapping, we have exactly the definition of matrix-matrix multiplication. This is a big win, because from the plot 5.3, we can now take advantage of the extremely optimized OpenBLAS dgemm routine.

One complication is that the symmetry organized three-body basis grouped the matrix into blocks, and we don't want to perform matrix-matrix multiplication on the entire matrices together, keeping track of many zero elements. The solution is that within each symmetry

block ξ_{pqr} , the column index B of w_B^A will still match perfectly with the row index of t_I^B , as in the two-body case described before. This means that we can just loop over the set of all symmetry blocks $\{\xi_{pqr}\}$, and do a block-to-block matrix-matrix multiply.

$$\frac{1}{8} \sum_{\{\xi_{pqr}\}} \sum_B w_B^{A(\xi)} t_I^{B(\xi)} \quad (5.5)$$

where the superscript (ξ) is denoting that we now also have a dependence on the symmetry blocks. This computational strategy is seen across a variety of many-body calculations. In CC theory, there are many terms like Eqn. (5.5), and in IM-SRG there are terms like

$$\frac{1}{2} \sum_{uv} \langle qr|\eta|uv\rangle \langle uv|\Gamma|st\rangle \stackrel{block}{=} \frac{1}{2} \sum_{\{\xi_{uv}\}} \sum_U \langle Q|\eta|U\rangle^{(\xi)} \langle U|\Gamma|S\rangle^{(\xi)}, \quad (5.6)$$

for $qr \rightarrow Q, uv \rightarrow U$ and $st \rightarrow S$, where the right-hand side has been written in block matrix notation to show that these terms can also be written as matrix-matrix products. Any operator which conserves the symmetries of the two-body states can be written as a block diagonal structure, allowing for the efficient storage of non-zero matrix elements and the usage of efficient matrix-matrix multiplication. While this work is largely focused on coupled cluster theory, it is important to stress that these tools have applicability to a large range of many-body methods.

A simple many-body method to consider is the expression for the correlation energy from MBPT2. We rewrite

$$\Delta E_{MBPT2} = \frac{1}{4} \sum_{abij} \frac{\langle ij|\hat{v}|ab\rangle \langle ab|\hat{v}|ij\rangle}{\epsilon_{ij}^{ab}}, \quad (5.7)$$

by defining the matrices \hat{A} and \hat{B} with new indices $I = (ij)$ and $A = (ab)$. The individual

matrix elements of these matrices are

$$A_{IA} = \langle I|\hat{v}|A\rangle,$$

and

$$B_{AI} = \frac{\langle A|\hat{v}|I\rangle}{\epsilon_I^A}.$$

We can define the intermediate matrix \hat{C} as

$$C_{IJ}^{(\xi_I)} = \sum_{A_\xi} \frac{\langle I|\hat{v}|A\rangle^{(\xi)} \langle A|\hat{v}|J\rangle^{(\xi)}}{\epsilon_I^A}, \quad (5.8)$$

which is the matrix product over the blocks of $(\hat{A})(\hat{B})$. We have written A with a subscript ξ as notation to restrict this sum to the symmetry block ξ_I defined by the left-hand side of the equation. From there we can rewrite the correlation energy from MBPT2 as

$$\Delta E_{MBPT2} = \frac{1}{4} \sum_{\{\xi_{ij}\}} \sum_{I_\xi} C_{II}^{(\xi)}, \quad (5.9)$$

which is the trace over the blocks of the matrix product $\hat{C} = \hat{A}\hat{B}$. Again the (ξ_{ij}) is denoting the block defined by the quantum numbers of the two-body states $|ij\rangle$, and the sum over I_ξ is denoting the restricted sum over two-body states contained within the symmetry block. By writing the inner sum over the A index as a series of matrix-matrix products between the blocks (ξ) of matrices A and B defined above, the entire expression is almost computed. Only the sum over the hole indices is left, which is taken care of by the trace.

Figure 5.4 shows the difference between the brute force summation over single-particle states of Eq. (5.7) and the block matrix set up, that is Eq. (5.8). In these calculations we

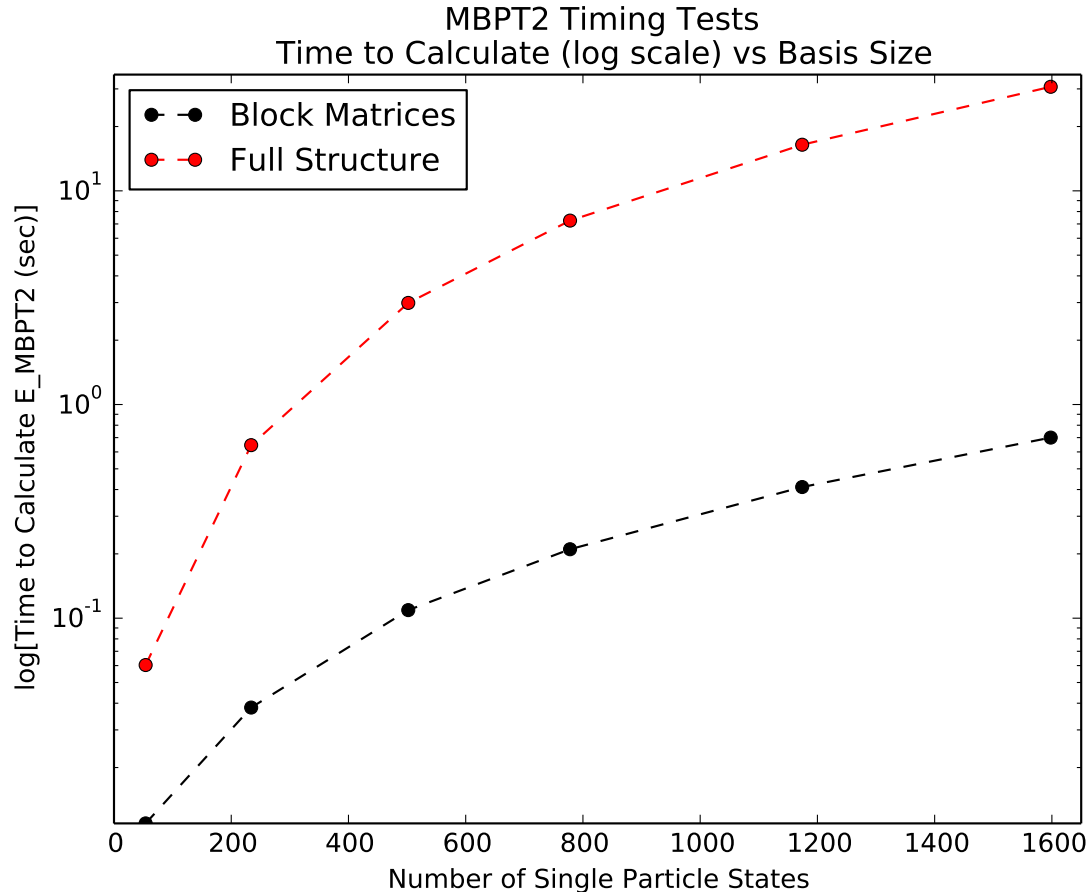


Figure 5.4: MBPT2 contribution to the correlation for pure neutron matter with $N = 14$ neutrons and periodic boundary conditions. Up to approximately 1600 single-particle states have been included in the sums over intermediate states in Eqs. (5.7) and (5.8)

have only considered pure neutron matter with $N = 14$ neutrons and a density $n = 0.08 \text{ fm}^{-3}$ and plane wave single-particle states with periodic boundary conditions, allowing for up to 1600 single-particle basis states. The Minnesota interaction model [53] has been used in these calculations. With 40 single-particle shells for example, we have in total 2713 single-particle states. Using the block matrix algorithm the final calculation time is 2.4 s (this is the average time from ten numerical experiments). The total time using the brute force summation over single-particle indices is 100.6 s (again the average of ten numerical experiments), resulting in a considerable speed up. It is useful to dissect the final time in

terms of different operations. For the block matrix algorithm most of the time is spent setting up the matrix elements for the two-body channels and to load the matrix elements. The final matrix-matrix multiplication takes only 1% of the total time. For the brute force algorithm, the multiplication and summation over the various single-particle states takes almost half of the total time. This is how code optimization typically progresses, take a section which is the current computational bottleneck and tackle that. At which point the next most expensive subroutine become prominent and must be tackled until the code runs sufficiently fast for the task at hand.

This performance speed up is very nice, but unfortunately it is not always so easy. There are many terms in the CCD equations where the tensor contractions do not have their indicies aligned as matrix-matrix products. For example,

$$-\hat{P}(ab|ij) \sum_{ld} \langle lb|X|id\rangle \langle ad|t|lj\rangle, \quad (5.10)$$

where

$$\langle lb|X|id\rangle = \langle lb|\hat{v}|id\rangle - \frac{1}{2} \sum_{em} \langle lm|v|ed\rangle \langle eb|t|im\rangle. \quad (5.11)$$

We can see that the contracted indices do not match up bra to ket in either of these cases, so some additional work must be done.

Looking at Eqn. (5.10), we can write the sum as a matrix product if we permute the indices by

$$-\hat{P}(ab|ij) \sum_{ld} \langle a\bar{j}|t|l\bar{d}\rangle \langle l\bar{d}|X|i\bar{b}\rangle, \quad (5.12)$$

where the bar over the index represents that it has been permuted from bra to ket or from ket to bra. Normally, this would be a relatively straightforward transpose type operation where the elements of the tensor are reshuffled, but due to the symmetry block structure of the tensors it gets a bit more complicated. This can be seen most strikingly with the t -amplitudes which are always in the format of two-particle two-hole excitations t_{pp_hh} , but when permuted get shuffled into a form that looks like t_{ph_hp} . This structure does not exist for the t -amplitudes, which is why we must be careful to put the bars over the indices to indicate this non-standard placement.

To maintain the block diagonal structure of this permuted tensor, we must rewrite what the symmetry blocks represent. A conservation law for $\langle ab|t|ij\rangle$ that looked like $\mathbf{k}_a + \mathbf{k}_b = \mathbf{k}_i + \mathbf{k}_j$ will now look like $\mathbf{k}_a - \mathbf{k}_j = \mathbf{k}_i - \mathbf{k}_b$ for $\langle a\bar{j}|t|i\bar{b}\rangle$. This is still the same conservation law, just shuffled around. Since the momenta are subtracted, this is functionally a time reversed state which is why the bar symbol for the anti-particle is used here.

Now that Eqn. (5.12) has been permuted, it would also help to write the intermediate in terms of the permute indices as well,

$$\langle l\bar{d}|X|i\bar{b}\rangle = \langle l\bar{d}|\hat{v}|i\bar{b}\rangle - \frac{1}{2} \sum_{em} \langle l\bar{d}|v|e\bar{m}\rangle \langle e\bar{m}|t|i\bar{b}\rangle. \quad (5.13)$$

Plugging these in together we get

$$-\hat{P}(ab|ij) \sum_{l\bar{d}} \langle a\bar{j}|t|l\bar{d}\rangle \left(\langle l\bar{d}|\hat{v}|i\bar{b}\rangle - \frac{1}{2} \sum_{e\bar{m}} \langle l\bar{d}|v|e\bar{m}\rangle \langle e\bar{m}|t|i\bar{b}\rangle \right), \quad (5.14)$$

where now we see that we have rewritten the tensor contractions as matrix products: one over $l\bar{d}$ and one over $e\bar{m}$. The resulting t -amplitude will then be in the format of $\langle a\bar{j}|t|i\bar{a}\rangle$,

so an additional permutation must be done to get it back into the correct format. It is interesting now to think if all of this was worth it. After all, the main point of the matrix-matrix product was to take advantage of efficient data movement, but this now looks like a lot of wasted inefficient data movement. While the t -amplitudes do need to be permuted and un-permuted every iteration, the two-body interaction elements do not. The permuted two-body matrix elements only need to be calculated once at the beginning of the code, and can then be used for every loop of the CC iterations.

5.5 Parallel Computing

The next step to increase the performance of the code is parallelization. If the block matrix strategy is still not yet fast enough to target a physical system of interest, then the next step is to look towards a faster computer. While Moore's law has continued the increased transistor density, this has not lead to a one-to-one increase in processor speed. To continue the exponential growth of computational power, modern computers have begun to increase the number of processing cores available per computer. This trend has been going strong for a couple of decades now, with supercomputers capable of performing hundreds of quadrillions of floating point operations per second (hundreds of petaFLOPs), and the next generation of supercomputers is predicted to break into the exaFLOP era of computing. However, accessing this level of performance brings many challenges, as the parallel paradigm requires rethinking algorithms and data structures at a fundamental level. Programs which are written and optimized for a single thread of execution, which is called a serial program, often have to be completely overhauled to run in parallel.

The first step to take advantage of parallel computing is to identify regions of the program

where a many computations are performed that are independent of each other. This usually corresponds to regions of the code for which many iterations of a loop need to be done, and the execution of the loop entries can be done in any order. For example let's examine an algorithm to compute the correlation energy of many-body perturbation theory at second order (MBPT2), that is, Eqn. (5.7). An algorithm which implements this expression in a straight forward way can be seen in Algorithm 3. The only necessary data structures are a list of hole states, a list of particle states, the two-body interaction, and an array of the single-particle energies. The energy can be calculated with a simple set of nested loops.

```
energy = 0.0;
```

```
omp parallelization directive goes here for  $i \in \text{hole states}$  do
```

```

| for  $j \in \text{hole states}$  do
| | for  $a \in \text{particle states}$  do
| | | for  $b \in \text{particle states}$  do
| | | | numerator = twoBodyInteraction(i,j,a,b);
| | | | numerator = numerator*numerator;
| | | | denominator = spEnergy[i] + spEnergy[j] - spEnergy[a] - spEnergy[b];
| | | | energy += 0.25*numerator/denominator;
| | | end
| | end
| end
end
```

```
end
```

Algorithm 3: Basic algorithm for calculating the many-body perturbation theory energy at second order.

If the number of single-particle states is large, then this type of pattern is perfect for parallelization, since all of the computations are independent of one another. Parallelizing a

loop like this is as simple as including a compiler directive from the Open Multi-Processing (OpenMP) [69] application programming interface (API) before the first loop. OpenMP is typically used to parallelize code where a single computational node has multiple cores, allocating one thread of execution for each computation core by default. OpenMP's compiler directives create multiple threads of execution to distribute the work from loops to the available processors, cutting down to overall time to compute. The only thing to take care of here, is that each thread needs to have its own copy of the "energy" variable so that they are not trying to overwrite each other. Then, each thread can combine its partial sum into a total energy upon exiting the loop using the "reduce" directive.

Unfortunately, this seems like we have taken a step backwards to take a step forwards, since we have only parallelized the brute force version of this calculation. This was to illustrate cases where parallelization is very easy, and much can be gained for a small amount of effort. This is a case where it is significantly easier to parallelize the simple implementation of the code, but the advantage we gain by compressing the matrices into blocks is too good to give up. An algorithm for the more optimized block matrix implementation for MBPT2 is in algorithm 4, where the loops are now over the block diagonal structure.

```

energy = 0.0;
for block  $\in$  symmetryBlock.blocks do
  for row  $\in$  symmetryBlock(block).rows do
    for col  $\in$  symmetryBlock(block).cols do
      i = symmetryBlock(block,row,col).holeIndex1;
      j = symmetryBlock(block,row,col).holeIndex2;
      a = symmetryBlock(block,row,col).particleIndex1;
      b = symmetryBlock(block,row,col).particleIndex2;
      numerator = twoBodyBlockInteraction(block,row,col);
      numerator = numerator*numerator;
      denominator = spEnergy[i] + spEnergy[j] - spEnergy[a] - spEnergy[b];
      energy += 0.25*numerator/denominator;
    end
  end
end

```

Algorithm 4: Block diagonal algorithm for calculating the many-body perturbation theory energy at second order.

One consequence of looping over only the non-zero matrix elements is that a new data structure, here called “symmetryBlocks” needs to keep track of how many total blocks there are, how many rows and columns are within each block, and the single-particle indices that generated each matrix element. While this is a worthwhile trade-off, it does make the parallelization more difficult. While putting the usual parallelization directive at the top most loop will again split the amount of work up and distribute it to the different threads. However, the basic directives will distribute a roughly equal number of blocks to

each thread, and the blocks vary in size considerably. This leads to what is called “load imbalance”, where some processors have a much larger amount of work to be done than others. Once the processors with the least amount of work finish, they just sit idle while the other processors keep going. Thus the time it takes to complete the parallel section is completely bottlenecked by which thread was given the most amount of work. In Fig. 5.5, a cartoon of the problem is shown with an example of four threads of execution. Even if the

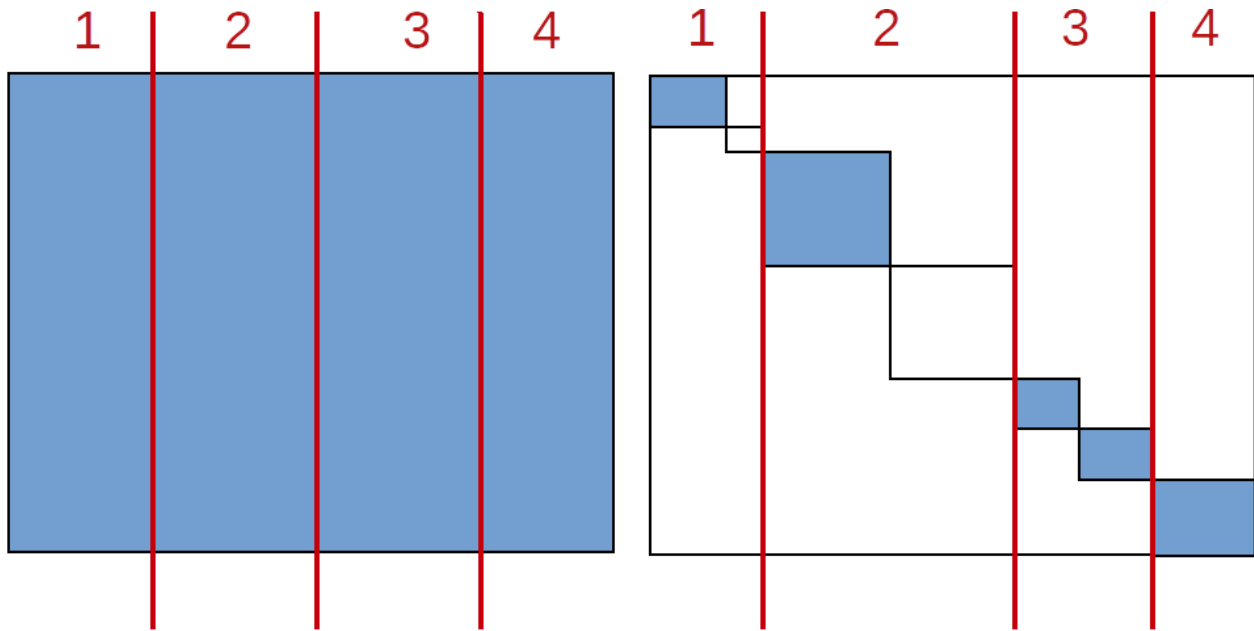


Figure 5.5: A cartoon of how the interaction matrix might be split into work loads for different threads of execution for the naive storage and the block storage schemes.

parallelization scheme is terribly load balanced the block matrix implementation will still be significantly faster, but optimizing the parallelization of the blocks can be tricky since the sizes of the blocks varies considerably as seen in Fig. 5.2. This load imbalance becomes worse and worse the larger the matrices become, and the more threads that are used for parallelization.

5.6 Distributed Memory Parallelization

As the system increases in size, even the block diagonal compression of the full interaction becomes insufficient, as the memory required to store the blocks becomes too large to contain in RAM. So the speed of the computation becomes an irrelevant question, as the computation is impossible. This memory wall can be circumvented with distributed memory parallelization, where multiple computational nodes are linked together via a network and work together. This allows the combined RAM of multiple nodes to be leveraged to solve larger problems. In practice, this is done with the Message Passing Interface (MPI) API, which launches a copy of a program on each node, and allows the communication of the copies amongst each other. For this application, the OpenMPI [70] implementation was used. While the increased memory of many compute nodes helps with the memory problem, it does not circumvent the load balancing problem. Whereas OpenMP allows each thread of execution to view the whole matrix in memory, the load imbalance was more a matter of which thread is responsible for which computations. With distributed memory parallelism each copy of the program, or “rank” as they are called in MPI, can only access the matrix elements on other ranks via costly communication across the network. Now Fig. 5.5 can represent the difficulty in distributing the interaction matrix across multiple compute nodes. If we distribute the blocks of the interaction matrix such that each MPI rank has an equal number of blocks (with no consideration of block size), then the ranks with the smallest number of matrix elements finish much faster than the ranks with more work to do. This disparity can be seen in Fig. 5.6, where the time between the fastest rank and the slowest rank becomes increasingly larger for increasing number of MPI ranks.

To correct for this, before the matrix elements are computed, the block sizes are computed

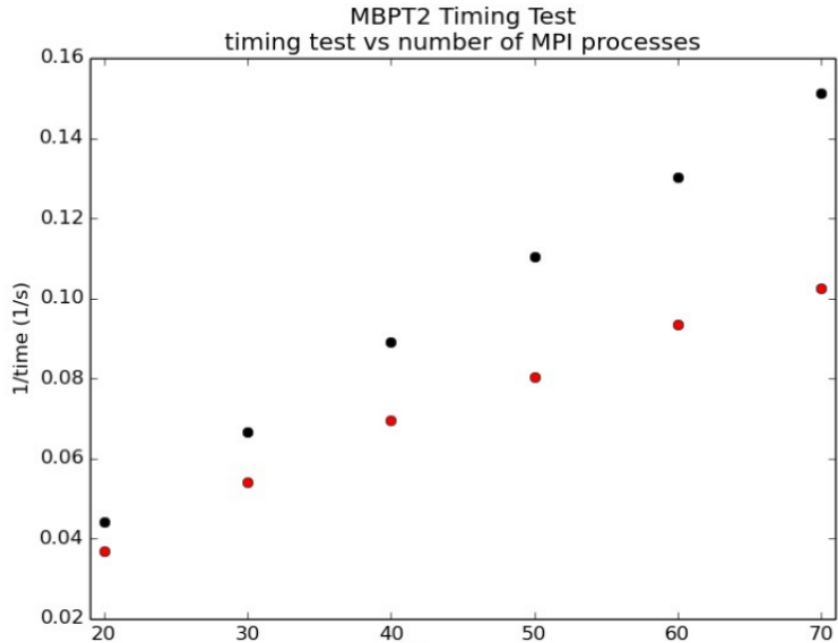


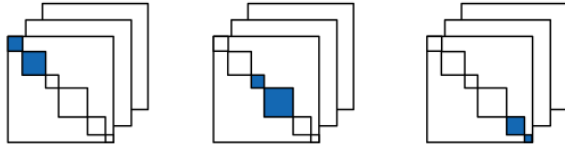
Figure 5.6: Performance of MBPT2 calculations with increasing number of MPI ranks. The speed of the calculation is measured in s^{-1} , the black data are the inverse time required to finish the calculation on the fastest rank, and the red data are the speeds of the slowest rank.

and sorted so that they can be distributed such that each rank is responsible for roughly the same number of non-zero matrix elements, rather than the same number of blocks. This has the added benefit that the calculation is load balanced for the computation of the matrix elements, such that the time it takes to load the matrices is roughly equal among the ranks as well. In the case of calculations for infinite matter, the two-body basis forms many more small blocks than large blocks. The blocks can be passed to the ranks by a bin-packing algorithm, which passes the largest blocks to the ranks starting from the largest block. Once the largest blocks have been distributed, the small blocks can be passed in to keep all of the ranks roughly even with respect to number of non-zero matrix elements.

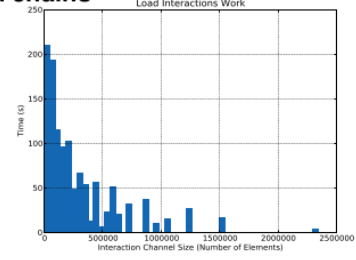
5.7 Final Parallel Algorithm

We finally have all of the ingredients to describe the distributed memory algorithm for performing coupled cluster calculations implemented for this work. The full algorithm is shown via a series of cartoons and histograms below to illustrate the work flow. These figures and this distribution scheme were a joint effort by the author, Stephanie Lauber and Peter Ahrens. The first step is to pre-compute the size of the two-body basis blocks, and assign the blocks to MPI ranks in a way to minimize load imbalance. This is shown in Fig. 5.7, where the three columns represent three MPI ranks, and the blocks colored in blue represent which blocks each rank is responsible for. The stacked layers of the matrices represents that this is happening for multiple sectors of the interaction matrix, although due to its size, most of this discussion is focusing on the v_{pp-pp} sector. On the right side of the figure is a histogram of the time required to load the matrices as a function of block size for an example calculation neutron matter with the Minnesota potential using the CCD approximation, although the results are largely general to any infinite matter calculation. The highest peak is at the first bin, which shows that loading the blocks with 50,000 or less non-zero matrix elements constitutes the most total compute time at this stage in the calculation. The distribution has a fairly long jagged tail with the final bin being a single block with about 2.5 million non-zero matrix elements. The next step is to perform the tensor contractions, starting with the terms which require some permutation to be aligned as a matrix-matrix product. In CCD, one such term is

$$\frac{1}{2} \sum_{dl} \langle kl|v|cd\rangle \langle db|t|lj\rangle \quad (5.15)$$

Step 1**Initialization and memory balancing of interaction chains**

WORKFLOW



The dimensions of the blocks are pre-computed; the load balancer takes in these dimensions and evenly distributes the work load. Each processor constructs a local piece of the total interaction matrix.

There are many small blocks and few outliers, making it easy to balance.

Figure 5.7: The blocks are distributed to the ranks to try and keep the number of non-zero matrix elements equal among ranks. The histogram shows that the time it takes to load these blocks is dominated by an enormous amount of small blocks, which is ideal for load balancing.

where the inner indices are not aligned, and so a permutation step is required to write this as

$$\frac{1}{2} \sum_{dl} \langle \chi(kc)|v|\chi(dl) \rangle \langle \chi(dl)|t|\chi(jb) \rangle, \quad (5.16)$$

where the χ represents the permutation operation which remaps the data to align the tensor contraction as a matrix-matrix multiply. In Fig. 5.8, the tall skinny blocks represent the t -amplitudes, since they are always of the form t_{pp_hh} , the particle dimension is always considerably larger than the hole dimension. Secondly, tensor elements are now colored in yellow to represent the fact that for a given rank the permutation operation requires t -amplitudes which are on other ranks. Here, the overall time to compute these diagrams is smaller than the loading step, but it is interesting to see from the histogram that it is now the large blocks which are taking the longest. The actual matrix-matrix product is not very costly here, most of the time in this step is spent receiving and transmitting data across the network for the permutation operation. Furthermore, the communication pattern can be entirely pre-computed before the first iteration. This allows for efficient communication across the network, as each rank can group all of the elements that need to be sent into a

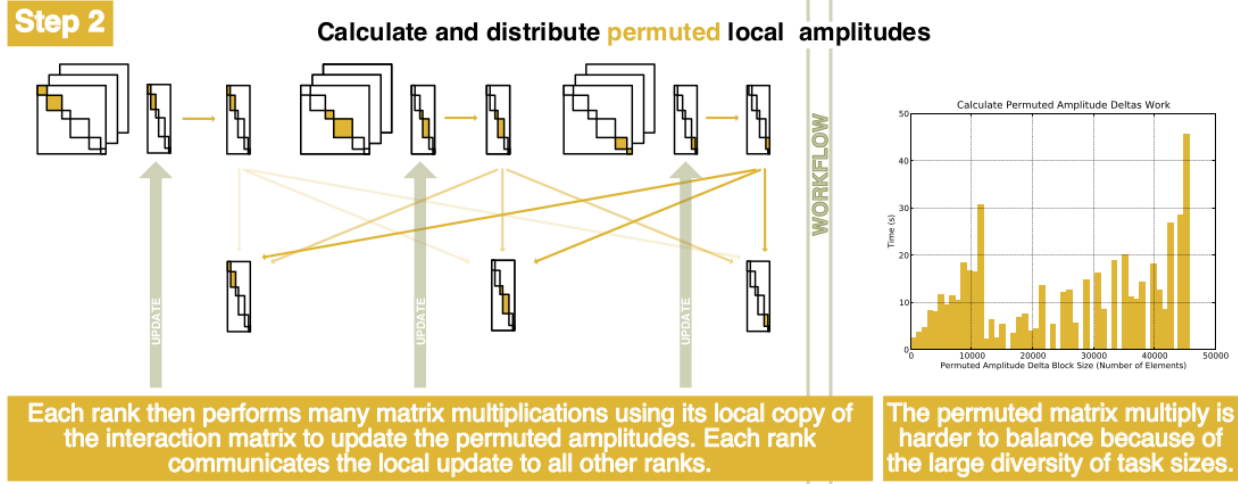


Figure 5.8: The t -amplitudes are permuted as needed for the tensor contractions which are not aligned as a matrix-matrix product. In the histogram, the larger blocks have begun to take more of the total time relative to the previous step.

separate buffer from each other rank that needs the data.

The next step is to compute the tensor contractions which do not require any permutation to be expressed as a matrix-matrix product. This step includes the most costly term, that of

$$\frac{1}{2} \sum_{cd} \langle kl|v|cd \rangle \langle cd|t|ij \rangle \quad (5.17)$$

which needs the $v_{pp,pp}$ sector of the two-body interaction. The histogram in Fig. 5.9 shows that the work is much more even across block sizes than the load step. This is because loading the matrices scales as N^2 for a matrix of row size N , and a matrix-matrix product scales as N^3 . So the large dense matrices take proportionally longer than adding together many small matrix products.

The last step, shown in Fig. 5.10, is to update the t -amplitudes using the partial sums from the various diagrams. Once each rank has updated the t -amplitudes, it computes its partial sum of the CCD correlation energy, and a global reduce between all of the ranks sums the final energy for that step. If the energy is still changing rapidly (above some set

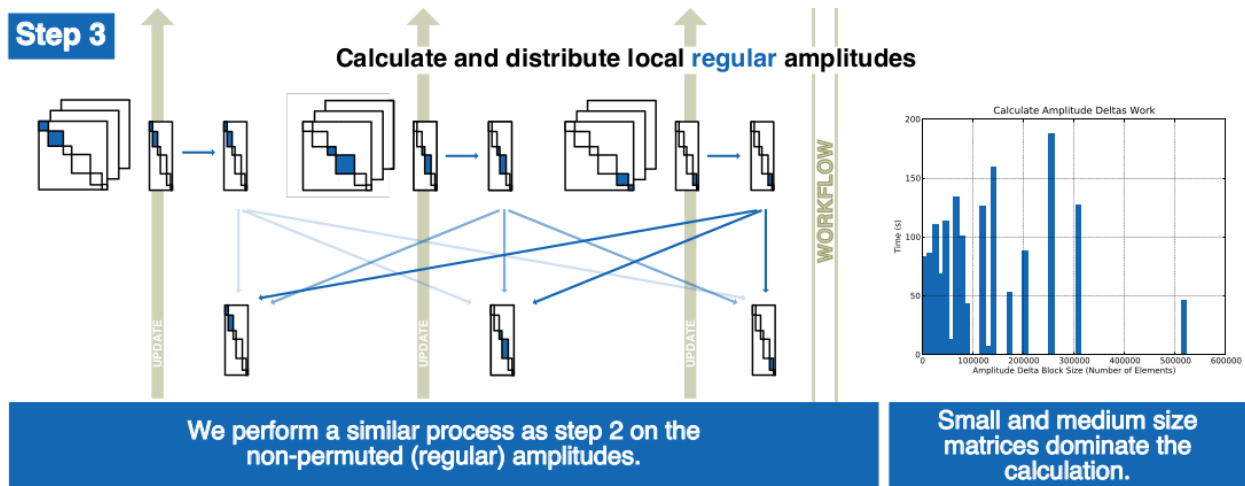


Figure 5.9: The largest tensor contractions are now performed, which are already aligned as matrix-matrix products. The $\mathcal{O}(N^3)$ scaling of the matrix-matrix product causes the larger matrices to contribute significantly to the total processing time in this step.

tolerance) compared to the previous iteration, these new amplitudes are used for the next iteration, which begins at step 2 of the algorithm. Step 1 does not need to be recomputed each step, since the interaction matrices only need to be loaded once at the beginning of the calculation.

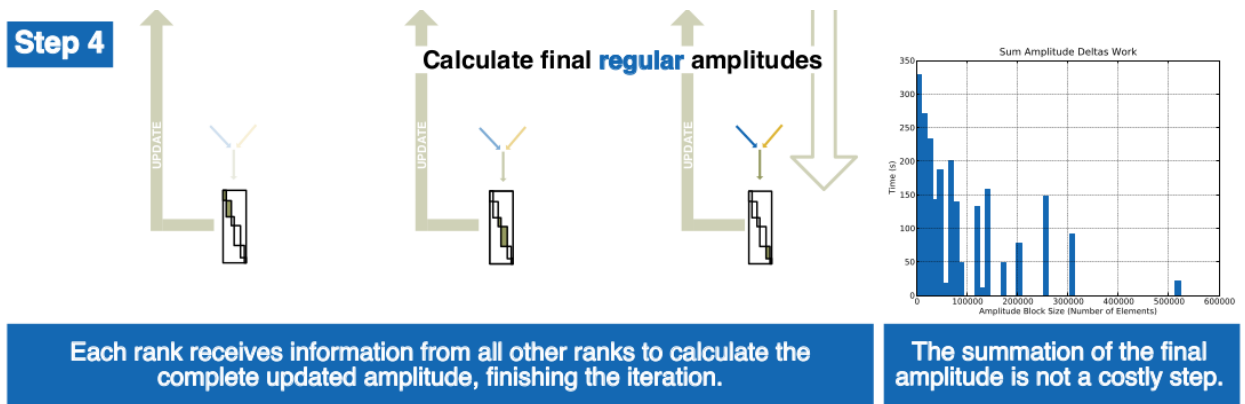


Figure 5.10: The t -amplitudes are summed together and the correlation energy is calculated. If the energy has not converged to the set tolerance, another iteration of the CC equations are performed, using these new t -amplitudes in step 2.

Once the energy has converged, the CC correlation energy for the ground state of the system has been found. The results for some selected physical systems and more concrete

performance tests can be seen in Chapter 6.

Chapter 6

Results

One quantity of interest to many physical scientists is the equation of state for different forms of matter. The equation of state describes some state variables of matter under certain conditions. For example, Boyle's law which describes the relationship between the pressure and volume of an ideal gas. If the gas is in a plunger and you push down on it, the equation of state describes how much pressure pushes back on the plunger. The equation of state of nuclear matter is of great importance in understanding the interior of neutron stars.

This matter has enormous gravitational pressure on it, and understanding the equation of state of such dense matter, how hard the matter pushes back, would allow the mass-radius relationship of neutron stars to be calculated. This is observationally very difficult due to how small and dim neutron stars are, so a first principles calculation of the equation of state is of great interest to the nuclear astrophysics community. One way to simulate the interior of a neutron star is to calculate the energy of a large slab of neutrons with the many-body Schrödinger equation. As outlined in previous chapters, by choosing a single particle basis of plane waves in a box with periodic boundary conditions, we can systematically increase the number of states, the number of neutrons, and the size of the box to better approximate this extreme environment. Due to the computational demand of adding additional single-particle states and number of neutrons, a polynomially scaling many-body method like coupled cluster (CC) theory is a great choice.

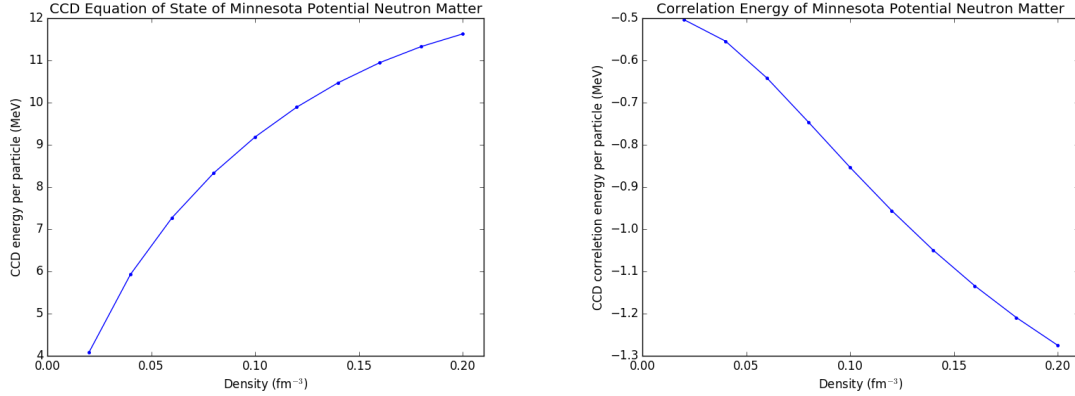
To find the equation of state it is standard to calculate the energy of the system at a

range of densities. This energy-density relationship provides a similar insight into nuclear matter, as the pressure-volume relationship of Boyle’s law provides for an ideal gas. A detailed calculation would use a state-of-the-art chiral effective field theory (χ -EFT) [6, 7] derived neutron-neutron interaction with three-body forces. As a proof-of-concept, the results in the chapter will present calculations of neutron matter using the simple nuclear force model called the Minnesota potential, and show capabilities of the CC code on the most computationally demanding term of full three-body force calculation.[53] These are the essential ingredients for a future project which is being planned to leverage the computational power of a supercomputing center for such a highly accurate *ab initio* calculation of the nuclear equation of state.

6.1 Neutron Matter

Fig. 6.1a is a plot of the equation of state of neutron matter with the Minnesota potential. We see that as the density increases the energy per particle of the system monotonically increases. To get an idea for how much of this calculation is beyond mean field contributions, we look at just the CCD correlation energy in Fig. 6.1b. With this system, due to the short range nature of the nuclear force, the many-body correlations become more and more important as the density increases.

The next plot of interest increases not only the size of the basis, but also the number of particles in the box. The limit where the number of nucleons A goes to infinity, as the volume V of the system goes to infinity and $N/V = \text{const}$ is called the thermodynamic limit. Figure 6.2a shows the convergence of the system towards the thermodynamic limit as function of the number of particles for the CCD approximation with the Minnesota interaction model



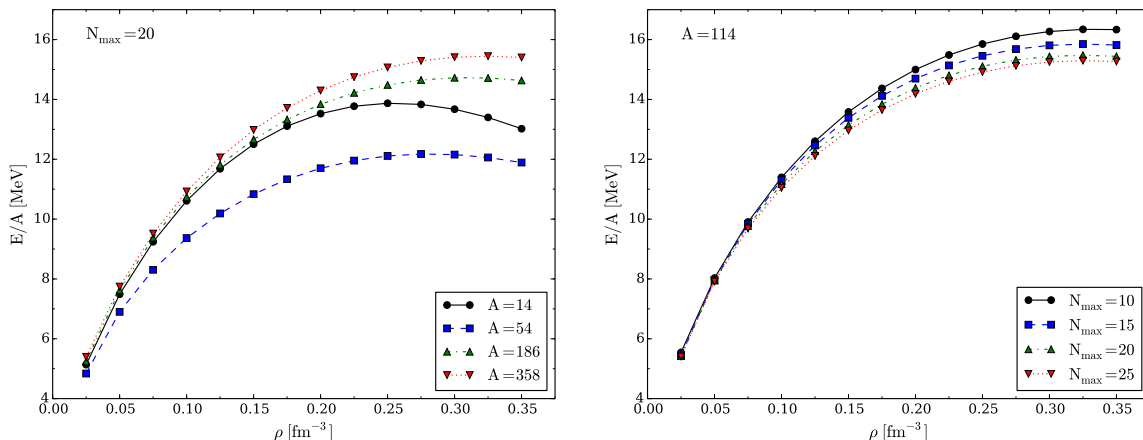
(a) The equation of state for pure neutron matter with the Minnesota potential. (b) Correlation energy per particle as a function of density.

Figure 6.1: Two different energy per particle plots at low densities of neutron matter with the Minnesota potential [53] computed in the CCD approximation with 54 neutrons and an $N_{\max} = 100$ truncation (100 plane-wave energy shells), corresponding to 10754 single particle states.

[53] with $N_{\max} = 20$.

Notice that $A = 54$ is lower than $A = 14$ and $A = 186$ is above. This shows that the convergence towards the thermodynamic limit is not monotonic. Before worrying about this limit however it is necessary to check, for an individual calculation at fixed particle number, that the calculation has converged within the basis.

Figure 6.2b shows the convergence in terms of different model space sizes with a fixed number of neutrons $N = 114$. The EoS lines appear to get closer together in Figure 6.2b, and $N_{\max} = 25$ seems to be relatively converged. To get a more quantitative look at convergence, it is better to look at the relative error among model spaces of a particular density on the plot. These types of calculations are important to get a grasp on basis truncation errors. There is active work in fitting the energy curves and extrapolating to the infinite basis limit, and while this is a powerful technique, it is necessary to actually calculate quantities with large basis sets to validate the extrapolation. It is also important to ask about the universality



(a) Equations of state for different numbers of particles with $N_{\max} = 20$ (874 single particle states) (b) Equations of state for different model space sizes with $A = 114$.

Figure 6.2: Energy per particle of pure neutron matter computed in the CCD approximation with the Minnesota interaction model [53].

of basis convergence. In the case of neutron matter, Figure 6.3 shows how for different numbers of particles, the convergence of the calculation can be dramatically different. For 14 neutrons, one-thousand basis states quickly converges. However for larger calculations, like 114 neutrons, the calculation is only stable to 3-4 digits at 3,500 basis states.

The final piece to mention on the topic of basis set convergence is about extrapolating to the thermodynamic limit of infinite matter. Since this matter is meant to simulate an effectively infinite expanse of neutrons or electrons, it is important to also increase the number of particles in the system. The thermodynamic limit of bulk matter is when $N \rightarrow \infty$, $V \rightarrow \infty$ and $N/V \propto \text{const}$. Here it is helpful to reconsider the “box” the calculation is being done in. The periodic boundary conditions (PBC) $\phi(x_i) = \phi(x_i + L)$ are arbitrarily chosen boundary conditions that constrain the wavefunctions. Any number of other boundary conditions could have been chosen, like anti-periodic boundary conditions $\phi(x_i) = -\phi(x_i + L)$. Studies have shown that the difference between these two choices gives an idea of how much the correlation energy is affected by this basis truncation [71, 72, 23].

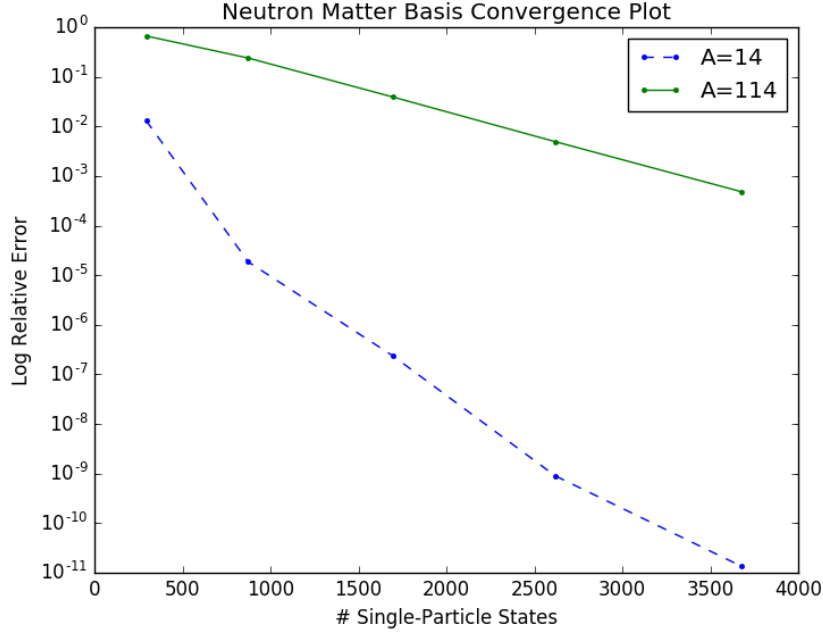


Figure 6.3: The relative error shows how much the CCD correlation energy is changing between subsequent calculations at different model spaces sizes ranging from $N_{\max} = 10$ to 70 for neutron matter with the Minnesota potential at density 0.2 fm^{-3} .

One solution to this problem is by integrating over solutions between periodic and anti-periodic conditions, known as twist-averaging [73]. This is an attempt at allowing more freedom in the basis functions at the boundary. The single-particle states are multiplied by a phase for each direction, characterized by a twist-angle, θ_i ,

$$\phi_{\vec{k}}(\vec{x} + \vec{L}) \rightarrow e^{i\vec{\theta}} \phi_{\vec{k}}(\vec{x}). \quad (6.1)$$

For periodic boundary conditions (PBC) $\theta_i = 0$ and $\theta_i = \pi$ for anti-periodic boundary conditions (APBC)

$$\vec{k} \rightarrow \vec{k} + \frac{\vec{\theta}}{L} \quad (6.2)$$

$$\epsilon_{\vec{k}} \rightarrow \epsilon_{\vec{k}} + \frac{\pi}{L} \vec{k} \cdot \vec{\theta} + \frac{\pi^2}{L^2}. \quad (6.3)$$

These twist phases effectively change the momentum of the basis states. This yields new single-particle energies. This correction disappears as $L \rightarrow \infty$, which is desired, since all boundary conditions should become irrelevant in that case. Since the single particle energies are changing, this changes the shell structure of the basis. Depending on the twist chosen, certain particle states can jump to holes or holes to particles. It is therefore necessary to fill hole states separately for each $\vec{\theta}$ since the CC framework developed so far is only effective for a closed-shell reference state. Integration over a quantity is approximated by a weighted sum, such as Gauss-Legendre quadrature, over the quantity for each set of twist angles. The algorithm is described in Algorithm 1. By using twist-averaged boundary conditions,

```

Build mesh points and weights for each direction;
 $E_{\text{twist}} = 0$ ;
for  $(\theta_{x_i}, w_{x_i}) \in \{\theta_x, w_x\}$  do
  for  $(\theta_{y_i}, w_{y_i}) \in \{\theta_y, w_y\}$  do
    for  $(\theta_{z_i}, w_{z_i}) \in \{\theta_z, w_z\}$  do
      Build Basis States with  $k_i \rightarrow k_i + \frac{\theta_i}{L}$ ;
      Order States by Energy and Fill Holes;
      Get Result  $E$  (T,HF,CCD);
       $E_{\text{twist}} = E_{\text{twist}} + \frac{1}{\pi^3} w_x w_y w_z E$ ;
    end
  end
end
end

```

Algorithm 5: Twist-Averaged Boundary Condition Algorithm

the extrapolation towards the thermodynamic limit is significantly smoother. However, this comes at a price, since a full CCD calculation is done at each of these steps. If, for example, 10 twist angles (called TABC10) in each direction are used, this requires 1000 full CCD calculations. For a computationally cheaper glimpse into the effects of twist-averaging, it is easy to calculate the kinetic energy per particle and the Hartree-Fock energy per particle, which avoids the full CCD calculation. It is clear in Figure 6.4a how much more stable the

energy calculations are with respect to particle number. These calculations can be compared to the exact values for infinite matter, which are calculated by integrating the relevant values up to the Fermi surface. The kinetic energy is given by

$$T_{\text{inf}} = \frac{3\hbar^2 k_f^2}{10m},$$

while the potential energy to first order (corresponding to the Hartree-Fock contribution) reads

$$\text{HF}_{\text{inf}} = \frac{1}{(2\pi)^6} \frac{L^3}{2\rho} \int_0^{k_f} d\vec{k}_1 \int_0^{k_f} d\vec{k}_2 \langle \vec{k}_1 \vec{k}_2 | \hat{v} | \vec{k}_1 \vec{k}_2 \rangle.$$

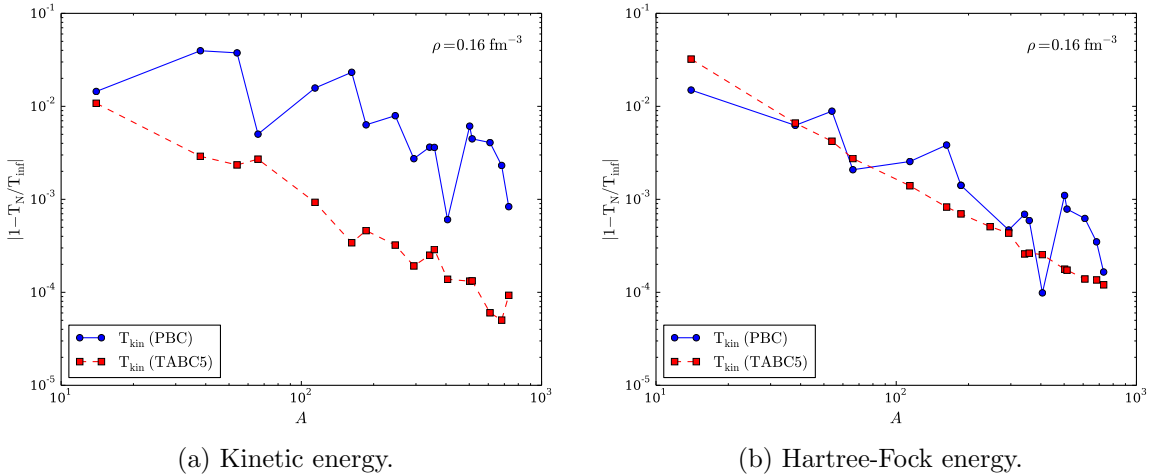
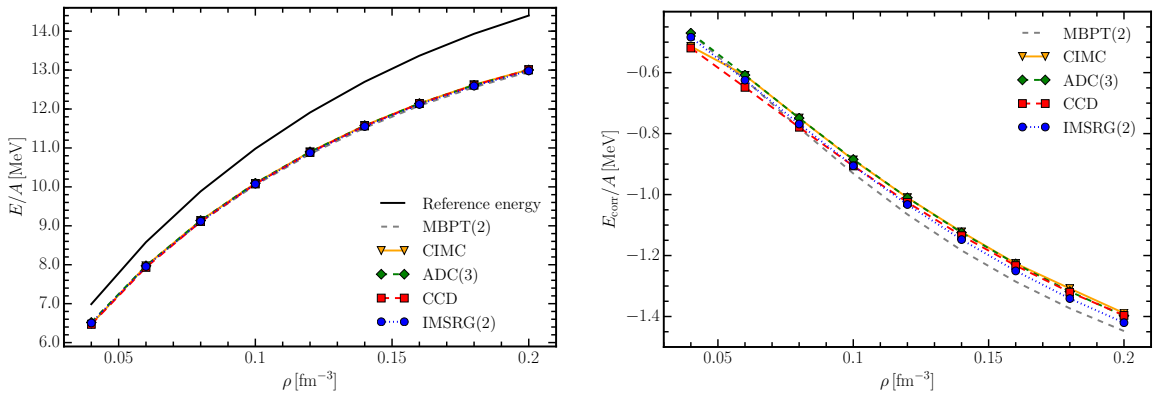


Figure 6.4: Finite-size effects in different energies of pure neutron matter computed with the Minnesota interaction model [53] as a function of the number of particles for both periodic boundary conditions (PBC) and twist-averaged boundary conditions (TABC5).

Similarly, Fig. 6.4b displays the corresponding Hartree-Fock energy (the reference energy as defined in Chapter 2) obtained with the Minnesota interaction using both periodic and twist-averaged boundary conditions. The results show again a weaker dependence on finite size effects. These are some of the tools needed to push towards the realistic thermodynamic limit calculations that are necessary. Of course these calculations will require a more sophis-

ticated nuclear potential, so it is instructive to examine another infinite matter system to check for similarities and discrepancies.

To conclude this section, a comparison of pure neutron matter calculations for several different many-body methods is presented in Fig. 6.5. Configuration interaction Monte Carlo (CIMC) and the algebraic diagrammatic construction (ADC) of the self-consistent Green’s function scheme [74, 75, 76], were not detailed in this text, but are other many-body methods of interest to many researchers [77]. We see that all of these methods add configurations that contribute correlations much beyond the reference energy. Additionally, they all have the same qualitative features. This is as expected, since they are all solving the same system, any differences between the methods are due to differences in many-body correlations they add. The collaborative work of [77] provides a detailed comparison of the many-body methods for the Minnesota potential.



(a) The equation of state for pure neutron matter. (b) The correlation energy per particle for each method.

Figure 6.5: Energy per particle for pure neutron matter with the Minnesota potential [53]. Here the calculations have been performed with IM-SRG(2), CCD, CIMC [77], and the ADC(3) Self-Consistent Green’s Function scheme [77].

6.2 Homogeneous Electron Gas

In Figure 6.6, a similar procedure using CCD to calculate the ground state energy of the homogeneous electron gas (HEG) at a range of densities has been calculated. While nuclear matter calculations are computed with respect to the particle density ρ , HEG calculations are usually phrased in terms of the Wigner-Seitz radius (r_s), so the energy per particle vs. Wigner-Seitz Radius forms an equation of state for the HEG. The Wigner-Seitz radius is defined as

$$\frac{4}{3}\pi r_s^3 = \frac{1}{\rho}, \quad r_s = \left(\frac{3}{4\pi\rho}\right)^{1/3}. \quad (6.4)$$

The plots in this chapter will give r_s in units of the Bohr radius, $r_b = \frac{\hbar}{m c \alpha}$, where m is the electron mass, c is the speed of light, and α is the fine structure constant. Unlike the nuclear force, the Coulomb force between electrons is well known, and so the electron gas has been studied much more extensively. [23, 78].

Increasing in the independent variable in Figure 6.6, r_s , corresponds to decreasing the density of the system. The plot shows that as the particles are squeezed tighter together the repulsive force increases the energy of the system, similar to the case with the Minnesota potential.

What might be less intuitive is how the many-body contributions look. Subtracting out the reference energy and plotting just the CCD correlation energy, as seen in Figure 6.7, shows that as the electrons spread apart (r_s increasing), the many-body correlations from CCD monotonically increase. However, this is a bit misleading, since the absolute magnitude of the energy is very large as seen for the smallest r_s regime of the EoS. Figure 6.8 shows that at small r_s (high densities), the reference energy is very nearly 100% of the total, whereas at $r_s = 1.0$, many-body correlations make up about 5% of the total energy, which is a very

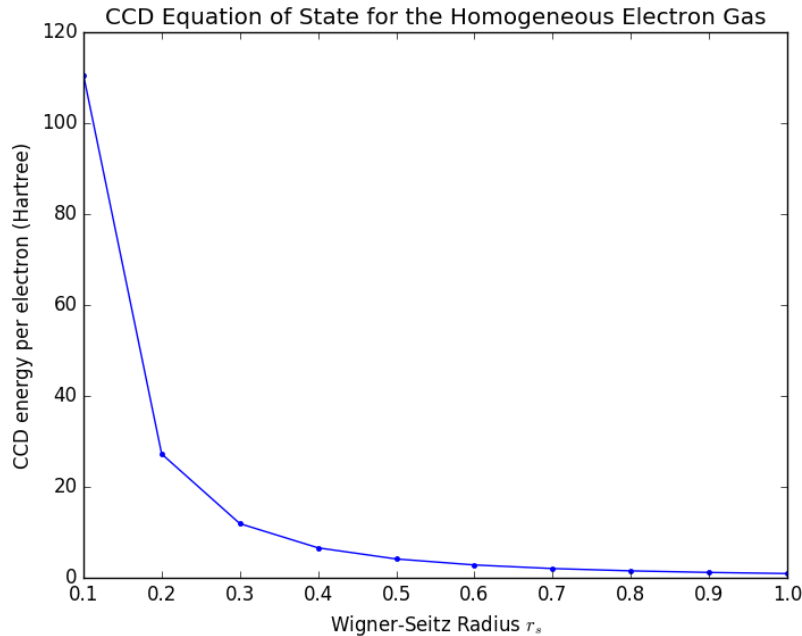


Figure 6.6: The CCD energy per particle for the homogeneous electron gas for a range of Wigner-Seitz Radii with $A = 14$ electrons

significant contribution in the high accuracy field of quantum chemistry. This means that at high densities, the reference (Hartree-Fock) energy contributes the vast majority of the total energy and the state is well approximated by a single Slater determinant. Conversely, as the electrons spread out, the many-body correlations become increasingly important.

Again, it is necessary to check the convergence of the calculations with respect to the single particle basis size. Figure 6.9 shows the relative error of the CCD correlation energy for the HEG with $r_s = 1.0$ and $A = 14$ electrons. The results are quite striking when compared with Figure 6.3, which shows that at 2500 basis states the relative error for $A = 14$ was down to 10^{-9} , whereas here, the relative error is still at 10^{-3} ! This is much closer to the $A = 114$ particle case, showing that for the same number of particles, electron gas calculations need a much larger basis to converge.

This convergence is significantly slower, meaning that the HEG needs much larger basis

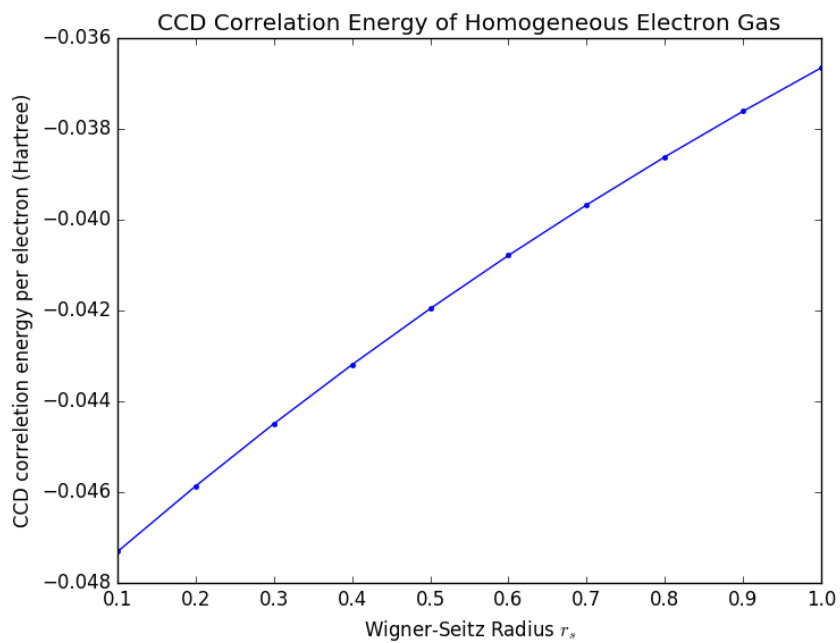


Figure 6.7: Contributions to the energy from purely CCD many-body correlations.

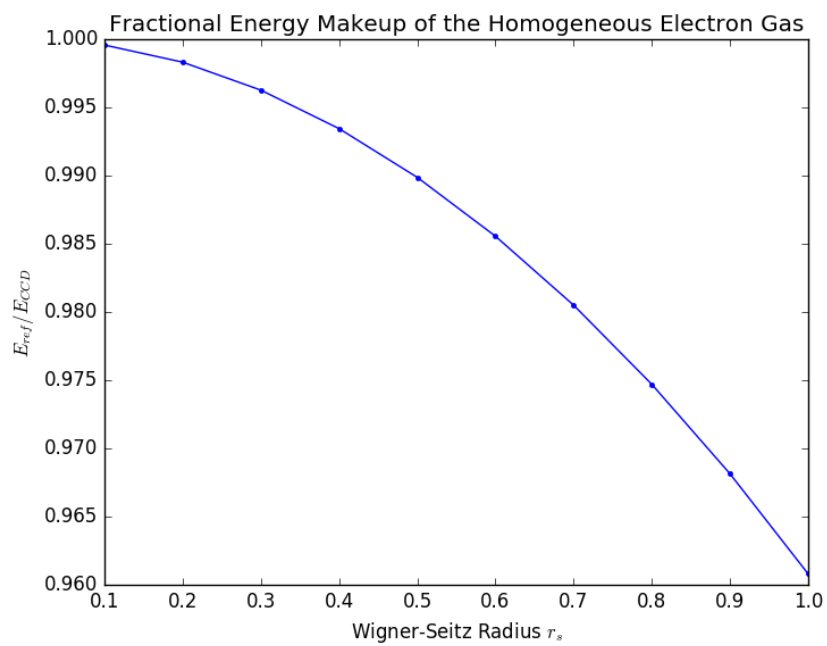


Figure 6.8: Fractional contribution to the energy from the Hartree-Fock reference state.

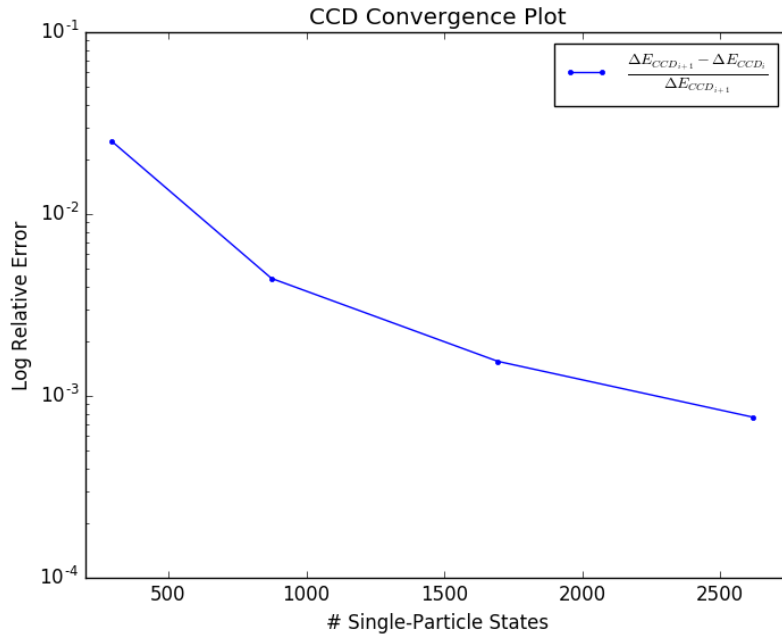


Figure 6.9: The relative error shows how much the CCD correlation energy is changing between model spaces sizes ranging from $N_{\text{max}} = 10$ to 60 for the electron gas at $r_s = 0.5$.

sets for the same level of precision when compared to neutron matter. This is again due to the very long range tail of the Coulomb potential coupling electrons across large distances and thus calculations for the HEG need a larger “box” to perform the calculation in. However, it is hard to make a direct comparison, when the densities and Wigner-Seitz radii have not been tuned to be equivalent. To gain some insight to how significant this is, Figure 6.10 shows the same plot, but at a much higher density of $r_s = 0.1$. This shows that the convergence trend is not dependent on densities for the electron gas, and that it has more to do with the nature of the Coulomb force than particle number.

6.3 Computational Results

To get an idea of just how slow the basis convergence is for the HEG or for neutron matter with a large number of particles, a calculation using an extremely large basis set was ran on

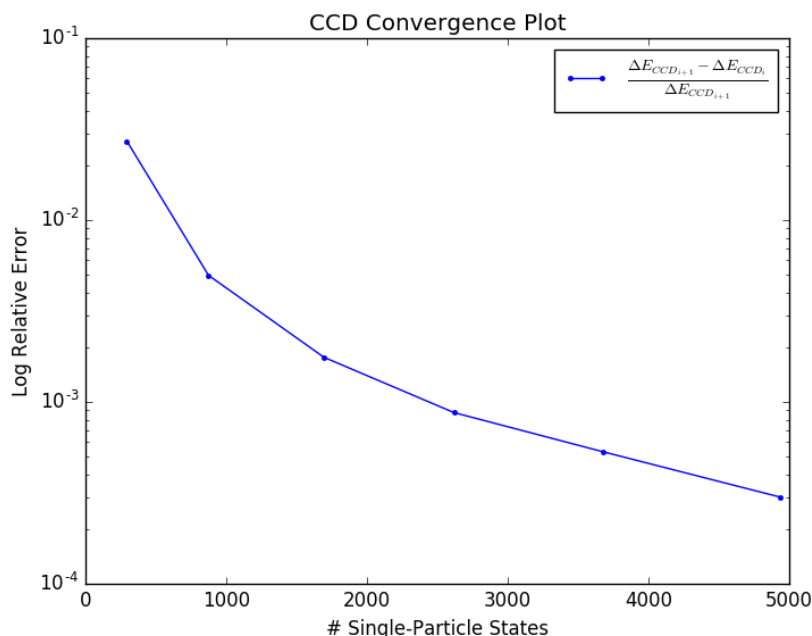


Figure 6.10: The relative error shows how much the CCD correlation energy is changing between model spaces sizes ranging from $N_{\max} = 10$ to 60 for the electron gas at $r_s = 0.1$.

2048 of the XE compute nodes on the Blue Water supercomputer. Each of these nodes has 32 cores, totalling 65,536 cores for this calculation. Figure 6.11 shows that it is not until around 25,000 basis states that the calculation approaches the $\sim 10^{-9}$ level of accuracy of the much smaller basis used for the Minnesota potential calculation. In this calculation, the tolerance for the CCD iterative solver was set to $\sim 10^{-9}$, so the drop at the final data point is just a random fluctuation as it is beyond the convergence tolerance.

However, with large calculations like this, choosing the proper basis size for the calculation at hand can be done via an interpolation, which is generally a more accurate method of prediction than extrapolation.

Even with just a two-body force, this calculation required 54,000 Gigabytes of memory to store the interaction tensor. This proved to be an excellent case to validate the distributed memory implementation described in Chapter 5. Figure 6.12 shows the time

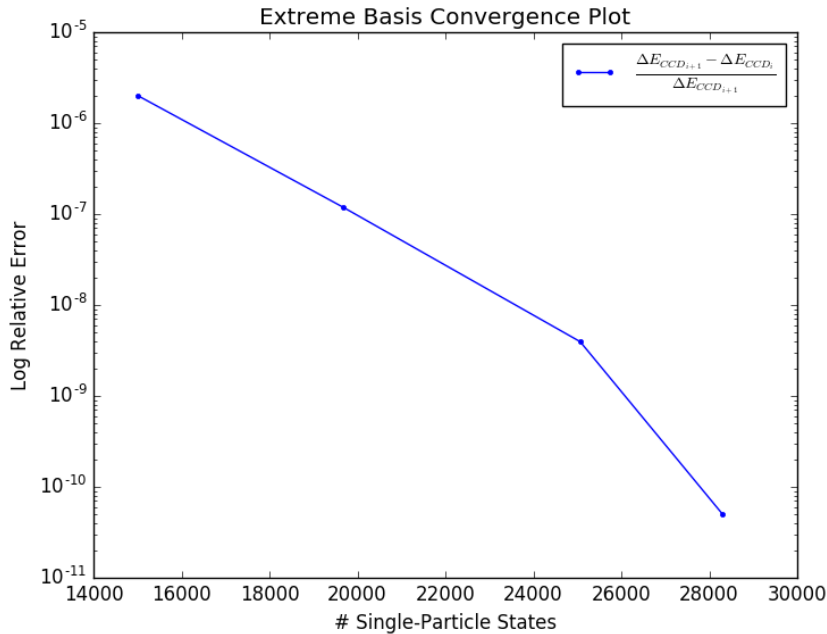


Figure 6.11: The relative error of the CCD correlation energy is changing between model spaces sizes ranging from $N_{\max} = 100$ to 200 for the neutron matter with the Minnesota potential at $A = 54$ and $\rho = 0.08$.

required to compute each data point from the above plot, as well as the breakdown of the major computational kernels. First, it is worth noting that despite the extreme memory requirements even the largest calculation here took less than 2 hours due to the high level of parallelism that can be exploited. Understandably, the tensor contractions are the most expensive component of these calculations, since even though the computations are dense in floating point operations, it is also this stage of the calculations that has the most communication overhead across the network. The line labeled setup is the nearly serial bottleneck at the beginning of the code, and this part of the code has since been parallelized, but it is difficult to run another timing test of this scale. Lastly, the load step is calculating all of the Minnesota potential matrix elements required for the interaction tensors. In a more realistic calculations, this would be the file I/O step, which could hopefully employ a similar level of parallelism.

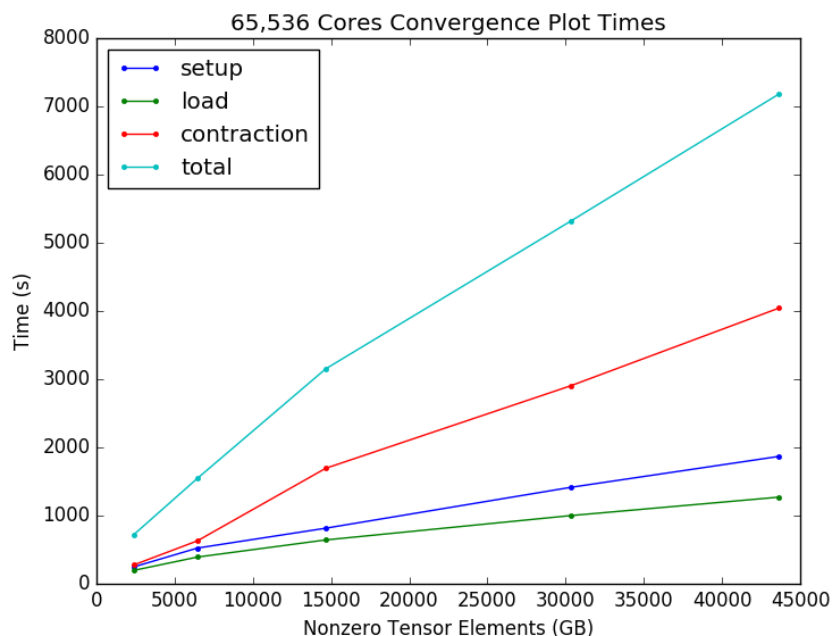


Figure 6.12: The time required for the large basis set Minnesota potential calculations.

To get an idea of how well the code is parallelized, it is common to look at strong and weak scaling. Ideal strong scaling is when doubling the amount of processors doubles how fast the code runs. This can be seen in many cases that are called “embarrassingly parallel”, where the calculation can be perfectly divided among compute cores, without any communication between cores needed. However, many calculations have parts of the code that run in serial, or communication overhead which causes the speedup to not follow the ideal case. Figure 6.13 is a strong scaling plot for the distributed memory implementation described in the computational methods chapter, with a line plotted to show what ideal strong scaling would look like. The code scales quite well up to about 100 cores for this calculation, but ceases to gain much speedup from increasing the cores beyond that, diverging more and more rapidly from the strong scaling line. While ideal strong scaling would be nice, it is not much of a surprise that this is not the case here. Any calculation which is even *possible* on a single core is a case where 1,000 cores is entirely unnecessary. The parts of the code that are highly

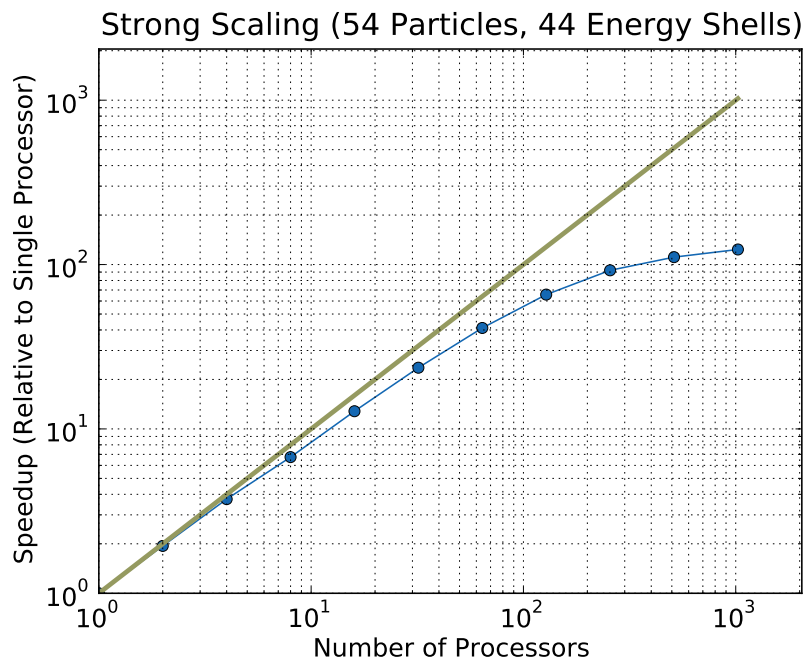


Figure 6.13: Strong scaling of distributed memory code, dark green line shows ideal case.

parallel are being computed almost instantly, leaving just the serial parts of the code which now take up 99% of the compute time.

However, in many-body physics, it is not often the case that parallelism is used to solve the same problem faster, but to solve larger and larger problems to increase the accuracy of calculations. This is where weak scaling is a more useful metric. Weak scaling is the idea that, given 1000 times more cores, can a problem 1000 times larger be tackled? If so, the ideal case would be that a problem size 1000 times larger would take the same amount of time if given 1000 times more cores. However, it is sometimes hard to easily quantify the problem size, since to compare apples to apples it would need to be measured in total floating point operations (FLOPs). In the case of CC calculations however, the limiting factor is the memory for the interaction tensors. How many gigabytes of memory are needed to store the matrix is typically what dictates how many nodes are allocated, and thus how many cores are used. To plot the weak scaling of the code, Figure 6.14 shows “problem size” vs. time to

complete calculation. A calculation is chosen to run on one core, which requires some amount of gigabytes to store the interaction matrix. This matrix size is now the unit which the other quantities are measured against. A problem which has an interaction matrix roughly 1,000 times larger and is then run on 1,000 cores. This procedure is done for many points, trying to increase the matrix size and number of processors proportionally. The green line shows the ideal weak scaling case, which the code is again diverging from. However, by choosing problem size equal to the matrix size we should not expect ideal weak scaling since for a square matrix of row size N , the matrix size scales as N^2 while matrix-matrix multiplication scales as N^3 . From the plot we can see that solving a system which needs 1000 times more memory from some base case only takes 2.5 times as long as this case is given 1000 times more processors. This is encouraging, as it shows that given the computational resources, the distributed memory algorithm is capable of solving proportionally larger and larger problems without too much additional overhead.

While extreme basis sets for CCD with two-body forces is nice, the real motivation here is to handle even modest basis sets for CCDT or three-body force calculations. To get an idea of how large the $\langle abc|w|def\rangle$ tensor is, Figure 6.15 shows the naive N^6 amount of matrix elements as well as the number of non-zero elements that the compressed block-diagonal structure has.

While these are large numbers, a more pragmatic calculation of the size of the three-body tensor in gigabytes is in Figure 6.16.

From this plot, we can see that even “small” basis sets over 700 single-particle states would require a billion gigabytes of memory naively. Even with the 10^4 compression factor of the block-diagonal tensor, this calculation will require 10 to 100 terabytes of memory. While this is a staggering number, it is not out of reach of modern supercomputers. Since

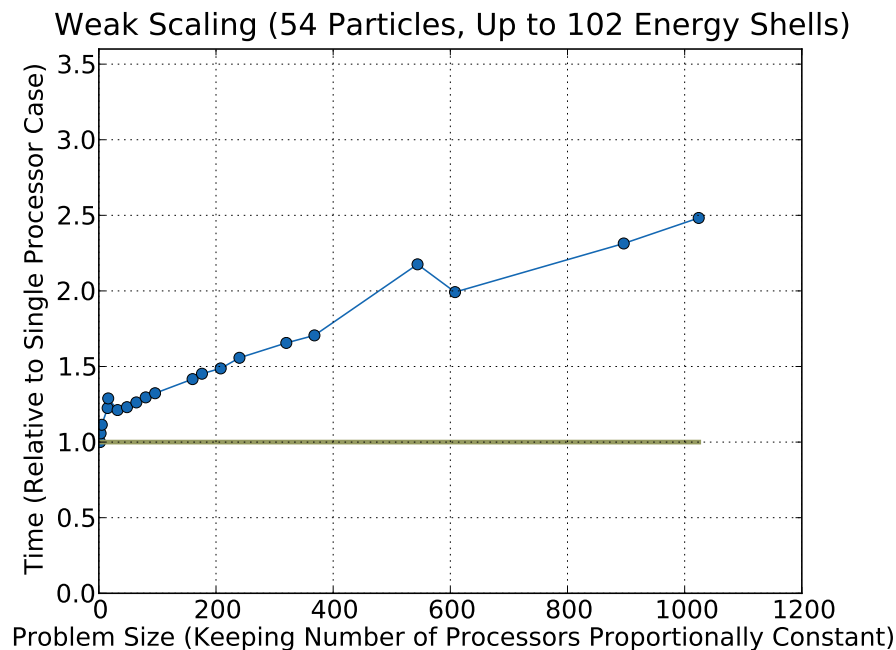


Figure 6.14: Weak scaling of distributed memory code, the dark green line shows the ideal case.

the basis for the electron gas and nuclear matter is so similar, this feature is universal across these calculations. Coupled cluster theory frequently runs into these memory issues, which could be circumvented by not storing the interactions, but by computing them on-the-fly [79]. This method has had success in quantum chemistry, but the nuclear potential has proven to be too costly to employ this method. However, as the computational power of these machines grows, it is not unthinkable that this could be done in the future.

These calculations would need to be highly optimized at the node level, exploiting as much parallelism as possible for many-core and GPU architectures. Figure 6.17 shows the on-node timing tests for computing the $\langle abc|w|def\rangle \langle def|t|ijk\rangle$ tensor contraction which, scaling at N^9 , is the most expensive component of a full CCDT calculation with three-body forces. Understanding this term and developing and optimizing it will be extremely important for future calculations. The primary challenge is performing hundreds of thousands of matrix-

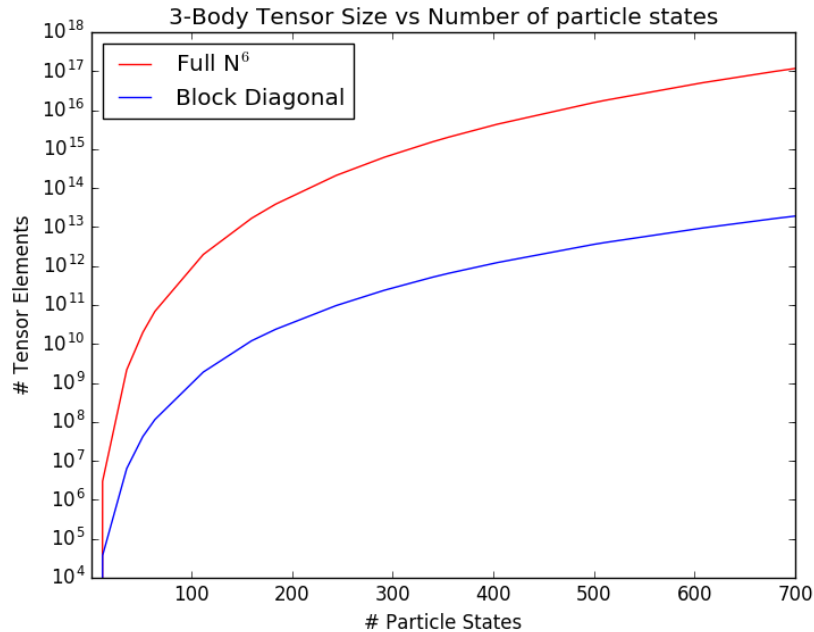


Figure 6.15: Number of tensor elements required for the 3-body force in the infinite matter basis with and without block-diagonal compression.

matrix multiplications across all of the symmetry blocks. In the plot, three methods were tested: OpenMP [69] parallelization over the blocks, serial batching of cuBLAS on the blocks, and serial batching of multithreaded OpenBLAS zgemm (complex double matrix-matrix multiplication) calls. The different BLAS operation calls typically have a leading character that determines the data type, d for double, z for complex double. OpenBLAS [68] was used for the CPU implementation of BLAS, and cuBLAS was used for the GPU implementation, where the “cu” in cuBLAS is a reference to CUDA, a programming model for writing software for Nvidia GPUs [80]. From this plot, we can see that the multi-threaded zgemm calls are the fastest, while the OMP parallelized loops are the slowest, not much faster than cuBLAS. The many-core calculations were ran on a node which has two 2.4Gz 14-core Intel Xeon processors and the GPU calculations were ran on an NVIDIA Tesla K80. By raw performance, the GPU calculations should run faster, but there are difficulties in

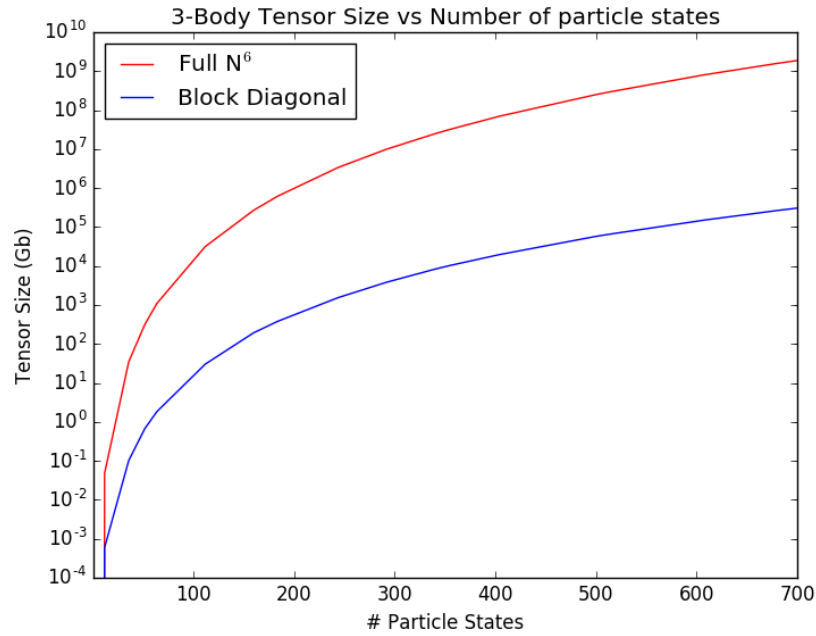


Figure 6.16: Size of tensor in gigabytes required for the 3-body force in the infinite matter basis with and without block-diagonal compression.

getting the calculations to run efficiently. The large disparity between the thousands of tiny matrix-matrix multiplies versus the relatively few large matrix-matrix multiplies means that a hybrid scheme will likely be necessary for doing batched calls for the small matrices and regular gemm calls for the large matrices. However, since this calculation is just doing tens of thousands of cuBLAS calls, the benefit of the GPU speed is overcome by the enormous amount of call overhead.

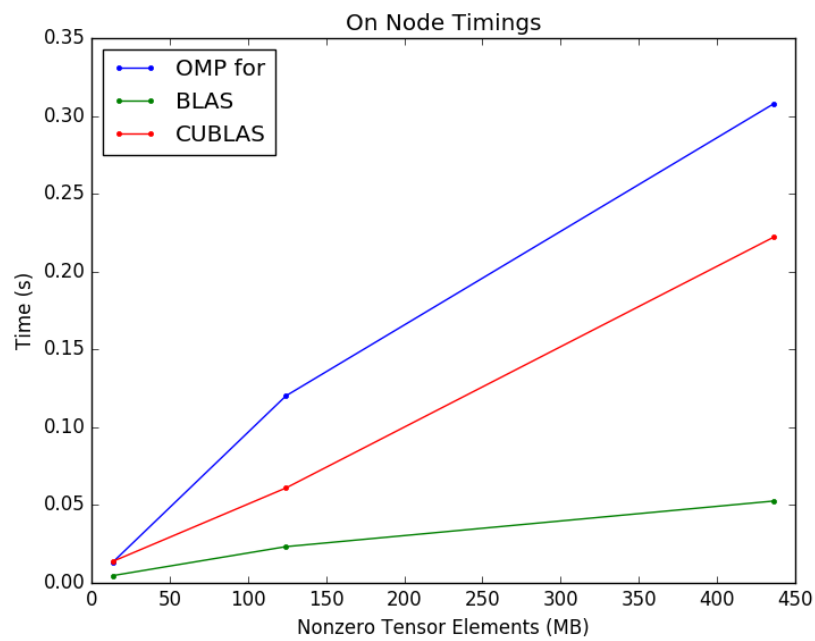


Figure 6.17: On node timing tests for the tensor contraction of three-body force diagrams.

Chapter 7

Conclusions and Perspectives

The future of *ab initio* many-body physics is bright, especially in nuclear theory where methods like coupled cluster (CC) theory and in-medium similarity renormalization (IM-SRG) are still relatively young to the field. Accurate calculations with predictive power are necessary for answering questions where experimental data are lacking. In systems like neutron stars, theory and computation could be our only tools for answering questions about their internal structure. In this thesis, we reviewed and implemented the formalism for several many-body methods, with a focus on coupled cluster theory which is capable of computing properties of very large systems while maintaining a link to all of the fundamental degrees of freedom.

The computer program that implements these many-body methods is designed with accuracy as the first goal. Analytical techniques were used to validate the accuracy of the program before any other considerations were made. The code is designed in a modular way which allows any physical system to be included without modifying any of the existing infrastructure. This allows properties of the pairing model, the homogeneous electron gas and infinite nuclear matter to be computed with minimal additional effort, and allows the addition of other systems in the future. Importantly, the program implements distributed memory algorithms and data structures which allow the code to run at high-performance computing centers. Investigating the strong and weak scaling showed that the program can perform increasingly large calculations as long as a proportional increase in computational

resources is provided. This enables extremely large basis sets to be used for physical systems to reach levels of precision that would otherwise be impossible.

Looking towards the future, with these data structures and algorithms implemented, the program can be extended to tackle many interesting topics in many-body theory and computational physics. Coupled cluster theory with doubles and triples excitations (CCDT) calculations of the homogeneous electron gas with twist-averaged boundary conditions is a likely first target. The addition of triples correlations will likely provide a significant correction to the correlation energy of the system. While approximate triples contributions have been included, it is currently unknown how important the role of the full triples correlations are in this system. Next, the inclusion of full three-body forces in calculations of nuclear matter with chiral effective field theory Hamiltonians has up until now been avoided due to the extreme memory requirements of the full three-body forces and the computational effort required for the tensor contractions. Tackling this calculation will be a serious undertaking in high performance computing, but with the next generation of high-performance computing facilities, we may be able to handle the increased dimensionality. The data structures and algorithms to handle the large number of matrix elements and computationally expensive tensor contractions are largely in place. Further work on the GPU implementation is on-going, which would allow the program to deploy on some of the modern supercomputers. The next step is to include all of the less computationally heavy, but necessary three-body diagrams. With these in place, the program will be in position to examine several important many-body questions:

1. What is the role of the full three-body interaction in infinite matter using chiral effective field theory? How much the normal ordered 0-,1-, and 2-body terms miss? Can the inclusion of the full three-body interaction lead to the accurate prediction of the nuclear

saturation density?

2. Can we quantify the errors of approximated triples by implementing full triples? Are there patterns in these errors to predict the errors of approximated triples in regions where full triples are too expensive?
3. What is the role of full triples in the homogeneous electron gas?
4. How does the nuclear equation of state differ at various neutron to proton fractions? What about at β -stable equilibrium?

Along with CC calculations, the distributed memory data structures and algorithms implemented can be quickly ported into a new many-body method, namely IM-SRG with the Magnus expansion. A distributed memory implementation of IM-SRG does not currently exist, but due to the modular nature of the program and the generic nature of the data structures, adding IM-SRG functionality is a logical next step forward. This would alleviate many of the memory constraints of the method, allowing the calculation of many new physical systems under a new theoretical perspective.

BIBLIOGRAPHY

BIBLIOGRAPHY

- [1] J. M. Lattimer, “The nuclear equation of state and neutron star masses,” *Annu. Rev. Nuc. Part. S.*, vol. 62, p. 485, 2012.
- [2] G. Baardsen, A. Ekström, G. Hagen, and M. Hjorth-Jensen, “Coupled-cluster studies of infinite nuclear matter,” *Phys. Rev. C*, vol. 88, p. 054312, 2013.
- [3] S. R. Stroberg, A. Calci, H. Hergert, J. D. Holt, S. K. Bogner, R. Roth, and A. Schwenk, “Nucleus-dependent valence-space approach to nuclear structure,” *Phys. Rev. Lett.*, vol. 118, p. 032502, 2017.
- [4] S. Bogner, R. Furnstahl, and A. Schwenk, “From low-momentum interactions to nuclear structure,” *Prog. Part. Nuc. Phys.*, vol. 65, p. 94, 2010.
- [5] R. Roth, J. Langhammer, A. Calci, S. Binder, and P. Navrátil, “Similarity-transformed chiral $NN + 3N$ interactions for the ab initio description of ^{12}C and ^{16}O ,” *Phys. Rev. Lett.*, vol. 107, p. 072501, 2011.
- [6] E. Epelbaum, H.-W. Hammer, and U.-G. Meißner, “Modern theory of nuclear forces,” *Rev. Mod. Phys.*, vol. 81, p. 1773, 2009.
- [7] R. Machleidt and D. Entem, “Chiral effective field theory and nuclear forces,” *Phys. Rep.*, vol. 503, p. 1, 2011.
- [8] J. C. Slater, “The theory of complex spectra,” *Phys. Rev.*, vol. 34, p. 1293, 1929.
- [9] E. U. Condon, “The theory of complex spectra,” *Phys. Rev.*, vol. 36, p. 1121, 1930.
- [10] R. F. Bacher, “The interaction of configurations: $sd - p^2$,” *Phys. Rev.*, vol. 43, p. 264, 1933.
- [11] C. W. Ufford, “Configuration interaction in complex spectra,” *Phys. Rev.*, vol. 44, p. 732, 1933.
- [12] J. Čížek, “On the correlation problem in atomic and molecular systems. calculation of wavefunction components in urselltype expansion using quantumfield theoretical methods,” *J. Chem. Phys.*, vol. 45, p. 4256, 1966.

- [13] J. Čížek and J. Paldus, “Correlation problems in atomic and molecular systems iii. rederivation of the coupled-pair many-electron theory using the traditional quantum chemical methodst,” *Int. J. Quantum Chem.*, vol. 5, p. 359, 1971.
- [14] J. Čížek and J. Paldus, “Coupled cluster approach,” *Phys. Scr.*, vol. 21, p. 251, 1980.
- [15] P. Piecuch, K. Kowalski, I. S. O. Pimienta, and M. J. McGuire, “Recent advances in electronic structure theory: Method of moments of coupled-cluster equations and renormalized coupled-cluster approaches,” *Int. Rev. Phys. Chem.*, vol. 21, p. 527, 2002.
- [16] I. Shavitt and R. J. Bartlett, *Many-Body Methods in Chemistry and Physics: MBPT and Coupled-Cluster Theory*. Cambridge Molecular Science, Cambridge University Press, 2009.
- [17] F. Coester, “Bound states of a many-particle system,” *Nuc. Phys.*, vol. 7, p. 421, 1958.
- [18] F. Coester and H. Kmmel, “Short-range correlations in nuclear wave functions,” *Nuc. Phys.*, vol. 17, p. 477, 1960.
- [19] H. Kümmel, K. Lührmann, and J. Zabolitzky, “Many-fermion theory in exps- (or coupled cluster) form,” *Phys. Rep.*, vol. 36, p. 1, 1978.
- [20] G. Hagen, T. Papenbrock, D. J. Dean, and M. Hjorth-Jensen, “Ab initio coupled-cluster approach to nuclear structure with modern nucleon-nucleon interactions,” *Phys. Rev. C*, vol. 82, p. 102, 2010.
- [21] G. Hagen, T. Papenbrock, D. J. Dean, and M. Hjorth-Jensen, “Coupled-cluster computations of atomic nuclei,” *Rep. Prog. Phys.*, vol. 77, p. 096302, 2014.
- [22] B. D. Day, “Current state of nuclear matter calculations,” *Rev. Mod. Phys.*, vol. 50, p. 495, 1978.
- [23] J. J. Shepherd, A. Grüneis, G. H. Booth, G. Kresse, and A. Alavi, “Convergence of many-body wave-function expansions using a plane-wave basis: From homogeneous electron gas to solid state systems,” *Phys. Rev. B*, vol. 86, p. 035111, 2012.
- [24] S. Beane, P. Bedaque, A. Parreo, and M. Savage, “Two nucleons on a lattice,” *Phys. Lett. B*, vol. 585, p. 106, 2004.
- [25] S. R. Beane, E. Chang, S. D. Cohen, W. Detmold, H. W. Lin, T. C. Luu, K. Orginos, A. Parreño, M. J. Savage, and A. Walker-Loud, “Light nuclei and hypernuclei from

- quantum chromodynamics in the limit of $su(3)$ flavor symmetry,” *Phys. Rev. D*, vol. 87, p. 034506, 2013.
- [26] A. Ekström, G. Baardsen, C. Forssén, G. Hagen, M. Hjorth-Jensen, G. R. Jansen, R. Machleidt, W. Nazarewicz, T. Papenbrock, J. Sarich, and S. M. Wild, “Optimized chiral nucleon-nucleon interaction at next-to-next-to-leading order,” *Phys. Rev. Lett.*, vol. 110, p. 192502, 2013.
- [27] A. Ekström, G. R. Jansen, K. A. Wendt, G. Hagen, T. Papenbrock, B. D. Carlsson, C. Forssén, M. Hjorth-Jensen, P. Navrátil, and W. Nazarewicz, “Accurate nuclear radii and binding energies from a chiral interaction,” *Phys. Rev. C*, vol. 91, 2015.
- [28] F. Gieres, “Dirac’s formalism and mathematical surprises in quantum mechanics,” *Rept. Prog. Phys.*, vol. 63, p. 1893, 2000.
- [29] J. C. Slater, “The theory of complex spectra,” *Phys. Rev.*, vol. 34, p. 1293, 1929.
- [30] A. Fetter and J. Walecka, *Quantum Theory of Many-particle Systems*. Dover Books on Physics, Dover Publications, 2003.
- [31] V. Fock, “Konfigurationsraum und zweite quantelung,” *Zeit. Phys.*, vol. 75, p. 622, 1932.
- [32] J. Goldstone, “Derivation of the brueckner many-body theory,” *Proc. R. Soc. Lond. A Math. Phys. Eng. Sci.*, vol. 239, p. 267, 1957.
- [33] N. Hugenholtz, “Perturbation theory of large quantum systems,” *Physica*, vol. 23, p. 481, 1957.
- [34] G. C. Wick, “The evaluation of the collision matrix,” *Phys. Rev.*, vol. 80, 1950.
- [35] D. R. Hartree, “The wave mechanics of an atom with a non-coulomb central field. part i. theory and methods,” *Math. Proc. Camb. Philos. Soc.*, vol. 24, p. 89, 1928.
- [36] V. Fock, “Näherungsmethode zur lösung des quantenmechanischen mehrkörperproblems,” *Zeit. Phys.*, vol. 61, p. 126, 1930.
- [37] C. Møller and M. S. Plesset, “Note on an approximation treatment for many-electron systems,” *Phys. Rev.*, vol. 46, 1934.

- [38] J. Hubbard, “The description of collective motions in terms of many-body perturbation theory,” *Proc. R. Soc. Lond. A Math. Phys. Sci.*, vol. 240, p. 539, 1957.
- [39] L. Brillouin, “Les problèmes de perturbations et les champs self-consistents,” *J. Phys. Radium*, vol. 3, p. 373, 1932.
- [40] J. Rayleigh, *The Theory of Sound*. Macmillan, 1894.
- [41] E. Schrödinger, “Quantisierung als eigenwertproblem,” *Ann. Phys.*, vol. 80, p. 437, 1926.
- [42] K. Tsukiyama, S. K. Bogner, and A. Schwenk, “In-medium similarity renormalization group for nuclei,” *Phys. Rev. Lett.*, vol. 106, p. 222502, 2011.
- [43] K. Tsukiyama, S. K. Bogner, and A. Schwenk, “In-medium similarity renormalization group for open-shell nuclei,” *Phys. Rev. C*, vol. 85, p. 061304, 2012.
- [44] H. Hergert, S. Binder, A. Calci, J. Langhammer, and R. Roth, “Ab initio calculations of even oxygen isotopes with chiral two-plus-three-nucleon interactions,” *Phys. Rev. Lett.*, vol. 110, p. 242501, 2013.
- [45] S. K. Bogner, H. Hergert, J. D. Holt, A. Schwenk, S. Binder, A. Calci, J. Langhammer, and R. Roth, “Nonperturbative shell-model interactions from the in-medium similarity renormalization group,” *Phys. Rev. Lett.*, vol. 113, p. 142501, 2014.
- [46] H. Hergert, S. K. Bogner, T. D. Morris, S. Binder, A. Calci, J. Langhammer, and R. Roth, “Ab initio multireference in-medium similarity renormalization group calculations of even calcium and nickel isotopes,” *Phys. Rev. C*, vol. 90, p. 041302, 2014.
- [47] H. Hergert, “In-medium similarity renormalization group for closed and open-shell nuclei,” *Phys. Scr.*, vol. 92, p. 023002, 2017.
- [48] S. R. Stroberg, H. Hergert, J. D. Holt, S. K. Bogner, and A. Schwenk, “Ground and excited states of doubly open-shell nuclei from ab initio valence-space hamiltonians,” *Phys. Rev. C*, vol. 93, p. 051301, 2016.
- [49] F. J. Wegner, “Flow equations for hamiltonians,” *Nuc. Phys. B - Proceedings Supplements*, vol. 90, pp. 141 – 146, 2000.
- [50] T. D. Morris, N. M. Parzuchowski, and S. K. Bogner, “Magnus expansion and in-medium similarity renormalization group,” *Phys. Rev. C*, vol. 92, p. 034331, 2015.

- [51] S. R. White, “Numerical canonical transformation approach to quantum many-body problems,” *The Journal of Chemical Physics*, vol. 117, p. 7472, 2002.
- [52] W. Magnus, “On the exponential solution of differential equations for a linear operator,” *Commun. Pure Appl. Math*, vol. 7, 1954.
- [53] D. Thompson, M. Lemere, and Y. Tang, “Systematic investigation of scattering problems with the resonating-group method,” *Nuclear Physics A*, vol. 286, p. 53, 1977.
- [54] P. Piecuch and K. Kowalski, “In search of the relationship between multiple solutions characterizing coupled-cluster theories,” in *Computational Chemistry: Reviews of Current Trends* (J. Leszczynski, ed.), vol. 5, p. 1, Singapore: World Scientific, 2000.
- [55] P. Piecuch, S. Zarrabian, J. Paldus, and J. Čížek, “Coupled-cluster approaches with an approximate account of triexcitations and the optimized-inner-projection technique. ii. coupled-cluster results for cyclic-polyene model systems,” *Phys. Rev. B*, vol. 42, p. 3351, 1990.
- [56] K. Kowalski, D. J. Dean, M. Hjorth-Jensen, T. Papenbrock, and P. Piecuch, “Coupled cluster calculations of ground and excited states of nuclei,” *Phys. Rev. Lett.*, vol. 92, p. 132501, 2004.
- [57] G. Hagen, T. Papenbrock, D. J. Dean, A. Schwenk, A. Nogga, M. Włoch, and P. Piecuch, “Coupled-cluster theory for three-body hamiltonians,” *Phys. Rev. C*, vol. 76, p. 034302, 2007.
- [58] M. Włoch, D. J. Dean, J. R. Gour, M. Hjorth-Jensen, K. Kowalski, T. Papenbrock, and P. Piecuch, “Ab-initio coupled-cluster study of ^{16}O ,” *Phys. Rev. Lett.*, vol. 94, p. 212501, 2005.
- [59] J. R. Gour, P. Piecuch, M. Hjorth-Jensen, M. Włoch, and D. J. Dean, “Coupled-cluster calculations for valence systems around ^{16}O ,” *Phys. Rev. C*, vol. 74, p. 024310, 2006.
- [60] D. Thouless, “Stability conditions and nuclear rotations in the hartree-fock theory,” *Nuc. Phys.*, vol. 21, p. 225, 1960.
- [61] B. H. Brandow, “Linked-cluster expansions for the nuclear many-body problem,” *Rev. Mod. Phys.*, vol. 39, p. 771, 1967.
- [62] P. Szakács and P. R. Surján, “Stability conditions for the coupled cluster equations,” *Int. J. Quantum Chem.*, vol. 108, p. 2043, 2008.

- [63] C. G. Broyden, “A class of methods for solving nonlinear simultaneous equations,” *Math. Comput.*, vol. 19, p. 577, 1965.
- [64] Y. S. Lee and R. J. Bartlett, “A coupled cluster approach with triples excitations,” *J. Chem. Phys.*, vol. 81, p. 5906, 1984.
- [65] G. Hagen and H. A. Nam, “Computational aspects of nuclear coupled-cluster theory,” *Prog. Theor. Phys. Supplement*, vol. 196, p. 102, 2012.
- [66] A. Signoracci, T. Duguet, G. Hagen, and G. R. Jansen, “Ab initio bogoliubov coupled cluster theory for open-shell nuclei,” *Phys. Rev. C*, vol. 91, p. 064320, 2015.
- [67] V. Strassen, “Gaussian elimination is not optimal,” *Numer. Math.*, vol. 13, p. 354, 1969.
- [68] “For documentation of openblas, see.” <http://www.openblas.net>, accessed June, 2019.
- [69] “For documentation of openmp, see.” <http://openmp.org>, accessed June, 2019.
- [70] E. Gabriel, G. E. Fagg, G. Bosilca, T. Angskun, J. J. Dongarra, J. M. Squyres, V. Sahay, P. Kambadur, B. Barrett, A. Lumsdaine, R. H. Castain, D. J. Daniel, R. L. Graham, and T. S. Woodall, “Open MPI: Goals, concept, and design of a next generation MPI implementation,” in *Proceedings, 11th European PVM/MPI Users’ Group Meeting*, (Budapest, Hungary), p. 97, 2004.
- [71] C. Gros, “The boundary condition integration technique: results for the hubbard model in 1d and 2d,” *Zeitschrift fr Physik B Condensed Matter*, vol. 86, p. 359, 1992.
- [72] C. Gros, “Control of the finite-size corrections in exact diagonalization studies,” *Phys. Rev. B*, vol. 53, p. 6865, 1996.
- [73] C. Lin, F. H. Zong, and D. M. Ceperley, “Twist-averaged boundary conditions in continuum quantum monte carlo algorithms,” *Phys. Rev. E*, vol. 64, p. 016702, 2001.
- [74] V. Somà, C. Barbieri, and T. Duguet, “Ab initio gorkov-green’s function calculations of open-shell nuclei,” *Phys. Rev. C*, vol. 87, p. 011303, 2013.
- [75] V. Somà, C. Barbieri, and T. Duguet, “Ab initio self-consistent gorkov-green’s function calculations of semi-magic nuclei: Numerical implementation at second order with a two-nucleon interaction,” *Phys. Rev. C*, vol. 89, p. 024323, 2014.

- [76] V. Somà, A. Cipollone, C. Barbieri, P. Navrátil, and T. Duguet, “Chiral two- and three-nucleon forces along medium-mass isotope chains,” *Phys. Rev. C*, vol. 89, p. 061301, 2014.
- [77] M. Hjorth-Jensen, M. P. Lombardo, and U. van Kolck, *An Advanced Course in Computational Nuclear Physics - Bridging the scales from quarks to neutron stars*, vol. 936 of *Lecture Notes in Physics*. Springer, 2017.
- [78] J. J. Shepherd, G. Booth, A. Grüneis, and A. Alavi, “Full configuration interaction perspective on the homogeneous electron gas,” *Phys. Rev. B*, vol. 85, p. 081103, 2012.
- [79] S. Reine, E. Tellgren, and T. Helgaker, “A unified scheme for the calculation of differentiated and undifferentiated molecular integrals over solid-harmonic gaussians,” *Phys. Chem. Chem. Phys.*, vol. 9, 2007.
- [80] “For documentation of cuda, see.” <http://developer.nvidia.com>, accessed June, 2019.